Optimality of Commercial Resins and Functionalized Chitosan Derivatives for the Recovery and Reuse of Pd(II) from Synthetic Electroless Plating Solutions

Thesis submitted in partial fulfillment of the

requirements for the degree of

DOCTOR OF PHILOSOPHY

by

Nagireddi Srinu

Department of Chemical Engineering

Indian Institute of Technology Guwahati

Guwahati–781039, India

Optimality of Commercial Resins and Functionalized Chitosan Derivatives for the Recovery and Reuse of Pd(II) from Synthetic Electroless Plating Solutions

Srinu Nagireddi

Optimality of Commercial Resins and Chitosan Derivatives for the Recovery and Reuse of Pd(II) from Synthetic Electroless Plating Solutions

Thesis submitted in partial

fulfillment of the requirements for the degree of

DOCTOR OF PHILOSOPHY

by

Nagireddi Srinu
Roll No.: 146107039

Department of Chemical Engineering

Indian Institute of Technology Guwahati

Guwahati – 781039, India

May 2019

Dedicated

to

my parents and family members

Department of Chemical Engineering
Indian Institute of Technology Guwahati
Guwahati – 781039, Assam, India

CERTIFICATE

It is to certify that the Ph.D. thesis entitled **"Optimality of Commercial Resins and Functionalized Chitosan Derivatives for the Recovery and Reuse of Pd(II) from Synthetic Electroless Plating Solutions"** (submitted by **Mr. Nagireddi Srinu)** was carried out under our joint supervision at the Department of Chemical Engineering, Indian Institute of Technology Guwahati.

(Prof. Ramagopal V. S. Uppaluri)
Department of Chemical Engineering
IIT Guwahati, Guwahati - 781039

(Prof. Animes K. Golder)
Department of Chemical Engineering
IIT Guwahati, Guwahati - 781039

Department of Chemical Engineering
Indian Institute of Technology Guwahati
Guwahati – 781039, Assam, India

DISCLAIMER

The experimental, modelling and characterization related data presented in this Ph.D. thesis was carried out by me and is reported after due verification. To the best of my knowledge, the work summarized in this Ph.D. thesis is not submitted elsewhere for the award of any other degree or diploma.

(Mr. Nagireddi Srinu)

Acknowledgement

Firstly, I would like to express my sincere gratitude to my advisors **Prof. Ramagopal V.S. Uppaluri** and **Prof. Animes Kr. Golder** for their continuous support, patience, motivation and immense knowledge sharing discussions during my Ph.D. tenure at IIT Guwahati. Their guidance significantly assisted my needs throughout the tenure of my research and thesis writing. With such gracious consideration, I do not wish to imagine having better advisors and mentors for my Ph.D.

Besides my advisors, I would like to thank honourable doctoral committee members of my thesis namely **Prof. Vimal Katiyar**, **Prof. Chandan Das**, and **Prof. Saswati Chakraborty**, for their highly relevant insights, comments and thought provoking questions that served as an incentive to widen the domain of my research.

My sincere thanks is also due to scientific officers of Chemical Engineering Department, Centre for the Environment and Central Instruments Facility for providing me all support to utilize research facilities. Without their precious support, the thesis would not have had a subjective edge in terms of surface characterization results.

I would also like to thank Council of Scientific & Industrial Research (CSIR, India) and Department of Chemical Engineering for providing the financial support to carry out the conducted research.

I thank my labmates and juniors for their friendly support and timely assistance and help. Special thanks to Mr. Prabhat Kumar Patel for his assistance and co-operation towards few lab experiments and final thesis editing work. Also I thank my friends Dr. Mothe Gopi Kiran, Dr. D Narendra Naik, Dr. Mood Mohan, Dr. G. Radha Krishna, Mr. Satyannarayana Edubilli, Dr. Ch Venkatanarasimha Rao, Mr. Mallikarjuna Reddy, Mr. T Ramesh, Mr. Y Santosh, Mr. V

Kartheek, Mr. K Durga Prasad, Mr. Sunku Prasad, Mr. Shashidhar Reddy, Mr. P Rajashekar Reddy for their friendly support and timely assistance in due course of the degree. In particular, I am grateful to **Dr. Gopi Krishna** for his immense help to make me understand chemistry aspects of my research.

A special thanks to my family. Words cannot express how grateful I am to my mother, father, sister and brother in-law for all sacrifices they made for me to reach to this destination in my life. Your prayers and continuous support to me sustained me this far and I am indebted to all of you for such positive and friendly environment in the crucial juncture of my education.

Srinu Nagireddi

(srinunagireddi830@gmail.com)

Abstract

Adsorption based recovery, removal and reuse of noble metals from spent waste solutions is a challenging area of research. With data confining towards simpler aqueous solutions, the available literature does not elaborate towards Pd(II) adsorption and desorption characteristics associated to complex adsorbate systems. Further, comparative assessment of performance and cost indices is not available. With abundance of nitrogen functional groups and significant ability to undergo cross-linking with suitable functional groups, chitosan has been investigated to a moderate extent towards its efficacy for noble metal recovery and reuse from only aqueous solutions. In this regard, promising performance has been inferred by our research group with respect to glutaraldehyde based functionalize chitosan derivative. However, other derivatives including nitrogen and sulfur functionalized chitosan materials have not been addressed for their efficacy for Pd(II) recovery and reuse. Considering these lacunae, the PhD thesis targets the efficacy of commercial and chitosan based resins for the recovery, removal and reuse of Pd(II) from synthetic electroless plating (ELP) solutions, which is characterized to have a moderate solution complexity. The thesis consists of four major sections namely:

a) Evaluation of Pd(II) speciation in synthetic ELP solutions and efficacy of raw chitosan towards Pd(II) removal and recovery.
b) Efficacy of commercial resins (Amberlyst A21, Amberlite IRA958 and Dowex Marathon MSA) for Pd(II) removal and recovery from synthetic ELP solutions.
c) Synthesis, characterization, batch adsorption and desorption studies of nitrogen functionalized chitosan resins (melamine cross-linked chitosan (CH-ME) and triethylenetetramine cross-linked chitosan (CH-TETA)) for the Pd(II) removal and recovery from synthetic ELP solutions.

d) Synthesis, characterization, batch adsorption and desorption studies of nitrogen and sulfur functionalized chitosan resins (thiosemicarbazide cross-linked chitosan (CH-TSC) and 3-amino-1,2,4-triazole-5-thiol cross-linked chitosan (CH-AZ)) for the Pd(II) removal and recovery from synthetic ELP solutions.

e) Comparative assessment in terms of adsorption, desorption and cost based performance indices for all resins considered in the thesis and identification of most competent resin from adsorption, desorption and cost perspective.

The surface characterization studies have been conducted for both commercial and synthesized chitosan based derivatives. These include FTIR, BET, XRD, TGA and FESEM-EDX analyses.

The overall methodology adopted in the thesis for various investigations have been summarized as follows. Firstly, Pd(II) speciation in synthetic ELP solutions was evaluated using visual MINTEQ (open source) software. Further, appropriate modification of chitosan with suitable nitrogen or nitrogen and sulfur functional groups was achieved by adopting displacement and elimination reaction techniques. For all adsorbents, batch adsorption studies were carried for a variation in batch adsorption process parameters as 0.5−10 pH, 10-100 mg adsorbent dosage, 5-1080 min contact time and 50-300 mg L^{-1}Pd(II) initial solution concentration. For comparative assessment, the adsorptive and desorptive performance of all resins was also evaluated for Pd(II) aqueous solution systems at corresponding optimized batch process parameter values. For the resin-synthetic ELP solution system, the experimentally evaluated batch equilibrium, kinetic and thermodynamics of Pd(II) adsorption were evaluated for their fitness with suitable equilibrium (Langmuir and Freundlich models), kinetic (Pseudo-first-order, Pseudo-second-order and intraparticle diffusion models) and Van't Hoff thermodynamic model respectively. The desorption efficiencies of all the adsorbents were carried out using simple and cheaper eluents at

the concentration range from 0.1−2 M for the spent adsorbents obtained with 50 mg L^{-1} initial Pd(II) solution concentration. Finally, cost effectiveness of all the adsorbents were targeted by evaluating cost indices based on the retail costs associated to their fabrication for synthesized resins and retail cost of commercial resins.

Speciation analysis inferred that Pd(II) ions were mostly available in $PdEDTA^{-2}$and $Pd(NH_3)_4^{2+}$ forms in acidic (1-6 pH) and basic (8-10 pH) range of pH respectively. For raw chitosan case, poor Pd(II) desorption efficiencies (6.31%) were achieved and the solubility resistance analysis confirmed that the chitosan is soluble from 0.5 – 5 pH. Hence, suitable modification of chitosan structure with relevant functional groups is justified from the perspective of its sustainability in acidic aqueous media. Among all commercial resins, Dowex Marathon MSA resin provided best performance for Pd(II) adsorption and desorption from synthetic ELP solutions. From cost efficacy perspective, compared to the Dowex Marathon MSA resin, Amberlyst A21 is the most inexpensive resin with marginally lower adsorption and desorption efficiencies. Among all laboratory fabricated chitosan derivatives, CH-AZ provided better adsorptive performance but provided poor desorptive efficiencies. From cost perspective, poor cost indices were obtained for CH-AZ (0.3219), CH-ME (0.333), CH-TSC (0.4418) resins and marginally better values for CH-TETA (0.6038).From desorption perspective, best performance index value was confirmed for CH-TSC derivative (0.6227).

Therefore, among all adsorbents, commercial Amberlyst A21 resin can be inferred to have excellent performance characteristics from adsorption, desorption and cost perspectives. Besides these, the carried out investigations enabled useful insights into the irrelevance of HSAB theory as a generalized rule of thumb to screen and scope potential adsorbents for noble metal recovery and reuse. In summary, the thesis provided useful insights into the desorption and cost efficacy

perspectives of studied resins and thereby provides the necessary framework to further enhance the applications of adsorption technology towards noble metal recovery and reuse from complex adsorbate systems such as real waste water samples.

Contents

List of Tables

List of Figures

Nomenclature

Abbreviation

PGM's	Platinum Group Metals
ELP	Electroless Plating
EDTA	Ethylenediaminetetraacetic acid
CTAB	Cetyl Trimethyl Ammonium Bromide
HSAB	Hard and Soft Acid Base
CH	Raw Chitosan
CH-ME	Melamine Cross-linked Chitosan
CH-TETA	Triethylene tetramine Cross-linked Chitosan
CH-TSC	Thiosemicarbazide Cross-linked Chitosan
CH-AZ	3-amino-1,2,4 triazole,5-thiol Cross-linked Chitosan
DMF	*N*,*N*-dimethylformamide
FTIR	Scanning Electronic Microscope
BET	Brunauer-Emmett-Teller
AAS	Atomic Absorption Spectrometer
EDX	Energy Dispersive X-ray spectrometer
FESEM	Field Scanning Electronic Microscope
TGA	Thermo Gravimetric Analyser
XRD	X-ray Powder Diffractometer

Notations

C_o	Initial Pd(II) solution concentration, mg L^{-1}
C_e	Equilibrium Pd(II) solution concentration, mgL^{-1}
W	mass of adsorbent, g
V	volume of solution, mL
Q_e	Equilibrium Pd(II) adsorption capacity, mg g^{-1}
Q_o	Maximum adsorption capacity, mg g^{-1}
b	Langmuir adsorption constant
R_L	Dimensionless equilibrium parameter
K_f	Freundlich isotherm coefficient
n	Amount of adsorbent taken per l L of aqueous solution, mg L^{-1}
t	Agitation time, min
K_1	Psuedo First order rate constant, min^{-1}
K_2	Pseudo second order rate constant, g $mg^{-1}min^{-1}$
K_{id}	Intra Particle rate constant ($time^{-1}$)
Q_t	Mass of solute adsorbed per mass of adsorbent at 't' min, mg/g
R	Universal gas constant (8.314 J mol^{-1} K^{-1})
T	Absolute temperature, K
ΔG^o	Change in Gibbs free energy,kJ mol^{-1}
ΔS^o	Change in Entropy, kJ $mol^{-1}K^{-1}$
ΔH^o	Change in Enthalpy, kJ mol^{-1}
K_c	Thermodynamic equilibrium constant
C_f	Final Pd(II) solution concentration subjected to adsorption study, mg L^{-1}
A	Initial Pd(II) concentration on adsorbent subjected to desorption study, mg L^{-1}
B	Initial amount of Pd(II) on adsorbent
V_{sol}	Volume of adsorbate solution, mL
$W_{adsorbent}$	Weight of adsorbent, mg
C	Final concentration of Pd(II) in eluent, mg L^{-1}
V_{eluent}	Volume of eluent solution, mL

Chapter 1:

Introduction and Literature Review

Chapter 1

Introduction and Literature Review

Section 1.1 of the chapter presents a brief summary on the need for Pd(II) recovery from waste streams, various competent technologies for the recovery and reuse of noble metals, prominence of adsorptive ion-exchange technologies, various Pd(II) adsorbate systems and promising adsorbents for Pd(II) recovery and targeted research perspectives. Section 1.2 addresses the available prior art for various adsorptive and ion exchange resins to foster competitive Pd(II) adsorption from aqueous and synthetic solutions. Thereafter, section 1.3 details on the scope for further research with emphasis towards Pd(II) adsorptive recovery and reuse from complex adsorbate systems. Finally, section 1.4 conveys the broad objectives of the thesis followed with thesis organization related details in section 1.5.

1.1 Preamble

1.1.1 Need for Pd(II) recovery and reuse

Bestowed with the promising features of high temperature stability, corrosion resistance, oxidation catalyst and ductility, Palladium has numerous commercial applications in catalytic converters and air purification equipments. Further, the noble metal is extensively used in jewellery, automobile, surgical instruments and electrical accessories industries. Continuous and ever increasing demand for the rare earth metals is emphasizing towards recovery and reuse of Pd(II) from spent sources such as used catalysts, industrial waste streams, etc., Usually Pd(II) recovery from spent catalysts is achieving through the dissolution of Pd(II) into acidic media and

recovering Pd(II) from leached solutions. In other words, it is very likely that Pd(II) recovery from several media involves cost competitive recovery from a liquid phase system that consists Pd(II) in a very dilute concentration with various Pd(II) species.

1.1.2 Technologies for Pd(II) recovery from waste streams

The recovery and reuse of Pd(II) from spent liquid phases is an interesting and challenging problem. Till date, numerous technologies such as membrane separation, ion exchange, electrochemical reduction, leaching, adsorption, chemical precipitation, biosorption, electro-kinetic process, magnetic nanoparticle based process, hydrothermal sulfidation floatation, foam fractionation, electrolysis and molecular recognition gel technology have been investigated for Pd(II) recovery and reuse from spent sources. Among various outlined techniques, very few methods qualify to address Pd(II) recovery from aqueous systems with very low solution concentrations (10–200 ppm). Also, few processes such as electrocoagulation generate metallic sludge as a by-product which needs further treatment (Volesky 2001). In addition, among these technologies, research commercialization for technology transfer is a further challenging task from the perspective of environmental sustainability, cost efficacy and recovery (Saniedanesh et al. 2013).

1.1.3 Prominence of adsorptive ion-exchange technologies

Among few competent technologies capable to address research commercialization avenues, chelating and ion-exchange resin based chemisorption/physisorption are highly relevant processes to recover noble metals with good metal recovery characteristics from aqueous systems with very low Pd(II) concentrations. Further, given their ease of production, lower cost and good separation technologies, compared to the synthetic cheating resins, biopolymers such

as chitosan have been suggested to be competitive (Niu and Volesky 2003). Compared to physisorption, chemisorption using chelating resins is promising given the fact that physisorption involves attraction of adsorbate Vander Waal's forces of attraction and chemisorption allows chemical bonding between metal and various prevalent functional groups in the chelating resins. Therefore, chemisorption facilitates better desorption characteristics by suitably deploying a reagent to recover Pd(II) from spent chelated resin to enhance Pd(II) reuse, minimal waste generation and better noble metal recovery. In this regard, despite offering good adsorption characteristics, commercial physisorbents such as activated carbon have been proven to be ineffective due to poor desorption characteristics (Rajesh 2014).

1.1.4 Overview of Pd(II) adsorption systems

Till date, several experimental investigations emphasized upon Pd(II) recovery from acidic (Ruiz et al. 2000, Guibal et al. 2001, Guibal et al. 2002, Chassary et al. 2005, Kanai et al. 2008, Butewicz et al. 2009, Zhou et al. 2009, Wang et al. 2010, Baba et al. 2011, Sopena et al. 2011, Pestov et al. 2012, Azarova et al. 2015, Yamashita et al. 2015, Bratskaya et al. 2016), aqueous (Fujiwara et al. 2007, Ramesh et al. 2008, Zhou et al. 2010, Sharififard et al. 2013) and chloride containing aqueous (Bratskaya et al. 2011) solutions. Among these, few articles focused upon the role of speciation in influencing adsorption characteristics. In these articles, it has been analyzed and inferred that for acidic media with lower pH (1–6), Pd(II) mostly exists as $PdCl^{+}$, $PdCl_2$, $PdCl^{3-}$ and $PdCl_4^{2-}$ species and in the higher pH range (6–12), Pd(II) exists in its hydroxide complex ($Pd(OH)_4^{2-}$) form (Hubicki 2009a, Hubicki 2009b). Thereupon, the researchers focused on the role of speciation to influence Pd(II) adsorption characteristics.

1.1.5 Adsorptive materials for Pd(II) recovery

Till date, wide varieties of chelating resins have been synthesized (Guibal et al. 2001, Guibal et al.2002, Baba et al. 2005). The specific functional groups that facilitate Pd(II) chemisorption have been identified to be nitrogen (e.g. in the form of N in amines, azo groups, amides and nitriles in resins such as Amberlyst A29, Amberlyst A21, Lewatit M-600, Purolite A-400TL, Glutaraldehyde cross-linked chitosan, L-lysine modified cross-linked chitosan, Chemically modified microalgal residue etc.), oxygen (e.g. carboxylic, hydroxyl, phenolic, ether, carbonyl and phosphoryl groups containing O in resins such as Melamine formaldehyde thiourea chelating resin, Activated carbon coated with chitosan, Thiourea modified chitosan microspheres etc.) and sulfur (e.g. S bound in thiols, thiocarbamates and thioethers groups in resins such as Duolite GT-73, Lewatit TP-214, XUS 43600.00, Thiourea derivative of chitosan, Rubeanic acid derivative of chitosan, 3-(((5-ethoxybenzenethiol)imino)methyl)-salicylic acid ligand etc.) functional groups (Pearson 1963, Zuo and Muhammed 1995, Bilba et al. 1998, Arrascue et al. 2003, Camel 2003, Atia et al. 2005, Donia et al. 2005).

The available literature in this area of research also indicates upon the need to develop new classes of bio-based materials for the recovery of noble metals from effluent streams. Among alternate biopolymers, chitosan, a partly acetylated glucosamine biopolymer is promising due to several features as non-toxicity, hydrophilicity, biodegradability, biocompatibility and antibacterial properties. While metal uptake is partly facilitated through few nitrogen functional groups in chitosan molecular structure, chitosan suffers with poor corrosion resistance in acidic media. Hence, suitable cross-linking agents and grafting procedures have been suggested. To further promote the application of cross-linked chitosan resin for Pd(II) adsorption, N and S containing functional groups can be introduced as chelating ligands. Other alternate resins for

Pd(II) recovery include melamine-formaldehyde thiourea resin, purolite, pyrogallal derived nano resin, etc., (Birinci et al. 2009, Wołowicz and Hubicki 2014, Nikoloski et al. 2015).

Deeper introspection into the above mentioned literature indicate that while information pertaining to resin chemistry is abundant, very little knowledge is available with respect to the promixity of the chelating resins for Pd(II) adsorptive recovery and reuse from complex adsorbate systems. Qualitative insights with respect to the chelating resin efficacy to foster Pd(II) adsorption can be obtained through the concept of hard and soft acids and bases (HSAB). According to the concept, precious metals such as Pt, Pd, Ag, Au and Hg are examples of soft acids and they form stronger bonds with soft bases such as functional groups containing S, O and N donor atoms (Pearson 1963). Further analysis conveys that the affinity of noble metal adsorption is as per the hierarchy S > N > O (Birinci et al. 2009). However, these insights are not adequate to serve as a competent tool for the comparative assessment of alternate synthetic and commercial resins for Pd(II) adsorption. This is due to the fact that while qualitative insights convey upon inherent Pd(II) adsorptive and desorptive mechanisms, they are not sufficient enough to provide insights into other issues such as toxicity of chemicals deployed for resin preparation, extent of S/O/N donor groups in the resin matrix and their contribution towards Pd(II) adsorptive and desorptive characteristics, complexity involved in resin fabrication, resin cost and resin efficacy to handle streams with diverse and complex chemical constituents. Further, systematic insights into the prevalent state-of-the-art will also be useful to streamline ongoing research activity towards commercial research and development.

1.1.6 Targeted perspectives

Thus, the major objective of the PhD thesis is to carry out a critical assessment of the available prior-art for developed and available Pd(II) adsorptive commercial and synthetic chelating resins. An objective oriented approach is targeted to analyze available literature in the following context:

a) Facilitate deeper insights into the chemistry of functional groups to correlate their functional role in influencing adsorption and desorption characteristics of alternate synthetic and commercial resins. Thereby, propose a road map towards identification and development of super-efficient resins (in terms of higher combinations of Pd(II) adsorption and desorption capacities) with relevant functional groups.
b) The role of adsorbate system solution chemistry in influencing sorption and desorption characteristics.

The above perspectives are anticipated to widen the scope of concurrent research pertaining to the development of cost effective, sustainable and non-toxic chelating resins for efficient Pd(II) recovery and reuse from waste streams characterized with complex combinations of chemical constituents.

1.2 Prior art

Based on the targeted research perspectives summarized in section 1.1.6, the available prior art in the field of Pd(II) adsorptive recovery and reuse from waste streams can be classified into the following themes:

a) Pd(II) speciation in acidic and chloride adsorbate systems.
b) Effect of pH variation and chloride concentration on Pd(II) uptake.

c) Relevance of functional groups chemistry on the Pd(II) uptake of synthetic and commercial resins.

d) Adsorption studies using commercial ion-exchange resins.

e) Pd(II) adsorption characteristics of chitosan and its derivatives.

f) Pd(II) adsorption characteristics of other chelating resins.

A brief overview of the available literature is presented in the following sub-sections.

1.2.1 Pd(II) speciation in acidic and chloride adsorbate systems

Pd(II) speciation primarily depends upon solution pH, chloride concentration, Pd(II) metal concentration and other metal ions and chemicals present in the solution. In the aqueous solution, Pd(II) exists in its most stable form. However, it can also form highly stable chloride, hydroxy-chloride and hydroxide complexes such as $PdCl^{+}$, $PdCl_2$, $PdCl_3^{-}$, $PdCl_4^{2-}$, $PdCl_3(OH)_2^{-}$, $PdCl_2(OH)_2^{2-}$, $PdCl(OH)_3^{2-}$ and $Pd(OH)_4^{2-}$ (Nachtigall et al. 1997, Pyrzynska and Trojanowicz 1999, Bernardis et al. 2005, Uheida et al. 2006, El-Safty et al. 2013). In the low pH range associated with acidic aqueous media and for higher concentrations of chlorides in aqueous systems, a significant proportion of the Pd(II) would exist in $PdCl_4^{2-}$ form. However, in the higher pH range associated with basic aqueous media, most Pd(II) forms hydroxy-chloride or hydroxide complexes (Dean 1999, Middlesworth and Wood 1999, Barakat et al. 2006). The following equations (Eqs. 1.1–1.8) summarize Pd(II) metal speciation with chloride and hydroxide ions (Ruiz et al. 2000, Hubicki and Wołowicz 2009):

$$Pd^{2+} + Cl^{-} \leftrightarrow PdCl^{+} \qquad (K=10^{4.47}) \qquad (1.1)$$

$$Pd^{2+} + 2Cl^{-} \leftrightarrow PdCl_2 \qquad (K=10^{7.76}) \qquad (1.2)$$

$$Pd^{2+} + 3Cl^{-} \leftrightarrow PdCl_3^{-} \qquad (K=10^{10.17}) \qquad (1.3)$$

$$Pd^{2+} + 4Cl^{-} \leftrightarrow PdCl_4^{2-} \quad (K=10^{11.54}) \quad (1.4)$$

$$Pd^{2+} + 2H_2O \leftrightarrow Pd(OH)^{+} + H_3O^{+} \quad (K=10^{-2.3}) \quad (1.5)$$

$$Pd^{2+} + 4H_2O \leftrightarrow Pd(OH)_2 + 2H_3O^{+} \quad (K=10^{-4.2}) \quad (1.6)$$

$$Pd^{2+} + 6H_2O \leftrightarrow Pd(OH)_3^{-} + 3H_3O^{+} \quad (K=10^{-12}) \quad (1.7)$$

$$Pd^{2+} + 8H_2O \leftrightarrow Pd(OH)_4^{2-} + 4H_3O^{+} \quad (K=10^{-14}) \quad (1.8)$$

In the above equations, palladium-hydroxide species have been indicated to have formed due to hydration in which the initial hydration shell is highly stable and strongly bounded and thereby leads to the formation of more complex species such as $Pd(H_2O)_4^{2+}$ or $PdCl_3(H_2O)^{-}$.

1.2.2 Effect of pH and chloride concentration variation on Pd(II) uptake

For an ion-exchange resin, the Pd(II) adsorption capacity is primarily dependent on the ionic charge of functional groups in the adsorbent, solution pH, acid/base used for pH adjustment and metal speciation. The metal speciation needs to consider ionic charge and ability to get hydrolyzed to form polynuclear species (Ruiz et al. 2000).

For various aqueous media based adsorbate systems, solution pH is usually altered and adjusted using either of HCl, H_2SO_4, HNO_3, NaOH and NH_4OH. In several conducted works, pH variation was brought forward through either HCl or NaOH and the effect of acid and base concentration has been evaluated on the Pd(II) adsorption characteristics. For the case in which HCl has been deployed for pH adjustment in the lower range, Pd(II) chloro-anioinc species form and their adsorption onto the protonated or activated functional groups is more favourable. However, for the case of H_2SO_4, due to non-existence of chloride ions, absorbable species are very likely to not form in the similar pH range (Chassary et al. 2005). For high HCl solution

concentrations, excess chloride ions induce strong competition and limit recovery of pertinent species in abundance ($PdCl_4^{2-}$). On the other hand, for higher pH, protonated amino groups get neutralized and hence ionic interaction reduces significantly (Guibal 2004) to detriment Pd(II) adsorption.

The effect of HCl and H_2SO_4 on Pd(II) adsorption using glutaraldehyde cross-linked chitosan resin was investigated by a research group (Ruiz et al. 2000). The authors inferred that for sulfuric acid based pH variation (for a pH of 2), Pd(II) was prevalent in the form of hydroxide and cationic (Pd^{2+} and $PdCl^{+}$) species. For such a case, metal species are favourable towards electrostatic interactions and sorption may occur due to ion exchange with protons adsorbed on amino sites. For HCl containing aqueous media at a pH of 2 and Cl^- concentration of 0.01 M, anionic species represented 75% of total Pd(II) species prevalent in the system. Due to favourable adsorption of these species onto chitosan, enhanced Pd(II) adsorption is expected in such media. For aqueous media containing higher Cl^- concentrations, $PdCl_4^{2-}$ species are in abundance and the species facilitate faster transport of Pd(II) species onto the ion-exchange resins. However, at even higher concentrations, the uptake capacity gets reduced (Hubicki and Wołowicz 2009).

In addition to the functionalization of the adsorbent, solution chemistry issues such as solution composition, pH and nature of constituents play a key role in governing the metal adsorption and desorption processes. Till date, most researchers focused on Pd(II) adsorption from aqueous solutions, where the solution pH is usually below neutral pH. Under these conditions, Pd(II) exists as Pd(II)-chloro complex. For such cases, Pd(II) complex interacts with protonated amine and other relevant functional groups to translate into effective Pd(II) adsorption (Birinci et al. 2009, Sharififard et al. 2013).

1.2.3 Functional groups chemistry associated to Pd(II) uptake of synthetic and commercial resins

The prevalent functional groups in the adsorbent profoundly contribute towards the noble metal adsorption process. As summarized in the introduction section of the thesis, functional groups containing S, N and O donor atoms facilitate effective Pd(II) adsorption. In this section, the associated mechanisms of various adsorbents containing O, S and N donor groups has been presented to cater towards effective Pd(II) adsorption from aqueous media systems.

Till date, several commercial and synthesized resins have been reported to serve as adsorbents to recover Pd(II) from aqueous waste media. Among these, very few articles focused towards pertinent adsorption mechanisms. Further, literature emphasis towards elaboration of desorption mechanism has been scanty.

For Pd(II) adsorption, two types of mechanisms have been proposed. The first mechanism involves ionic interaction between chloro-palladium complex and protonated amines and the second refers to chelation or co-ordination. Pd(II) adsorption can occur due to either mechanisms or both. The following equations (Eqs. 1.9–1.12) summarize these mechanisms (Ruiz et al. 2000, Ramesh et al. 2008, Birinci et al. 2009, Hubicki and Wołowicz 2009, Zhou, Xu et al. 2010, Wołowicz and Hubicki 2011, Wołowicz and Hubicki 2012, Awual et al. 2013, Wołowicz and Hubicki 2014, Zhou et al. 2015):

Ionic interaction:

$$(R_1R_2)NH + HCl_{(aq.)} \leftrightarrow (R_1R_2)NH_2^+Cl^-_{(sorb.)} \quad (1.9)$$

$$2(R_1R_2)NH_2^+Cl^-_{(sorb.)} + [PdCl_4]^{2-}_{(aq.)} \leftrightarrow [(R_1R_2)NH_2^+]_2[PdCl_4]^{2-}_{(sorb.)} + 2Cl^-_{(aq.)} \quad (1.10)$$

Chelation:

$$(R_1R_2)NH_2^+Cl^-_{(sorb.)} + [PdCl_4]^{2-}_{(aq.)} \leftrightarrow [(R_1R_2)NH][PdCl_3]^-_{(sorb.)} + H^+_{(aq.)} + 2Cl^-_{(aq.)} \quad (1.11)$$

$$(R_1R_2)C = S + [PdCl_4]^{2-}_{(aq.)} \leftrightarrow [(R_1R_2)C = S][PdCl_3]^{-}_{(sorb.)} + Cl^{-}_{(aq.)} \quad (1.12)$$

In the above equations, it is important to note that in the pH range of 1-6, $PdCl_4^{2-}$ groups predominate and hence the ionic interaction is expected to be significant for higher proton concentration. However, for high pH (eq. 1.11), chelation is highly favoured. Therefore, by varying the solution pH, ionic interaction can be preferably sought and this is considered to be the most relevant approach for resin regeneration.

For alternate resins possessing various amine groups, relevant mechanisms have been proposed by a research group (Wołowicz and Hubicki 2011). Among these, with the same functional group, three resins correspond to strong basic anion exchange resins namely amberlyst A26, amberlite IRA958 and amberlite IRA458 resins. These resins consist of quaternary ammonium, type-1 functional group ($-N^+(CH_3)_3$). Alternatively, the authors also considered lewatit M600 that contains quaternary ammonium type-2 functional group ($-N_2(CH_3)_2C_2H_4OH$). Compared to type-2 resins, type-1 resins have marginally higher basicity. Irrespective of the ionic form and pH, type 1 resins get dissociated completely. However, type-2 resins do exist independent of the protonation process in terms of their dissociation. The following equations (eq. 1.13–1.14) depict the electrostatic interaction of the functional groups with Pd(II) anionic complex at pertinent pH:

Electrostatic interaction for type-1 resin:

$$2R - CH_2 - N^+(CH_3)_3Cl^- + [PdCl_4]^{2-} \leftrightarrow [R - CH_2 - N^+(CH_3)_3]_2[PdCl_4]^{2-} + 2Cl^- \quad (1.13)$$

Electrostatic interaction for type-2 resin:

$$2R - CH_2 - N^+(CH_3)_2C_2H_4OHCl^- + [PdCl_4]^{2-} \leftrightarrow [R - CH_2 - N^+(CH_3)_2C_2H_4OH]_2[PdCl_4]^{2-} + 2Cl^- \quad (1.14)$$

The research group of Wolowicz also studied lewatit SR7 (containing quaternary ammonium functional group) and purolite A-400TL (containing quaternary ammmounium, type 1 ($-N^+(CH_3)_3$) functional group) resins (Wołowicz and Hubicki 2012, Wołowicz and Hubicki

2014). For the Pd(II)-chloride anionic complex, relevant functional group interactions for lewatit SR-7 have been presented in the following equations (eq. 1.15):

$$2R - CH_2 - N^+(C_3H_7)_3Cl^- + [PdCl_4]^{2-} \leftrightarrow [R - CH_2 - N^+(C_3H_7)_3]_2[PdCl_4]^{2-} + 2Cl^- \quad (1.15)$$

For purolite A-400TL, relevant functional group interactions have been depicted in Fig. 1.1. In the figure, it can be seen that the Pd-chloride anionic complex gets attached to the amine group through the replacement of chloride ions in the adsorbent. Hence, in the presented mechanism, Cl^- ionic concentration has a significant role and at higher concentration of Cl^-, $PdCl_4^{-2}$ formation is high for the constant pH case. Therefore, for an enhancement in Cl^- concentration from 0.1 to 1 M at a pH of 1, the $PdCl_4^{-2}$ concentration increased from 96.95-99.73%. In other words, trade-off exists with respect to Cl^- concentration in the said complexation reaction.

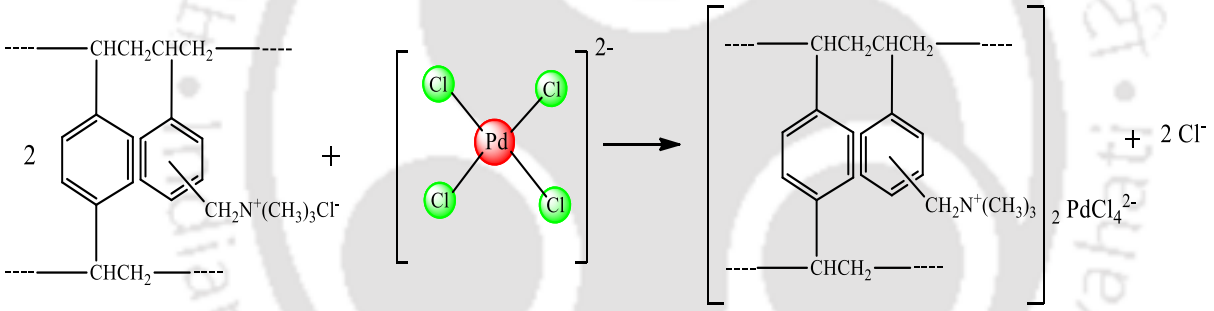

Fig. 1.1: Mechanism of Pd(II) adsorption onto Purolite A-400TL resin (Wołowicz and Hubicki 2014).

Hubicki et al., (2009) considered duolite GT73 and lewatit TP214 resins that possessed thiourea functional groups in the adsorbents to recover Pd(II) from aqueous media. The authors discussed both adsorption and elution mechanisms. The authors inferred that high Cl^- concentrations favour higher availability of $PdCl_4^{-2}$ species that enable faster transport of the species onto the ion-exchange resins. Hence, under these circumstances, Pd(II) uptake would be higher. However, at even higher Cl^- concentrations, the uptake would reduce significantly. The proposed mechanism based on the investigations of the authors can be summarized as in Fig. 1.2.

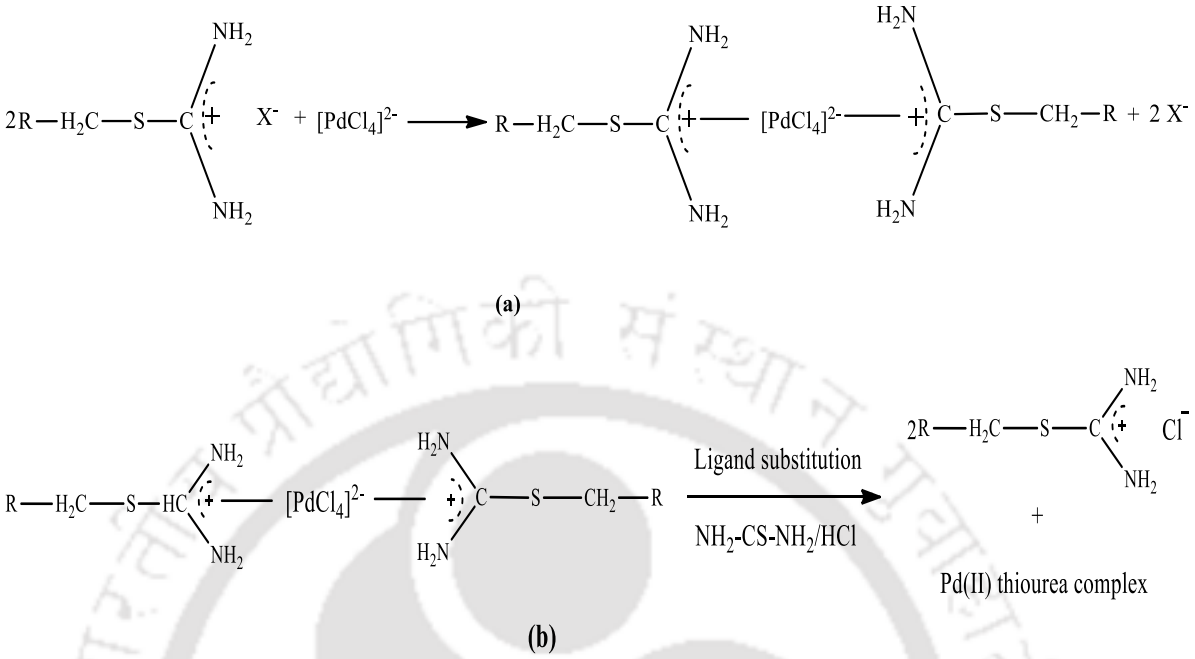

Fig. 1.2: (a) Adsorption and (b) Elution mechanisms with Lewatit TP214 resin.

The demonstrated mechanisms can be explained as follows. For the case of Pd(II) adsorption onto Lewatit TP214, the anion complex of $[PdCl_4]^{2-}$ binds to the acid conjugate form or thioureanium form of the resin through the anion exchange mechanism (Fig. 1.2a). For the case of elution of the same complex, the neutral thiourea ligands form positively charged Pd(II) complex (Fig. 1.2b). For the case of Duolite GT73 adsorbent, a charge transfer complex is formed between the ion exchanger matrix and the non-dissociated acid (H_2PdCl_4). For model chloride solution systems, the maximum Pd(II) ion-exchange capacities have been evaluated as 171.9-205.6 and 19.5-35.46 mg g^{-1} for both Lewatit TP214 and duolite GT73, respectively. These values respectively varied from 285.45-306.7 and 21.27-31.9 mg g^{-1} for chloride-nitrate solution systems. For both resins, desorption efficiencies lower than 99% have been obtained. Similar works have been reported by the authors for other resins such as purolite S920 and chelite S. From such investigations, their research group reported optimality of noble metal

uptake to follow the order: Lewatit TP214>Purolite S920>Chelite S>Duolite GT73 (Hubicki and Wołowicz 2009). Another research group reported the relevance of thioureanium functional group containing resin (XUS 43600) and reported adsorption and desorption capacities of 221.3 mg g^{-1} and 99.5%, respectively (Nikoloski et al. 2015).

A conjugate adsorbent was prepared by immobilizing 3-(((5-ethoxybenzenethiol)imino)methyl)-salicylic acid ligand (EBMS) by Awual et al., (2013). Pd(II) adsorption mechanism in the presence of thiourea has been depicted as shown in Fig. 1.3:

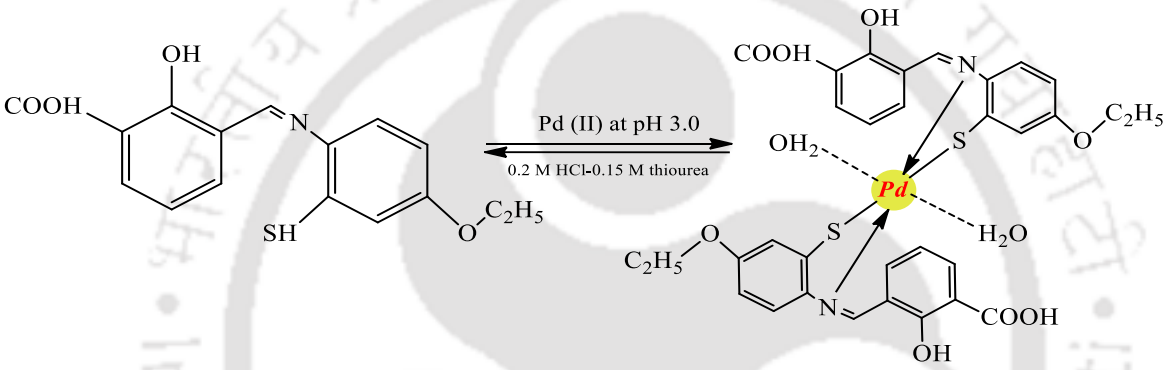

Fig. 1.3: Structure of EBMS ligand (reactant) and conceivable complexation mechanism of Pd(II) and EBMS (product).

For the adsorbent, maximum Pd(II) adsorption capacity was obtained as 164.2 mg g^{-1}. For 0.2 M HCl-0.15 M thiourea eluent system, the conjugate adsorbent provided a desorption efficiency of 98.72% (Awual et al. 2013). Resins with similar functional group interactions have been reported in the literature based on rubeanic acid derivative of chitosan and thiourea derivative of chitosan for Pd(II) removal (Guibal et al. 2002). For these resins, the authors reported a noble metal uptake of 352 and 277.5 mg g^{-1}, respectively. Similarly, another research group prepared amine and sulfur containing functional groups in a resin fabricated with polyacrylonitrile solvent. The resin exhibited Pd(II) adsorption capacity and removal of 14.93 mg g^{-1} and 93%, respectively (Morcali and Zeytuncu 2015).

1.2.4 Adsorption and desorption studies using commercial ion-exchange resins

In this section, a brief overview of various adsorption studies conducted till date with respect to the recovery and reuse of Pd(II) using commercial ion-exchange resins has been presented.

The effect of Zn(II) and Cu(II) ions in due course of Pd(II) adsorption onto Lewatit TP214 macroporous chelating commercial resin was investigated by Labosova et al., (2006). The authors inferred that the cations do not detriment or complement Pd(II) uptake characteristics for the chosen resin (Labosova et al. 2006). Using variant compositions of model chloride and chloride-nitrate solutions, Hubicki et al., (2009) carried out Pd(II) adsorption studies using S-donor atoms containing ion-exchange resins such as Duolite GT73 (cationic ion-exchange resin with thiol functional group) and Lewatit TP214 (chelating ion-exchange resin with thiourea functional group). Among the chosen resins, Lewatit TP214 exhibited better Pd(II) adsorption characteristics than Duolite GT73 (Hubicki and Wołowicz 2009).

In another investigation, the research group studied other resins namely (Amberlyst A21, a weakly basic resin) and Amberlyst A29 (a strongly basic resin) for Pd(II) adsorption from HCl-NaCl containing solutions. Among these resins, Amberlyst A21 possessed a dimethylamine group ($-N(CH_3)_2$) on a polystyrene skeleton and Amberlyst A29 comprised of a dimethyl-hydroxyethyl-quaternary amine group ($-N^+(CH_3)_2C_2H_4OH$) on a styrene-divinylbenzene skeleton. The authors found that Amberlyst A21 was more promising to adsorb Pd(II) chloro-complexes from acidic chloride solutions than Amberlyst A29 (Hubicki and Wołowicz 2009).

Liu et al., (2009) carried out detailed studies for the evolution of adsorption characteristics of Ag(I), Au(III), Pd(II) and Pt(IV) metal ions with 717 strongly basic anion-exchange resin. The authors observed that complete elution was not possible for all cases after adsorption process

reached saturation. It was further claimed that during adsorption process, the oxidation state of the metal ions is very likely to reduce them to their metallic form (Peng et al. 2009).

The research group of Hubicki furthered research towards Pd(II) adsorption characteristics of strongly basic anion exchange (SBA) resins, namely macroporous Amberlyst A26 resin, styrene–divinylbenzene functional group containing LewatitM600 resin with gel structure, macroporous Amberlite IRA958 resin, acrylic Amberlite IRA458 gel resins. Characteristic functional groups prevalent in the resins refer to $-N^{+}(CH_3)_3$ and $–N_2(CH_3)_2C_2H_4OH$ groups. Among the resins, Lewatit M600 resin exhibited better Pd(II) adsorption characteristics (Wołowicz and Hubicki 2011). Similar investigations were conducted for the evaluation of adsorption characteristics of Pd(II), Pt(IV), Ag(III), Cu(II), Co(II), Ni(II) and Zn(II) from acidic solutions using Lewatit Monoplus TP220 adsorbent by the research group of Hubicki. The authors inferred that for an increase in the Pd(II) concentration from 100 to 1000 mg L^{-1}, the equilibrium adsorption capacity enhanced from 10 to 99.95 mg g^{-1} (Wołowicz and Hubicki 2012).

In another investigation, the research group inferred that the inclusion of HCl, HNO_3 and $AlCl_3$ in the Pd(II) adsorbate system had a detrimental influence on the Pd(II) uptake for commercial mono-disperse Lewatit SR7 resin (Wołowicz and Hubicki 2012). For Purolite A-400TL resin (strongly basic anionic exchange resin) that was deployed for adsorption studies with noble metals such as Pd(II), Pt(IV) and Au(III), the maximum sorption capacity was 404.15 mg g^{-1} (Wołowicz and Hubicki 2014).

Another investigation targeted the recovery of Pt(IV) and Rh(III) using Lewatit Mono Plus (M+) MP-600 (with quaternary ammonium functional group), Purolite S985 (with polyamine functional group) and XUS 43600.00 (with thioureanium functional group) from chloride

solutions. For the chosen resins, XUS 43600.00 exhibited highest metal uptake for Pd(II) and Pt(IV).

Table 1.1 summarizes relevant data associated to the Pd(II) adsorption and desorption characteristics of commercial adsorbents.

1.2.5 Pd(II) adsorption and desorption characteristics of chitosan and its derivatives

Few research groups targeted the effectiveness of chitosan and chitosan coated activated charcoal adsorbents for the removal and recovery of Pd(II) and Pt(IV) from aqueous solutions. Among these, while both adsorbents exhibited promising affinity towards Pd(II) than Pt(IV), and chitosan provided good adsorption capacities than activated charcoal coated with chitosan (Sharififard et al. 2013). For L-lysine modified cross-linked resin (LMCCCR), other researchers indicated that among Au(III), Pt(IV) and Pd(II), Pt(IV) and Pd(II) uptake was significant for aqueous adsorbate systems (Fujiwara et al. 2007). Another investigation reported upon the superior performance of glycine modified cross-linked resin (GMCCR) for Pt(IV) and Pd(II) removal but not Au(III) from aqueous solutions (Ramesh, Hasegawa et al. 2008). Zhou et al., (2009) investigated adsorption characteristics of Pt(IV) and Pd(II) onto thiourea modified chitosan microspheres (TCS) (Zhou et al. 2009). Ethylenediamine-adjusted magnetic chitosan nanoparticles (EMCN) were used for the removal of Pt(IV) and Pd(II) from aqueous solutions. EMCN was synthesized through NaOH assisted precipitation in water-in-oil micro-emulsion system. For the EMCN, among Pd(II) and Pt(IV), Pt(IV) uptake efficiency was higher. The total sorption capacity was comparable to that of each metal individually. This indicates that the metals compete to get adsorbed onto the same sorption sites (Zhou et al. 2010).

The removal of Pd(II) using glutaraldehyde cross-linked chitosan derivatives was carried out by Ruiz et al., (2000). The authors targeted the role of acid deployed to control solution pH in the

presence of other competitor anions. The authors observed that compared to HCl, H_2SO_4 was unfavourable (Ruiz et al. 2000). Other researchers targeted sulfur groups (in thiourea and rubeanic acid compounds) grafted chitosan derivatives for Pd(II) removal and inferred that the rubeanic acid derivative of chitosan was efficient for Pd(II) uptake from dilute solutions (Guibal et al. 2002). Ding et al., (2006) investigated the adsorption properties of two types of diaza-crown ether cross-linked chitosan resins for Pd(II) and Ag(I) recovery. The authors produced diaza-crown ether chitosan (CTSDC) through grafting of N, N'-diallyldibenzo 18-crown-6 crown ether with chitosan. On the other hand, the alternative diaza-crown ether cross-linked chitosan (CCTSDC) was prepared through crosslinking of CTSDC and epichlorohydrine. For both Pd(II) and Ag(I) cases, CCTSDC outperformed CTSDC in terms of Pd(II) uptake (Ding et al. 2006).

Alternatively, persimmon tannin chitosan derivative (PTCS) was targeted for the Pd(II) adsorption and was inferred to possess a maximum adsorption capacity of 330 mg g^{-1}(Zhou et al. 2015). The Pd(II) adsorption capacity of ion-imprinted chitosan and extremely acidic solution system was investigated by Lin et al., (2015). The authors concluded that the highest metal uptake was about 324.6-326.4 mg g^{-1} (Lin et al. 2015).

Adopting ion-imprinting technique, Monier et al., (2016) prepared 2-aminobenzaldehyde modified chitosan Schiff's base (Pd-CAZ) resin for selective chelation of Pd(II). The authors evaluated thermodynamic, kinetic and isotherm parameters associated to Pd(II) adsorption onto Pd-CAZ and non-imprinted CAZ (NI-CAZ) resins. The authors reported maximum Pd(II) adsorption capacities of 275 and 114 mg g^{-1} for Pd-CAZ and NI-CAZ, respectively. Further, the resin regeneration and recovery experiments affirmed that 96% of the resin could be restored even after fifth adsorption-desorption cycle and hence highly promising performance.

Table 1.2 presents a summary of pertinent functional groups, adsorption and desorption capacities along with optimized experimental conditions for various chitosan based synthesized adsorbents.

The adsorption characteristics of competent chitosan based derivatives investigated for heavy metal adsorption would be worth consideration in the near future, given the fact that Pd(II) adsorption characteristics of such resins have not been studied on these till date. Hence, few resins have been identified and the available prior art has been presented in the following paragraphs:

Liao et al., investigated the triethylenetetramine derivative of chitosan for its ability to recovery Ni(II) from aqueous solutions. The authors reported performance efficiency of the resin under acidic conditions and indicated optimal adsorption capacity at about 4.5 pH. The maximum Ni(II) adsorption capacity of chitosan and chitosan derivatives have been evaluated to be 58.09 and 91.44 mg g^{-1}, respectively (Liao et al. 2016).

Wu et al., synthesized magnetic chitosan modified with melamine and evaluated its adsorption capacity for Cu(II) in aqueous solutions. The authors summarized a maximum Cu(II) adsorption capacity of 2.58 mmol g^{-1} for an optimal process parameter set of 5.5 pH, 25 min adsorption time and 5.0 mmol L^{-1} initial Pd(II) concentration (Wu et al. 2015).

Li et al., synthesized thiosemicarbazide modified chitosan (TCS) to recover Pb(II) and Cd(II) from aqueous solutions. The authors reported their adsorption capacities to be 325.2 and 257.2 mg g^{-1} for Pb(II) and Cd(II) respectively (Li et al. 2016).

Elwakeel et al., prepared 3-amino-1,2,4 triazole,5-thiol and melamine grafted chitosan derivatives for the removal of Reactive Black 5 from aqueous solutions. At an optimal pH of 3 and at 25 ^{o}C, the maximum adsorption capacities of the resins have been reported as 0.492 and

0.330 mmol g^{-1} for 3-amino-1,2,4 triazole,5-thiol and melamine grafted chitosan derivatives, respectively (Elwakeel et al. 2016).

Recently, our research group carried out experimental investigations that targeted Pd(II) removal and recovery from synthetic ELP solutions using glutaraldehyde cross-linked chitosan derivative (Nagireddi et al. 2017) and commercial Lewatit TP214 ion-exchange resin (Nagireddi et al. 2018). Optimal batch adsorption process parameters were 8 pH, 300 min contact time for both resins and 0.6 and 2 g L^{-1}adsorbent dosage for glutaraldehyde cross-linked chitosan and Lewatit TP214 ion-exchange resin respectively. Corresponding maximum adsorption capacity and desorption efficiency of the resins has been evaluated as 166.67 and 172.41 mg g^{-1} and 42.35 and 66.95 %, respectively. Based on these studies, Lewatit TP 214 anion exchange resin can be inferred to provide excellent Pd(II) removal and reuse characteristics from synthetic electroless plating solutions.

1.2.6 Pd(II) adsorption and desorption characteristics of other chelating resins

Facilitating the modification of poly(vinylbenzylchloride–acrylonitryle–divinylbenzene) matrix with ethylenediamine, bis(aminopropyl)amine, bis(aminohexyl)triamine or tris(2-aminoethyl)amine, Jermakowicz et al., (2005) prepared a resin towards sorption of platinum ions in the presence of other cations in an aqueous media. The authors inferred that in the presence of Cu(II), Ni(II) and Fe(III) complexes, the resin exhibited higher adsorption capacity for Au(III), Pt(IV) and Pd(II) chloro-complexes (Jermakowicz et al. 2005).

In the presence of Cu(II) and Zn(II) base metal ions, Birinci et al., (2009) investigated Pd(II) removal using melamine–formaldehyde–thiourea (MFT) resin. The resin exhibited a preferential sorption of Pd(II) from the multi-metal system and is hence promising (Birinci et al. 2009).

Using chemically modified microalgal residue prepared by immobilizing the functional groups of polyethyleneimine onto microalgae waste, a research group targeted Pd(II) and Pt(IV) removal from acidic solutions. For the chosen system, highest metal uptake was obtained at 0.1 M HCl (2.01 and 0.80 mmol g^{-1} for Pd(II) and Pt (IV), respectively) (Sayın et al. 2015).

The efficacy of ligand modified conjugate adsorbent prepared through immobilization of 3-(((5-ethoxybenzenethiol)imino)methyl)-salicylic acid onto meosoporous silica monolith carriers was investigated by a research group for Pd(II) adsorption. The adsorption process followed Langmuir isotherm with maximum adsorption capacity of 164.20 mg g^{-1} (Awual et al. 2013).

Deploying fire assay leaching solutions, Morcali et al., (2015) evaluated adsorptive and desorptive characteristics of Pd(II) onto glutaraldehyde cross-linked with polyacrylonitrile modified thiourea. For an optimal set of process parameters (1.5 pH, 360 min contact time, 5 g L^{-1} adsorbent dosage), the optimal metal uptake was 14.93 mg g^{-1} (Morcali and Zeytuncu 2015).

Pd(II) adsorption onto 1,3,5-Triazine-pentaethylenehexamine polymer (synthesized using cyanuric chloride and pentaethylenehexamine) was investigated from chloride aqueous systems. The adsorbent exhibited an optimal Pd(II) intake for 2 pH, 36 h contact time, 3.33 g L^{-1} dosage and pCl of 1. The optimal adsorption capacity was about 50% of the adsorbent quantity deployed for the work (Sayın et al. 2015).

For Pd(II) recovery from waste water samples, Md. RabiulAwual et al., (2015) prepared four adsorbents namely (3-(3-(methoxycarbonyl)benzylidene)hydrazinyl)benzoic acid, 5-tert-butyl-2-hydroxybenzaldehyde thiosemicarbazone, N,N'(octane-1,8-diylidene)di(2-hydroxy-3,5-dimethylaniline) immobilized mesoporous silica derivatives and fine-tuned functionalized mesoporous adsorbent. Corresponding adsorption capacities had been reported to be 184.50,

171.65, 213.67 and 191.35 mg g^{-1}, respectively. Using HCl-thiourea eluent system, all four adsorbents exhibited above 95% desorption efficiencies.

Mildan et al., (2015) considered poly(m-aminobenzoic acid) chelating polymer for the Pd(II) adsorption study. The authors inferred that for an optimal pH of 2, the adsorbent capacity was 24.21 mg g^{-1}. Sharma et al., (2016) synthesized Aliquat-336 (ionic liquid) impregnated SBA-15 mesoporous silica for Pd(II) adsorption. The authors reported that the adsorption followed Langmuir isotherm with an adsorption capacity of 212.76 mg g^{-1}. Chia-HsinYen et al., (2017) prepared magnetic nanoparticles that were modified with third-generation dendrimers (MNP-G3) and ethylenediaminetetraacetic acid modified MNP-G3 for the recovery of precious metals from aqueous media. The adsorbents indicated fitness towards Langmuir isotherm model with maximum adsorption capacity of 3.60, 3.58, 2.75 and 2.84 mg g^{-1} for Pd(IV), Au(III), Pd(II) and Ag(I), respectively. Further, MNP-G3 exhibited good regeneration capability as it sustained upto 6 cycles with 90-95% desorption efficiencies.

Using poly(glycidyl methacrylate) modified with 8-aminoquinoline derivative (AQ-PGMA), Zhang et al., (2018) reported the optimal Pd(II) adsorption capacity of 267.9 mg g^{-1} for HCl solution concentrations higher than 0.4 mol L^{-1}. Wojnicki et al., (2018) studied Pd(II) chloride complex adsorption onto activated carbon adsorbent. The authors obtained maximum sorption capacity of 42.4 and 67 mg g^{-1} at 294 and 323 K. Desorption studies were conducted using a solution of HCl and perchlorate acid and for a maximum period of 10 months, which indicated maximum desorption of 50-65% Pd(II) from the surface of the adsorbent.

A novel mesoporous polymer composite C7-BTBP/XAD-7 was prepared through the impregnation of polymeric XAD-7 carrier with 6,6'-bis(5,6-diheptyl-1,2,4-triazin-3-yl)-2,2'-bipyridine (C7-BTBP). The adsorbent was evaluated for Pd(II) in HNO_3 solution consisting of

several other metals. For 3.0 M HNO_3 solution, the adsorbent was inferred to provide best performance in terms of higher stability, strong adsorption affinity, high selectivity, and fast adsorption rate with a maximum Pd(II) adsorption capacity of 43.85 mg g^{-1} (Lu et al. 2018).

The efficacy of imidazoline functionalized nanosilica adsorbent to recover Pd(II) from aqueous solution was investigated by Bing Zhang et al., (2018). For an optimal pH of 4, the Pd(II) adsorptive and desorptive (thiourea-HCl system) efficiencies had been obtained as 69.6 mg g^{-1} and 87%, respectively.

For effective Pd(II) sorption from acidic solutions, the synthesis of glutaraldehyde cross-linked polyethylenimine (PEI) on algal beads (ABA/PEI) and PEI cross-linked alginate/algal mixture−glutaraldehyde beads (HABA/PEI) was targeted by Wang et al., (2019). Among these resins, HABA/PEI beads exhibited the highest Pd(II) uptake (158.57 mg g^{-1}) than ABA/PEI (120.25 mg g^{-1}) beads. Desorption studies affirmed similar performance (84.1%) using HCl-thiourea eluent.

A series of polyurethane foam (PUF) composites were prepared by Xue et al., (2019) using PUF matrix for Pd(II) recovery from acidic chloride solutions. The maximum Pd(II) uptake of the PUF matrix adsorbent was 784.5 mg g^{-1}. Using thiourea-HCl eluent system, the adsorbent exhibited 98% desorption efficiency at 80 ^{o}C.

Table 1.3 summarizes the adsorption and desorption characteristics and corresponding optimal process parameter values for all other resins investigated till date.

Table 1.1: Pd(II) adsorption and desorption characteristics of commercial resins reported in the literature.

Adsorbent Name	Metal ions	pH	Functional group	Metal ion concentration (mg L^{-1})	Adsorption capacity (mg g^{-1})	Desorption (%)	Reference
Duolite GT-73	Pd(II)	0-7	Thiol	195	19.5-35.46 21.27-31.9	>99	Hubicki and Wołowicz 2009
Lewatit TP-214		0-14	Thiourea		171.9-205.6 285.45-306.7		
Amberlyst A29	Pd(II)	0-8	Dimethylamine	100	0.023-0.006	-	Hubicki and Wołowicz 2009
Amberlyst A21			Quaternary amine		0.029-0.012		
717 anion-exchange resin	Ag(I), Au(III), Pd(II), Pt(IV)	3	-	5	701.5 g	-	Peng et al. 2009
Lewatit M-600	Pd(II)	0-11	Quaternary ammonium, type-2	100	0.0255	-	Wołowicz and Hubicki 2011
Amberlyst A26		0-14	Quaternary ammonium, type-2		0.023		
Amberlite IRA-458					0.006		
Amberlite IRA-958					0.004		
Lewatit MonoPlus TP-220	Pd(II), Pt(IV), Ag(III), Cu(II), Co(II), Ni(II), Zn(II),	-	Bis-picolylamine	100-1000	10-99.95	-	Wołowicz and Hubicki 2012
Purolite A-400TL	Pd(II), Pt(IV), Au(III)	0-14	$-N^{+}(CH_3)_3$ (type1)	100-1000	404.15	-	Wołowicz and Hubicki 2014
Lewatit MonoPlus (M^{+}) MP-600	Pd(II), Pt(IV), Rh(III)	0-14	Quaternary ammonium	23.0	342.18	91.4	Nikoloski et al. 2015
Purolite S985			Polyamine	25.3	236.	93.0	
XUS 43600.00		0-7	Thiouranium	13.26	221.	>99.5	

Table 1.2: Pd(II) adsorption and desorption characteristics of chitosan based synthesized resins reported in the literature.

Adsorbent Name	Metal ions	pH	Surface area ($m^2 g^{-1}$)	Functional group	Metal ion concentration ($mg L^{-1}$)	Adsorption capacity ($mg g^{-1}$)	Desorption (%)	Reference
Glutaraldehyde cross-linked chitosan	Pd(II)	2	-	Amine	400	180	-	Ruiz et al. 2000
Glutaraldehyde cross-linked chitosan				Amine		287.4		
Rubeanic acid derivative of chitosan	Pd(II)	2	-	Amine and Thiol	50	352.0	-	Guibal et al. 2001
Thiourea derivative of chitosan				Amine and Thiourea		277.5		
Diaza Crown ether cross-linked chitosan	Pd(II)	4	-	Amine group	30	248.1	-	(Ding, Zhang et al. 2006)
	Au(III)					215.4		
Diaza Crown ether chitosan	Pd(II)					157.8		
	Au(III)					85.1		
L-lysine modified cross-linked chitosan	Pd(III)	2	82.4	Primary amine	400	109.47	99.98	Fujiwara et al. 2007
	Pt(IV)	1				129.26	98.66	
	Au(III)	2				70.34	99.86	
Glycine modified cross-linked chitosan	Au(III)	2	121.62	Amide	500	169.98	99.94	Ramesh et al. 2008
	Pt(IV)					122.47	99.12	
	Pd(II)					120.39	98.27	
Thiourea modified chitosan microspheres	Pt(IV)	2	95.6	$-NH_2$, -OH	400	129.9	97	Zhou et al. 2009
	Pd(II)					112.4		
Ethylenediamine modified magnetic chitosan nanoparticles	Pt(IV)	2	-	NH, υCN	60	171	97.3	Zhou et al. 2010
	Pd(II)					138	90. 5	
Chitosan	Pd(II)	2	16.37	N-H	300	62.5	-	Sharififard et al. 2013
	Pt(IV)					66.6		
Activated carbon coated with chitosan	Pd(II)		362.3	N-H, C=O, C-O		43.48		
	Pt(IV)					52.63		
Ion-imprinted chitosan fiber	Pd(II)	1	-	Primary amines	800	326.4	20.82	Lin et al. 2015
Non-imprinted fibers						313.7	9.87	
Grafted chitosan on persimmon tannin extract	Pd(II)	5	-	N-H -NH	1000	315	-	Zhou et al. 2015
2-aminobenzaldehyde modified chitosan	Pd(II)	5	4.254	$-NH_2$	50-500	275	96	Monier et al., 2016

Table 1.3: Pd(II) adsorption and desorption characteristics of other synthesized resins reported in the literature.

Adsorbent Name	Metal ions	pH	Surface area (m^2 g^{-1})	Functional group	Metal ion concentration (mg L^{-1})	Adsorption capacity (mg g^{-1})	Desorption (%)	Reference
Vinyl(benzyl chloride-acrylonitryle-divinylbenzene)	Au(III) Pt(IV) Pd(II)	-	-	Amino	47.27 46.8 42.55	190 245 280	5	Jermakowicz et al. 2005
Melamine formaldehyde thiourea chelating resin	Pd(II)	4	-	NH_2, -OH	100	15.29	-	Birinci et al. 2009
Chemically modified microalgal residue	Pd(II) Pt(IV)	0.1 mol/L HCl	-	N-H, amine	10	354.6 156.5	96 95	Khunathai et al. 2013
3-(((5-ethoxybenzenethiol)imino)methyl)-salicylic acid ligand	Pd(II)	3	675.62	Imino and Thiol	60	164.3	98.7	Awual et al. 2013
Modified polyacrylonitrile based adsorbent	Pt(IV) Pd(II)	1.5	-	C=S N-H C-N C=N	26.63 42.59	10.26 14.93	3	Morcali and Zeytuncu 2015
1,3,5-Triazinepenta ethylene hexamine polymer	Pd(II)	2	10.981	-	300	17.72	-	Sayın et al. 2015
((3-(3-(methoxycarbonyl)benzylidene)hydrazinyl)benzoic acid) ligand	Pd(II)	3.50	591	Amine	2-70	184.5	95	Awual et al. 2015
5-tert-butyl-2-hydroxybenzaldehyde thiosemicarbazone ligand	Pd(II)	3.50	587	C=S N-H $-NH_2$	2-70	171.65	99	Awual et al. 2015
N,N'-(octane-1,8-diylidene)di(2-hydroxy-3,5-dimethylaniline) ligand	Pd(II)	1.50	537	NH_2, -OH	2-70	213.67	98	Awual et al. 2015
1E,1‘E,1‘‘E,1‘‘‘E (tetrakis(3-carboxysalicylidene))naphthalene-1,2,5,5-tetramine ligand	Pd(II)	2	591	N-H, -OH	2-70	191.35	95	Awual and Hasan 2015

Adsorbent Name	**Metal ions**	**pH**	**Surface area (m^2 g^{-1})**	**Functional group**	**Metal ion concentration (mg L^{-1})**	**Adsorption capacity (mg g^{-1})**	**Desorption** (%)	**Reference**
Aliquat-336 impregnated SBA-15	Pd(II)	4	928	$N–CH_2$ -OH	40	212.76	>95	Sharma et al. 2016
Third-generation dendrimers modified magnetic nanoparticles	Pd(IV) Au(III) Pd(II) Ag(I)	6.5	60	$-NH_2$ -OH -NH	20	3.60 3.58 2.75 2.84	>90	Yen et al. 2017
8-aminoquinoline-grafted poly(glycidyl methacrylate).	Pd(II)	0.4 mol/L HCl	-	-OH -NH	150-800	267.90	98	Zhang et al. 2018
Activated carbon	Pd(II)	1	1431	-		67	50-60	Wojnicki et al. 2018
6,6'-bis(5,6-diheptyl-1,2,4-triazin-3-yl)-2,2'-bipyridine/XAD-7 composite	Pd(II)		256.5			43.85		Lu et al. 2018
Nanosilica with imidazoline groups	Pd(II)	4	-	C≡N C-N-	100-600	71.43	85	Zhang et al. 2018
Glutaraldehyde cross-linked polyethylenimine (PEI) in algal beads	Pd(II)	1	-	-OH -NH	0.05 and 2 mmol $Pd\ L^{-1}$	120.25	70.2	Wang et al. 2019
PEI in alginate/algal mixture−glutaraldehyde cross-linking						158.57	84.1	
Poly-Cys-g-PDA@GPUF	Pd(II) Au(III) Pt(IV) Ru(III)	3	18.66	C-S -NH -OH		784.5 1082.6 573.9 285.3	98	Xue et al. 2019

1.2.7 Cost effectiveness and ranking of Pd(II) adsorptive chelating resins

The previous sections of the available prior-art deliberated upon the technical competence of various alternate adsorbents and chelating resins for Pd(II) recovery and reuse. An equally important issue associated to successful application of chelating resins for industrial and commercial Pd(II) recovery and reuse is associated to the process cost. Conceptual and rigorous cost analysis is a very important tool to further assist technical findings and improve decision making process based on the stringent criteria associated to process cost and environmental hazard of the suggested process and associated disposables of the process.

The cost of an adsorption process is primarily dependent upon the adsorbent cost deployed for the removal of metals from complex wastewater systems. Most adsorbents adopted for Pd(II) removal refer to functionally modified derivatives and commercial exchange resins which are all regarded to be highly expensive. The deployment of such adsorbents would be additionally burdening for developing countries such as India. Therefore, identification of low cost adsorbents is very important along with the identification of competent resins based on adsorption and desorption characteristics.

There is a significant lack of thrust and emphasis towards cost effectiveness of prepared and developed resins. A critical insight into the available literature indicates that even conceptual retail costs of various fabricated resins is very difficult to carry out, given the fact that several competent literatures do not present details with respect to stoichiometric quantities of deployed chemicals for the entire process. Hence, cost effectiveness of targeted resins is very important and shall be emphasized in this work.

Another important inference from carried out work is that the commercial resin Lewatit TP214 is expensive and despite indicating promising performance, other inexpensive commercial resins

can be explored to further improve cost effectiveness associated to Pd(II) recovery and reuse from complex adsorbate systems such as electroless plating solutions.

1.3 Possible scope for further research

1.3.1 Pd(II) speciation characteristics for complex adsorbate systems

Till date, numerous experimental studies have been conducted for the recovery of Pd(II) from aqueous solutions by targeting different types of synthesized and commercial resins. In several of these investigations, the researchers confined to the performance of resin types and their functional groups interaction with solution chemistry factors such as with Cl^- ions, pH, Pd(II) speciation and extent of complexation. Also, a considerable attention has been given to the affinity of metal ions towards the functional groups containing sulfur, nitrogen and oxygen atoms in the presence of competitor ion(s). However, for the case of treatment of industrial effluent, many potential secondary groups/species could chelate and/or react with the functional groups or with Pd(II) species or their complexes. For example, ethylene diaminetetraacetic acid (EDTA) (Pujari et al. 2014, Pujari et al. 2016), ammonia (Colombo 2007, Pujari et al. 2016) and surfactant (Pujari et al. 2014, Kato et al. 2016) could form Pd(II) complexes and these complexes may have variant adsorption and desorption characteristics in comparison with Pd(II) available in the aqueous solutions.

It has also been conveyed that a major application of Pd(II) precursors with ELP processes is with respect to their deployment for dense Pd(II) membrane and catalyst fabrication. The plating bath solution essentially includes a stabilizer like Na_2EDTA, a binding site enhancer such as a surfactant (Jana et al. 2000) in a highly alkaline solution containing ammonia (NH_4OH) liquor

(Pujari et al. 2014, Pujari et al. 2016). For such systems, speciation has not been addressed and therefore needs to be targeted.

1.3.2 Pd(II) adsorption and desorption characteristics of various adsorbents and complex adsorbate systems

Till date, numerous experimental studies have been conducted to recover Pd(II) from waste streams. Among them, most of the research focused on Pd(II) recovery from simple waste streams such as, acidic and chloride solutions (Ruiz et al. 2000, Guibal et al. 2001, Guibal et al. 2001, Guibal et al. 2002, Bernardis et al. 2005, Chassary et al. 2005, Jermakowicz et al. 2005, Ding et al. 2006, Labosova et al. 2006, Colombo 2007, Fujiwara et al. 2007, Ramesh et al. 2008, Birinci et al. 2009, Butewicz et al. 2009, Hubicki and Wołowicz 2009, Hubicki and Wołowicz 2009, Peng et al. 2009, Zhou et al. 2009, Zhou et al. 2010, Baba et al. 2011, Bratskaya et al. 2011, Sopena et al. 2011, Wołowicz and Hubicki 2011, Wołowicz and Hubicki 2012, Wołowicz and Hubicki 2012, Wołowicz and Hubicki 2012, Khunathai et al. 2013, Sharififard et al. 2013, Rajesh 2014, Wołowicz and Hubicki 2014, Awual and Hasan 2015, Awual et al. 2015, Kim et al. 2015, Lin et al. 2015, Morcali and Zeytuncu 2015, Nikoloski et al. 2015, Sayın et al. 2015, Zhou et al. 2015, Bratskaya et al. 2016, Monier et al. 2016, Sharma et al. 2016, Tokuyama et al. 2017, Wang et al. 2017, Lu et al. 2018, Wojnicki et al. 2018, Zhang et al. 2018, Xue et al. 2019). However, there might be other additives present in the solution that may affect the Pd(II) recovery in the case of industrial waste streams. For example, ELP solutions contain Na_2EDTA, NH_4OH and cetyl trimethyl ammonium bromide (CTAB) surfactant along with $PdCl_2$ (Bernardis et al. 2005, Pujari et al. 2014, Rajesh 2014, Pujari et al. 2016) and these additives could influence Pd(II) sorption characteristics. In this regard, the adsorption efficiencies of S, N, and O functionalized derivatives can be worth considering for Pd(II) recovery from complex solutions

such as ELP solutions. The HSAB theory states that, with all other factors maintained equal, soft acids (i.e. Pd^{2+}, Au^{+}, Pt^{2+} and Ag^{+}) react faster and form stronger bonds with soft bases (i.e. RS^{-} and SCN^{-}), whereas hard acids (i.e. Cr^{3+} and Cr^{6+}) react faster and form stronger bonds with hard bases (NH_3 and OH^{-}). This needs to be further explored for complex adsorbate system such as ELP. Based on the HSAB, chitosan and its functionalized derivatives and commercial derivatives can be investigated for the evaluation of their efficacy and competence towards Pd(II) recovery from complex adsorbate systems such as ELP solutions.

In summary, it can be seen that commercial resins have been explored for Pd(II) recovery from chloride and aqueous feed solutions with minimal solution chemistry complexity. S, N, and O functional groups containing commercial and chitosan based derivatives were explored for Pd(II) adsorption from aqueous solutions but not with solutions possessing stabilizers and surfactants at variant pH that strongly interfere with the Pd(II) adsorption characteristics. The role of pH, solute concentration, and chloride ion concentration have been targeted for few adsorbents without referring to the relevance or irrelevance of speciation in influencing Pd(II) adsorption characteristics. In other words, solution chemistry complexity needs to be given utmost significance in ongoing experimental investigations for commercial and chitosan based derivatives applicability towards Pd(II) recovery and reuse. Such investigations will be effective to promote industrial and commercial applicability of the said derivatives to mitigate effluent hazard and recover noble metal simultaneously.

Among various chitosan based derivatives with S, N and O functional groups, chitosan modified with triethylenetetramine, melamine, thiosemicarbazide and 3-amino-1,2,4 triazole,5-thiol derivatives could be promising for Pd(II) removal and recovery from synthetic ELP solutions. These resins have been investigated for heavy metal recovery from aqueous solutions and the

interaction of the functional groups with S/N/O atoms with the Pd(II) species in complex adsorbate system such as ELP would be useful to understand the pertinent adsorption mechanism, challenges apparent to enhance desorption characteristics and economic competitiveness in terms of resin fabrication cost.

1.3.3 Role of eluents on desorption characteristics

Till date, numerous desorption experimental studies have been carried out for the recovery of Pd(II) from spent adsorbent by using different types of eluents. In most of these, researchers used complex and expensive eluents such as EDTA, Thiourea, EDTA-H_2SO_4, Thiourea–HCl, and KCN–NaOH to recover Pd(II) from spent adsorbents, which are expensive, toxic and non-sustainable in industrial scale adsorption based recovery and reuse systems and methodologies (Fujiwara et al. 2007, Ramesh et al. 2008, Zhou et al. 2009, Zhou et al. 2010, Awual et al. 2015, Awual et al. 2015, Zhang et al. 2018, Zhang et al. 2018). Simpler acidic and basic eluents can enhance the potential of desorption based reuse of recovered Pd(II) and thereby pave the way to maximize Pd(II) reuse and recovery. For example, tetramine palladium chloride monohydrate can be recovered from spent adsorbents, since such simpler formulations achieved through ammonical eluent solutions can be used for electroless and electroplating systems without any further purification as these systems require liquid phase feed stocks and essentially don't need precipitation of the noble metal.

1.3.4 Identification of cost effective adsorbents for Pd(II) recovery from complex adsorbate systems

The literature presented in the previous sections elaborated towards experimental research that was conducted for Pd(II) recovery from acidic and chloride solutions. However, nominal inputs

have been provided in terms of their cost effectiveness. Therefore, there is a necessity to evaluate cost effectiveness of adsorbents for Pd(II) recovery from both simple and complex adsorbate systems. Such insights are very much needed to confine and assign economic competitiveness based benchmarks for the identification of low cost adsorbents and methodologies to further reduce the retail cost of fabrication of most competent resins.

1.4 Objectives of the thesis

Based on the identified gaps in literature, the broad objectives of the thesis have been outlined as follows:

a) Studies on Pd(II) complexation chemistry in ELP solutions.

b) Removal and recovery of Pd(II) onto raw chitosan from synthetic ELP solutions.

c) Performance of commercial Amberlyst A21, Amberlite IRA958 and Lewatit M600 resins.

i. Batch adsorption and desorption studies for Pd(II) removal and recovery from synthetic ELP solutions.

ii. Equilibrium, kinetic and thermodynamic modeling of Pd(II) adsorption process.

iii. Effect of surfactant in solution chemistry to influence Pd(II) adsorption characteristics.

d) Synthesis, characterization and application of chitosan derivatives with nitrogen functionalized derivatives for Pd(II) recovery from synthetic ELP solutions. These refer to melamine grafted chitosan and triethylenetetramine grafted chitosan derivatives, respectively.

e) Synthesis, characterization and application of chitosan derivatives with sulfur and nitrogen functionalized derivatives for Pd(II) recovery from synthetic ELP solutions. These refer to thiosemicarbazide grafted chitosan and 3-amino-1,2,4 triazole,5-thiol grafted chitosan derivatives, respectively.

d) Cost analysis of all adsorbents investigated in the work for the recovery and reuse of Pd(II) from synthetic ELP solutions.

1.5 Organization of the thesis

As elaborated in section 1.3 of the thesis, significant scope does exist to further research in the field of chelating and ion-exchange resins for Pd(II) adsorption from complex adsorption system such as electroless plating solutions. The objectives set for the Ph.D. thesis provide deeper insights for such central objective. In this section, a brief summary of all subsequent chapters of the thesis is presented in the following paragraphs.

Chapter 2 details upon the experimental and modeling approaches adopted for all investigations addressed in the thesis. These include procedures associated to a) evaluation of Pd(II) speciation in synthetic ELP solution media, b) batch adsorption and desorption characteristics of Pd(II) on to raw chitosan followed with modeling approaches to represent evaluated adsorption characteristics, c) Pd(II) batch adsorption and desorption characteristics of synthetic ELP solutions with commercial ion-exchange resins (such as, amberlyst A21, amberlite IRA958 and dowex marathon MSA resins), d) synthesis and characterization of chitosan based derivatives, and batch adsorption and desorption of Pd(II) on chitosan derivatives followed with modeling approaches to represent evaluated adsorption characteristics

Chapter 3 summarizes Pd(II) speciation in synthetic ELP solutions and results obtained for Pd(II) adsorption on raw chitosan. The optimality of adsorption parameters such as equilibrium, pH, Cl^- ions concentration (mg L^{-1}), adsorbent dosage (mg) and contact time (min) have been identified. Following this, the adsorption efficacy of raw chitosan was evaluated in terms of capacity and removal efficiency at various concentrations and temperatures. Finally, results

obtained from equilibrium, kinetic and thermodynamic modeling have been presented. In addition, the chapter also summarizes a comparative assessment of Pd(II) adsorption using various adsorbents from various waste streams.

Chapter 4 addresses Pd(II) adsorption and desorption characteristics of commercial ion-exchange resins (such as, amberlyst A21, amberlite IRA958 and dowex marathon MSA) with synthetic electroless plating solutions. Results obtained from relevant modeling efforts have also been elaborated to identify the best fit models for various cases. Finally, batch desorption characteristics of said commercial resins with simple eluents such as NaOH, KOH and HCl have been summarized to identify the best inexpensive eluent for Pd(II) recovery and reuse from synthesis ELP solutions.

Chapter 5 details upon the results obtained nitrogen functionalized chitosan derivatives. These refer to melamine grafted chitosan and triethylenetetramine grafted chitosan derivatives. Subsequently, Pd(II) batch adsorption characteristics and fitness of best equilibrium and kinetic models has been summarized for both derivatives. Finally, batch desorption characteristics of the nitrogen functionalized chitosan derivatives has been summarized for simple eluents such as NaOH, KOH and HCl.

Chapter 6 elaborates upon the results obtained for sulfur functionalized chitosan derivatives namely thiosemicarbazide grafted chitosan and 3-amino-1,2,4 triazole,5-thiol grafted chitosan derivatives. Pd(II) adsorption characteristics, best fit equilibrium and kinetic models, batch desorption using NaOH, KOH and HCl eluents have been presented to evaluate the technical competence of the sulfur functionalized chitosan derivatives for Pd(II) recovery and reuse from synthetic ELP solutions. Finally, conceptual retail cost analysis of the fabricated resins has been discussed to identify cost competitive resins for Pd(II) recovery and reuse from synthetic ELP

solutions and compare the chitosan based derivatives with commercial resins from technical as well as cost competitiveness perspectives.

Chapter 7 presents the most relevant conclusions deduced from the research findings of this work. Thereafter, the chapter also presents a brief overview of the research directions for future research in the field of noble metal recovery and reuse from complex adsorption systems.

Chapter 2:

Experimental, Analytical, and Modelling Methodologies

Experimental, Analytical, and Modelling Methodologies

The chapter summarizes experimental, and modelling approaches followed throughout the Ph.D. thesis in eight sections. The first section addresses the materials required for the preparation of palladium electroless plating (ELP) stock solutions, physio-chemical properties of commercial resins, and chitosan derivatives synthesis. The second section presents procedures adopted for the Pd(II) speciation study of synthetic ELP solutions. The third section elaborates upon synthesis procedures associated with various chitosan derivatives. The fourth section briefly presents solubility tests conducted for chitosan and its derivatives. The fifth section, surface characterization methodologies for proponed materials. Sections 2.6 and 2.7 briefly describe procedures followed for batch adsorption and desorption studies, respectively. Finally, section 2.8 presents modeling methods followed towards the fitness of measured equilibrium, kinetic, and thermodynamic data of Pd(II) adsorption.

2.1 Materials

2.1.1 Palladium stock solution precursors

Palladium chloride (99.9% pure obtained from SRL Chemicals Pvt. Ltd., India), Na_2EDTA (Merck, India), liquor ammonia (25%) (Merck, India) and millipore water (Make: milliQ) were used for the preparation of noble metal solutions in aqueous media. pH of the solution was adjusted using analytical grade HNO_3 (Merck, India), and NaOH (Merck, India) pH was measured using a pH meter (VSI-301).

2.1.2 Other chemicals

Chitosan (75–85% degree of deacetylation and medium molecular weight), epichlorohydrin (99%), melamine (99%), triethylenetetramine (≥97%), thiosemicarbazide (99%), 3-amino-1,2,4-triazole-5-thiol (95%) were procured from Sigma-Aldrich Corporation, Bangalore, India. *N*,*N*-dimethylformamide (DMF) was obtained from Merck India. Other chemicals like cetrimonium bromide (CTAB), acetic acid, acetone, and ethanol were purchased from SRL Chemicals Pvt. Ltd., India

2.1.3 Commercial resins

Amberlyst A21, Amberlite IRA958, and Dowex Marathon MSA commercial resins were procured from Sigma-Aldrich Corporation, Bangalore, India. Table 2.1 summarizes the physio-chemical properties of these commercial resins.

Table 2.1: Summary of physical characteristics of commercial anion exchange resins deployed in the thesis.

Description	Amberlyst A21	Dowex Marathon MSA	Amberlite IRA958
Make	Sigma-Aldrich Corporation, Bangalore, India		
Functional groups	Dimethylamine	Quaternary ammonium	
Ionic form as shipped	Free Base	Cl^- form	
Matrix	Styrene divinylbenzene	Polystyrene–divinylbenzene	Acrylic copolymer
Structure	Macroporous		
Total capacity (meq/mL)	1.3	1.0	0.8
Operating pH range	1−14		
Thermal stability (K)	373		353
Water retention (%)	56–62	56−66	66−72

2.1.4 Preparation of palladium stock solution

The synthetic ELP solution composition has been chosen based on the research work conducted by Murali et al., (2014 & 2016), who utilized initial Pd(II) solution concentrations of 500 mg L^{-1} for the fabrication of dense Pd(II) composite membranes using porous stainless steel supports. The authors reported an average conversion of about 35% (175 mg L^{-1}). Therefore, the spent electroless plating solution after such membrane fabrication is likely to have a Pd(II) solution concentration of 325 mg L^{-1}. Considering such spent solutions and reused spent solutions, the Pd(II) solution concentrations have been varied in the range of 50 – 300 mg L^{-1} in this work. For this purpose, the stock solution of $PdCl_2$ (1000 mg L^{-1}) was prepared using a synthetic electroless plating bath composition presented in Table 2.2. The synthetic solution was prepared by thoroughly mixing the specific constituents in 1000 mL deionized water in a shaking incubator (Labtop; LSI-125/R; India) at 120 rpm for 15 min. Subsequent solutions with reduced Pd(II) concentrations were prepared by diluting the stock solution. The synthetic ELP solution composition essentially refers to a stabilizer (Na_2EDTA), an optional cationic surfactant (CTAB) in a highly alkaline solution prepared with liquor ammonia. The Pd(II) concentration of the prepared stock solution varied between 50-300 mg L^{-1}.

Table 2.2: Composition of synthetic Pd(II) ELP solutions.

Name of the component	**Palladium solution concentration (mg L^{-1})**					
	50	**100**	**200**	**300**	**400**	**500**
$PdCl_2$ (mg L^{-1})	83.31	166.63	333.27	499.90	666.54	833.17
Na_2EDTA (g L^{-1})	1.39					
NH_3 solution (25%), mL L^{-1}	10.33					
CTAB, mg L^{-1} (if any)	335-1340					

2.2 Pd(II) speciation studies of synthetic ELP solutions

The Pd(II) speciation in ELP solutions was investigated using Visual MINTEQ 3.1 software (an open-source software: 2014-2015). The speciation of Pd(II) in EDTA enriched ELP solution was considered in the solution pH and Cl^- concentration range of 1-10 and 0.93-29.14 mM, respectively.

2.3 Synthesis of chitosan derivatives

Nitrogen and sulfur functionalized chitosan derivatives such as melamine, triethylenetetramine, thiosemicarbazide, and 3-amino-1,2,4-triazole-5-thiol were grafted onto epichlorohydrin treated chitosan. The detailed synthesis procedure has been elaborated in the following sub-sections.

2.3.1 Chitosan-Epichlorohydrin derivative

Six grams of chitosan was dissolved in 20% aqueous solution of acetic acid and was precipitated in 2.5 M NaOH solution. Thereby, the obtained gel was washed several times with distilled water and was suspended in 50 mL of DMF and 25 mL epichlorohydrin. This mixture was stirred for 24 h at 80 °C. The solid product obtained from the mixture was obtained from filtration and was washed several times with distilled water and ethanol. This product is referred to as cross-linked chitosan, whose structural interactions can be summarized through the following reaction 2.1 (Elwakeel et al. 2016).

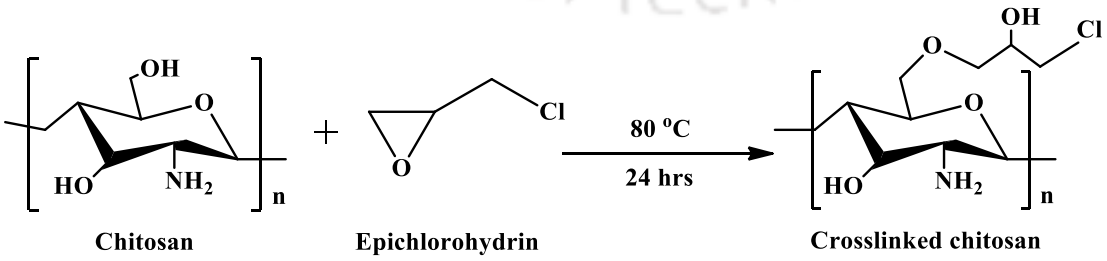

(2.1)

2.3.2 Chitosan-Melamine (CH-ME) derivative

Cross-linked chitosan was treated with melamine suspension (4 g of ME was dissolved in 150 mL hot distilled water). The reaction mixture was stirred at 100 ºC for 24 h. Thereafter, the product was filtered and washed with distilled water, methanol, and subsequently dried in air. This product is referred to as CH-ME in the Ph.D. thesis, whose structural interactions can be summarized through the following reaction 2.2 (Elwakeel et al. 2016).

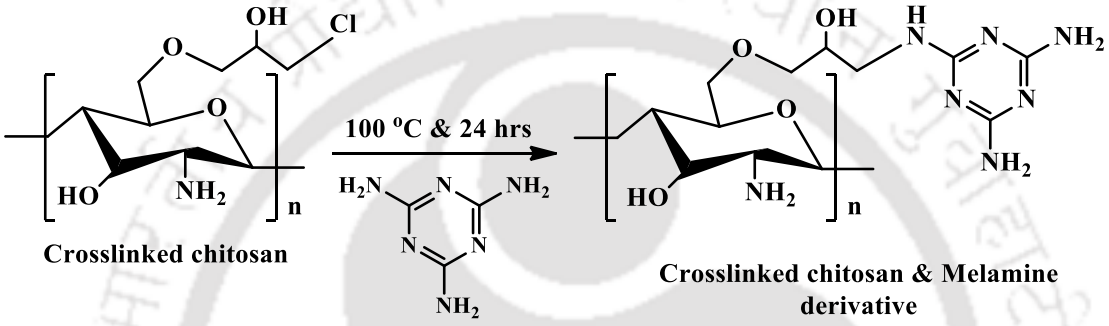

(2.2)

2.3.3 Chitosan-Triethylenetetramine (CH-TETA) derivative

The cross-linked chitosan was contacted with 150 mL of DMF at 50 ºC and was stirred for 30 min. Thereafter, 50 mL of TETA was slowly added to the solution. The mixture was stirred for 4 h, and precipitate was washed with ethanol and distilled water to remove the unreacted TETA. This product is referred to as CH-TETA in the Ph.D. thesis, whose structural interactions can be summarized through the following reaction 2.3 (Liao et al. 2016).

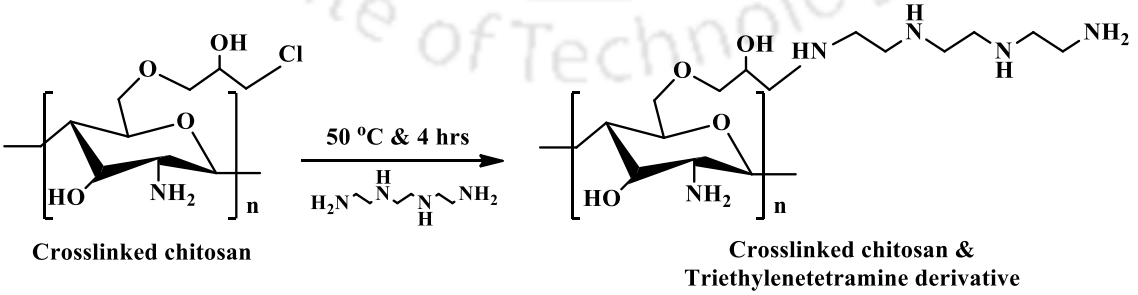

(2.3)

2.3.4 Chitosan-Thiosemicarbazide (CH-TSC) derivative

The cross-linked chitosan was treated with thiosemicarbazide suspension (4 g of TSC was dissolved in 150 mL hot distilled water). The reaction mixture was stirred at 100 ºC for 24 h. Finally, the product was filtered and washed with distilled water, methanol, and dried in air. This solid product is referred to as CH-TSC in the Ph.D. thesis, whose structural interactions can be summarized through the following reaction 2.4 (Ahmad et al. 2015).

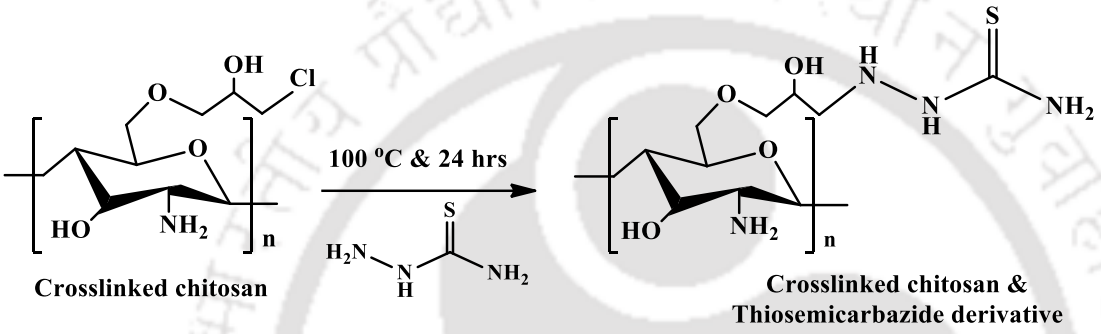

(2.4)

2.3.5 Chitosan-3-amino-1,2,4-triazole-5-thiol (CH-AZ) derivative

The grafting process involved treatment of cross-linked chitosan with 3-Amino-1,2,4 triazole,5-thiol solution (3 g of AZ was dissolved in 200 mL hot distilled water) under continuous stirring condition at 100 °C for 12 h. Thereby, the obtained product (CH-AZ) was filtered and washed with distilled water, methanol and acetone to subsequently dry in air. With a promising yield % of 95% for the CH-AZ adsorbent, the structural interactions can be summarized in the following reaction (2.5) (Elwakeel et al. 2016).

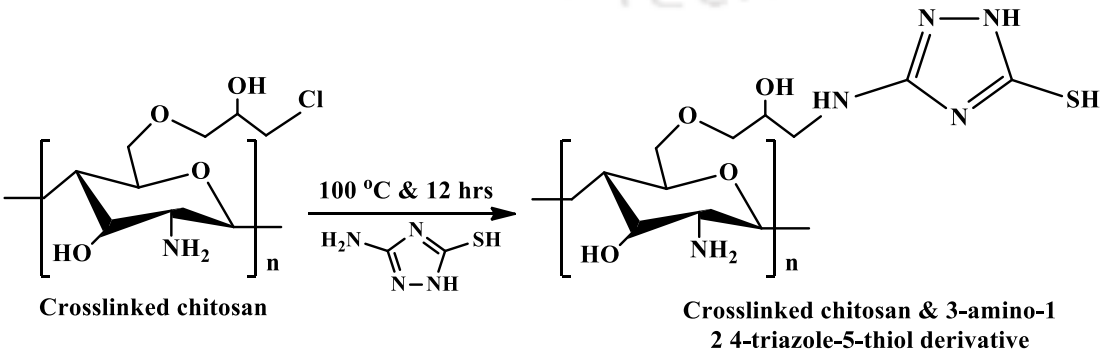

(2.5)

2.4 Solubility studies for chitosan and its derivatives

The solubility resistance of chitosan derivatives was evaluated in acidic media (pH < 7) by treating 50 mg of adsorbent with 30 mL HNO_3 (1 N) in a stirred condition for 12 h using an orbital shaker at 250 rpm. Subsequently, the mixture samples were taken out and filtered using Whatman filter paper (No. 1, pore size: 11 μm) to determine the residual derivative weight after drying for 3 h in an oven at 110 °C. The evaluated weight loss was used to determine solubility resistance in highly acidic media (Kim et al. 2006). Similar tests have been conducted with highly basic media using NaOH (1 N) solution.

2.5 Surface characterization

The surface and thermal characterization studies for both raw and Pd(II) loaded commercial resins, chitosan and its derivatives were carried out using Fourier Transform-Infrared Spectrophotometer (FTIR), Braummer-Emmet-Teller (BET), X-ray diffractometer (XRD), Thermo Gravimetric Analyser (TGA) and Field Emission Scanning Microscopy equipped energy dispersive X-Ray analyser (FESEM-EDX).

Atomic Absorption Spectrophotometer (AAS; Varian; Spectra AA 220 FS; Netherland) operated at a wavelength of 244.6 nm was used to determine the initial and final Pd(II) solution concentrations during adsorption and desorption experiments. Sampling procedures involved collecting at least three samples and determining the mean value of all measurements. These mean values have been reported in this work. Nitrogen gas adsorption-desorption isotherm data were measured using a relevant instrument (Quantachrome; Autosorb-IQ MP; USA) at 77 K for chitosan and its derivatives, using which pore size and surface area were determined. FTIR (Shimadzu; IR Affinity1; Japan) was used to determine prevalent functional groups in commercial resins, chitosan, modified chitosan derivatives, and Pd adsorbed derivatives samples. The instrument was

operated in the wavenumber range of 4000–400 cm^{-1}. XRD (Bruker; D8 Advance; Germany) was used to determine the crystalline properties of chitosan, chitosan derivatives, and Pd-loaded derivatives. Thermal properties of chitosan and its derivatives were measured using TGA (Mettler Toledo; TGA 851e/LF/1100; Switzerland). Glass transition temperature (Tg) and crystallization properties of the chitosan was obtained using differential scanning calorimetry (DSC; Mettler Toledo; No. 1; Switzerland). FESEM-EDX (Zeiss; Sigma; Germany) was used to obtain an elemental composition for both raw and Pd-loaded commercial resins, chitosan and its derivatives.

2.6 Batch adsorption studies

For batch adsorption studies, 50 mL of known Pd(II) solution concentrations were taken in 250 mL conical flasks and were contacted with 0.2-2 g L^{-1} of adsorbent at 250 rpm and 298 K in an orbital shaker. The optimality of adsorption process parameters, namely pH, chloride ion concentration, contact time, adsorbent dosage, temperature, and initial metal ion concentration was evaluated by considering the variation of only one parameter and maintaining all other parameters at specific values. Correspondingly, these parameters have been varied in the range of 0.5-12 pH, 298-333 K temperature, 0.2-2 g L^{-1} adsorbent dose, and 50-300 mg L^{-1} Pd(II) initial concentration for a contact time of 12 h. After mixing solutions for set contact time, the mixture was filtered using Whatman filter paper (No. 1, pore size: 11 µm), and the adsorbate was tested for residual Pd(II) solution concentration using AAS instrument. Each batch adsorption experiment was conducted at least three times, and the average value has been reported in the thesis. Using measured values, the % removal and adsorption capacity were evaluated using the following expressions (Eqs. 2.1 and 2.2).

$$\text{Removal} = \frac{C_o - C_e}{C_o} \times 100 \quad (\%) \tag{2.1}$$

$$\text{Adsorption capacity } (q_e) = \frac{C_o - C_e}{W} \times V \quad (\text{mg g}^{-1}) \tag{2.2}$$

where C_o, C_e, V, and W are initial Pd(II) solution concentration (mg L^{-1}), equilibrium Pd(II) solution concentration (mg L^{-1}), volume of solution (L), and mass of adsorbent (g), respectively.

2.7 Batch desorption experiments

2.7.1 Batch desorption of Pd(II) loaded chitosan

Using Pd(II) loaded chitosan, NaOH solutions with variant concentrations (0.1, 0.3, 0.5, 1, and 2 N) was deployed as the eluent. The Pd(II) loaded chitosan prepared with 50 mg L^{-1} initial Pd(II) concentration was washed about 5 times with deionized water and transferred into stoppered reagent bottles. To a known amount of adsorbent, NaOH of a specified amount (50 mL) was added, and the mixture was subjected to mechanical shaking for 520 min at room temperature. Eventually, the Pd(II) solution concentration in the eluent has been determined using AAS to determine Pd(II) metal recovery after desorption. The metal recovery for reuse was evaluated using a mass balance of Pd(II) concentration in the solution before and after desorption.

2.7.2 Batch desorption of Pd(II) loaded commercial resins

Using Pd(II) adsorbed Amberlyst A21 resin, eluents such as NaOH, KOH, and $N(CH_2CH_3)_3$ were deployed at desired solution concentrations to determine desorption characteristics. For Amberlite IRA958 and Dowex marathon MSA resins, desorption studies were carried out using NaOH, KOH and HCl eluents. The experimentation involved washing of Pd(II) loaded resins (prepared with

50 mg L^{-1}) samples in 5 cycles using deionized water. Thereafter, specific quantities of resins were kept in stoppered reagent bottles, and a specific quantity of eluent volume (50 mL) was added, and the mixture was subjected to mechanical shaking (200 rpm) for stipulated time interval at room temperature. Eventually, the final Pd(II) solution concentration was measured for the determination of desorption based Pd(II) metal recovery. The metal recovery for reuse was evaluated using a mass balance expression of the number of moles of Pd(II) existent before and after desorption.

2.7.3 Batch desorption of Pd(II) loaded chitosan derivatives

Using Pd(II) loaded chitosan derivatives, NaOH, KOH, and HCl solutions with variant concentrations (0.1, 0.3, 0.5, 1, and 2 N) were deployed as the eluents. The procedures adopted for the batch adsorption study have been presented elsewhere (Nagireddi et al. 2017). Pd(II) loaded derivatives prepared with 50 mg L^{-1} initial Pd(II) concentration was used for the desorption studies using 50 mL of eluent solution at room temperature. Mass balance expressions were deployed to evaluate desorption efficiency for various cases.

2.8 Fitness of equilibrium, kinetic and thermodynamic models

2.8.1 Equilibrium models

The batch equilibrium adsorption data were analysed using the Langmuir isotherm model, which hypothesizes monolayer Pd(II) adsorption onto the adsorbent active sites to evaluate the adsorption process. The data were also analysed using the Freundlich isotherm model, which hypothesizes multilayer Pd(II) adsorption based on the assumption of uniform energy surface heterogeneity.

The Langmuir isotherm equation (Eq. (2.3)) can be expressed in the linear form as follows (Langmuir 1918):

$$\frac{C_e}{Q_e} = \frac{C_e}{Q_o} + \frac{1}{bQ_o} \tag{2.3}$$

where, Q_e and C_e are equilibrium Pd(II) adsorption capacity (mg g^{-1}) and equilibrium Pd(II) solution concentration (mg L^{-1}), respectively. In the above expression, Q_o and b are maximum adsorption capacity (mg g^{-1}) and Langmuir adsorption constant, respectively. The values of Q_o and b were computed from the slope and intercept of the Langmuir plot of C_e versus C_e/Q_e. Based on the initial Pd(II) solution concentration C_o and Langmuir constant b, dimensionless equilibrium parameter R_L can be evaluated using the expression (Eq. 2.4).

$$R_L = \frac{1}{1 + bC_o} \tag{2.4}$$

The magnitude of R_L affirms one of the following regimes:

Favourable adsorption: $0 < R_L < 1$

Unfavourable and linear adsorption: $R_L > 1$ and $R_L = 1$

Irreversible adsorption: $R_L = 0$

The linearized Freundlich isotherm model (Eq. (2.5)) is expressed as (Freundlich 1906):

$$\log Q_e = \log K_f + \frac{1}{n} \log C_e \tag{2.5}$$

where, K_f and n are the Freundlich constants related to adsorption capacity and adsorption intensity, respectively.

If n = 1, then the partition between the two phases is to be regarded as independent of the concentration. If the value of 1/n is below one, it indicates normal adsorption. On the other hand, for the case of 1/n value cooperative adsorption is inferred (Mohan and Karthikeyan 1997). As the

temperature increases, the constants k and n vary to reflect the empirical observation that the quantity adsorbed increases more slowly, and higher concentration is required to saturate the surface. However, K_f and n are parameters characteristic of the sorbent-sorbate system, which must be determined by data fitting. Linear regression is generally used to determine the parameters of kinetic and isotherm models (Guadalupe et al. 2008). Specifically, the linear least-squares method and the linearly transformed equations have been widely applied to correlate sorption data. The term 1/n is a heterogeneity parameter, and a smaller value of 1/n indicates heterogeneity. The model expression reduces to a linear adsorption isotherm for the case of 1/n = 1. If n lies between one and ten, it is inferred to indicate a favorable sorption process (Goldberg 2005).

2.8.2 Kinetic models

For all cases, the Pd(II) adsorption kinetic analysis was conducted for 50 mg L^{-1} Pd(II) initial solution concentration, optimum adsorbent dose, solution pH, 298 K, and 250 rpm operating conditions. For the analysis, liquid samples have been taken at precise time intervals until equilibrium contacting time has been achieved to evaluate the time-dependent Pd(II) solution concentration. The Pd(II) adsorption kinetics obtained data have been tested for their fitness with pseudo-first (Aharoni and Ungarish 1977), pseudo-second-order models (Ho and McKay 1999) and intraparticle diffusion models, respectively expressed as:

$$\log (Q_e - Q_t) = \log Q_e - \frac{K_1 t}{2.303} \tag{2.6}$$

$$\frac{t}{Q_t} = \frac{1}{K_2 Q_e^{\,2}} + \frac{t}{Q_e} \tag{2.7}$$

$$Q_t = K_{id} t^{0.5} \tag{2.8}$$

where Q_t and Q_e are time-dependent and equilibrium resin Pd(II) adsorption capacities (mg g^{-1}), respectively. The model constants in the above expressions are pseudo-first-order rate constant (K_1, min^{-1}) and pseudo-second-order rate constant (K_2, g $mg^{-1}min^{-1}$). K_{id} corresponds to the rate constant evaluated using on intraparticle diffusion model. For the fitness of the pseudo-second-order model, the plot of t/Q_t against t needs to indicate a linear relationship. From such plot, Q_e and K_2 can be determined from the slope and intercept of the plot, respectively.

2.8.3 Thermodynamic model

The thermodynamic parameters of Pd(II) adsorption on adsorbent have been determined using data obtained at variant operating temperature values (298-333 K) and constant values for all other adsorption process parameters. For such batch adsorption data, the thermodynamic equilibrium constant was determined for various temperature data sets (Eq. 2.9).

$$K_c = \frac{C_{ae}}{C_e} \tag{2.9}$$

where C_{ae} and C_e are the Pd(II) equilibrium concentrations (mg L^{-1}) on the adsorbent and in the solution, respectively.

Subsequently, the enthalpy ($\Delta H°$, kJ mol^{-1}) and entropy ($\Delta S°$, kJ $mol^{-1}K^{-1}$) change associated to Pd(II) adsorption have been evaluated using intercept and slope respectively using the graphical representation of Vant Hoff equation, presented as (Eq. 2.10):

$$\log K_c = \frac{\Delta S°}{R} - \frac{\Delta H°}{RT} \tag{2.10}$$

where R and T refer to universal gas constant (8.314 J $mol^{-1}K^{-1}$) and absolute temperature (K), respectively.

The Gibbs free energy change ($\Delta G°$, kJ mol^{-1}) during Pd(II) adsorption process can be evaluated using the expression (Eq. 2.11) (Liu 2009):

$$\Delta G° = \Delta H° - T\,\Delta S° \qquad (2.11)$$

where, $\Delta H°$ and $\Delta S°$ refers to enthalpy change (kJ mol^{-1}) and entropy change (kJ $mol^{-1}K^{-1}$), respectively.

Chapter 3:

Pd(II) Speciation Characteristics of Synthetic ELP Solutions and Adsorptive Efficacy of Raw Chitosan

Chapter 3

Pd(II) Speciation Characteristics of Synthetic ELP Solutions and Adsorptive Efficacy of Raw Chitosan

In this chapter, the obtained results for Pd(II) adsorption from synthetic ELP solutions have been presented for raw chitosan. Sections 3.2 details upon Pd(II) speciation in synthetic ELP solutions. Section 3.3 summarizes the solubility resistance of raw chitosan in both acidic and basic media. Section 3.4 addresses batch Pd(II) adsorption characteristics followed with model fitness of measured adsorption equilibrium, kinetic, and thermodynamic data. Section 3.5 presents surface characterization results for raw and Pd(II) loaded chitosan samples. Section 3.6 presents batch desorption characteristics, followed by a summary of the research findings in section 3.7.

3.1 Introduction

This chapter addresses the Pd(II) speciation characteristics of synthetic ELP solutions and the efficacy of raw chitosan towards Pd(II) removal and recovery from synthetic ELP solutions. The Pd(II) batch adsorption experiments were carried out in the parametric range of 0.5–10 pH, 33–500 mg L^{-1} Cl^- concentration, 5–840 min, 298–333 K temperature, 10–100 mg adsorbent dose (0.2–2 g L^{-1}) and 50–300 mg L^{-1} Pd(II) initial concentration. Thereafter, for optimal process parameter based data, equilibrium, kinetic, and thermodynamic modelling of Pd(II) adsorption process have been addressed using various models. Eventually, batch desorption studies were carried out for Pd(II) adsorbed loaded chitosan using NaOH solutions with variant concentrations (0.1, 0.3, 0.5, 1, and 2N) as the eluent. Also, surface characterization studies have been carried out using Fourier transform infrared (FTIR) spectral analyser, Brummer-Emmett-Teller analyser

(BET), Thermogravimetric analyser (TGA), Differential scanning calorimetry analyser (DSC), X-ray diffractometer (XRD), CHNS elemental analyser and Field Emission Scanning Microscopy equipped energy dispersive X-Ray analyser (FESEM-EDX).

3.2 Pd(II) speciation characteristics of synthetic ELP solutions

The speciation of Pd(II) in synthetic ELP solution for variant solution pH and Cl^- concentration is illustrated in Fig. 3.1. These results have obtained using open source Visual MINTEQ 3.1 software (https://kth.app.box.com/s/gfycuk1rvedrigukrqrdcxkqcazmvvr7, 2014-2015). As analyzed, Pd(II) primarily exists as $PdEDTA^{2-}$, $PdCl_4^{2-}$, $PdCl_3^-$, $PdCl_2$ (aq), $PdCl^+$, $Pd(NH_3)_4^{2+}$ and $Pd(NH_3)_3^{2+}$. For low pH range (1 to 6) and high chloride concentration, Pd(II) mostly exists in $PdEDTA^{2-}$ form. In basic pH range, $Pd(NH_3)_4^{2+}$ are the predominant species.

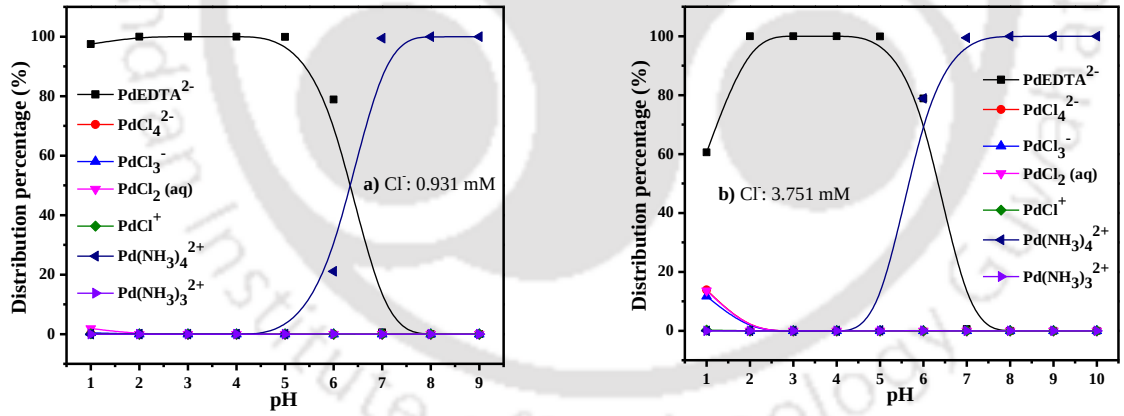

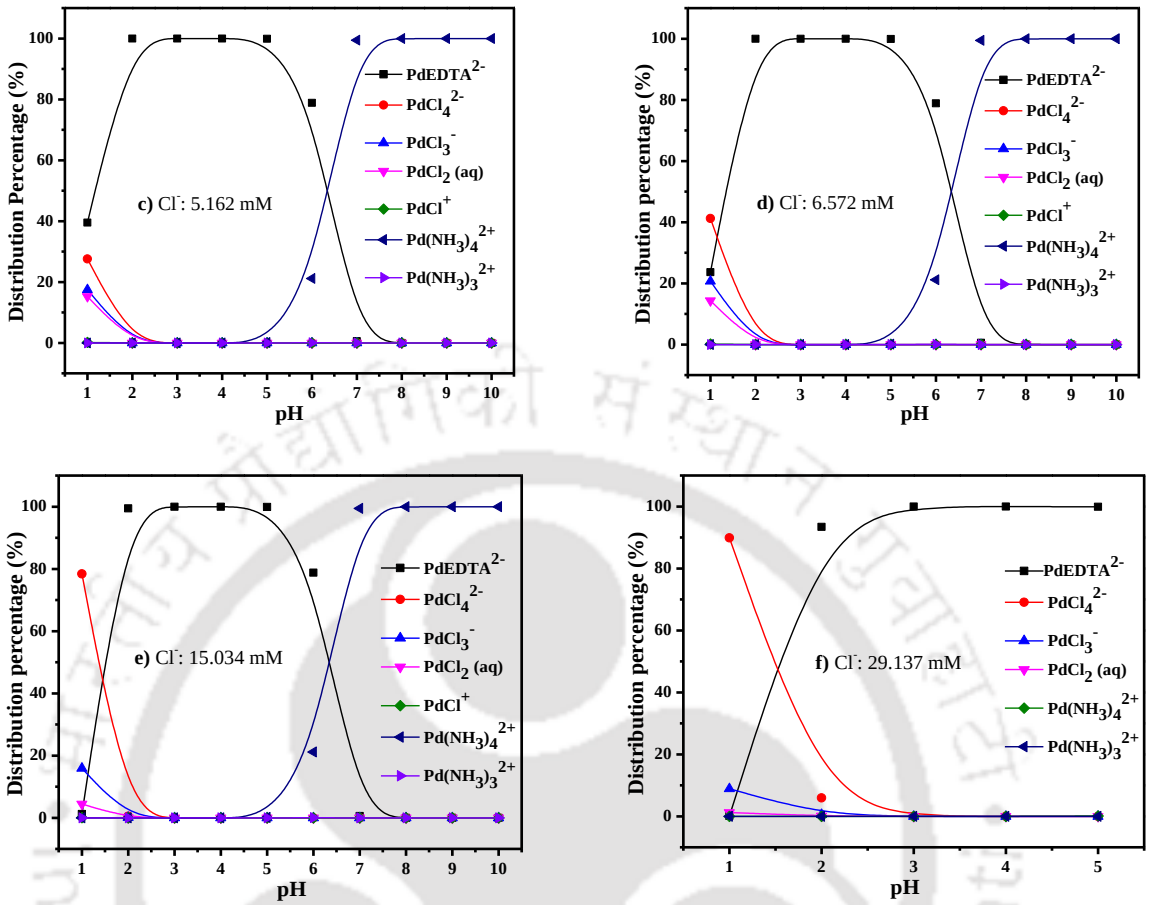

Fig. 3.1: Influence of pH and Cl- concentration on Pd(II) speciation characteristics of synthetic ELP solutions.

3.3 Solubility resistance based optimality of solution pH

Fig.3.2 presents the weight loss profile of chitosan as a function of solution pH. It can be seen that the weight loss of chitosan was rapid in the pH range of 2–5. Above 5 pH, the weight loss of chitosan was slow, and it almost reached ~~to~~ saturation. The weight loss % in the pH range of 2−5 has been evaluated to vary from 88.6−20.8%. At pH 6, the weight loss % is 10.9%. Therefore, adsorption capacity and % removal values obtained below a pH of 6 have been omitted for the results obtained in the pH variation studies associated with batch adsorption.

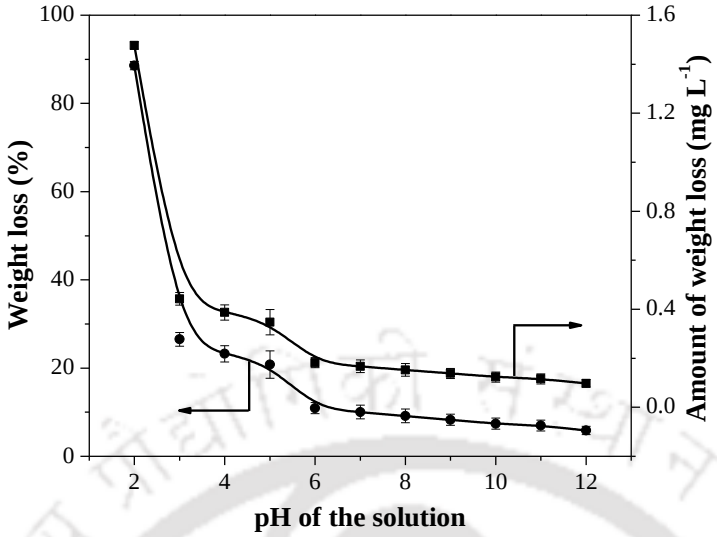

Fig. 3.2: Effect of solution pH on chitosan solubility.

3.4 Pd(II) adsorption characteristics of chitosan-ELP solution system

3.4.1 Effect of adsorption parameters on Pd(II) adsorption

Fig. 3.3a depicts pH effect on Pd(II) adsorption capacity and % removal profiles. For the case study, other parameters have been chosen to be 33 mg L^{-1}, 720 min, 1 g L^{-1}, and 50 mg L^{-1} for chloride ion concentration, contact time, adsorbent dosage, and Pd(II) concentration, respectively. The figure confirms maximum combinations of adsorption capacity (46.58 mg g^{-1}) and % removal (93.16%) at a pH of 2, which is not inferred to be the overall optimal pH value due to poor solubility resistance. Hence, pH of 6 as indicated by good solubility resistance of chitosan has been regarded to be the optimal pH for all further investigation. Therefore, the maximum adsorption capacity and removal % were achieved at pH 6 as 33.35 mg g^{-1} and 70.69%, respectively.

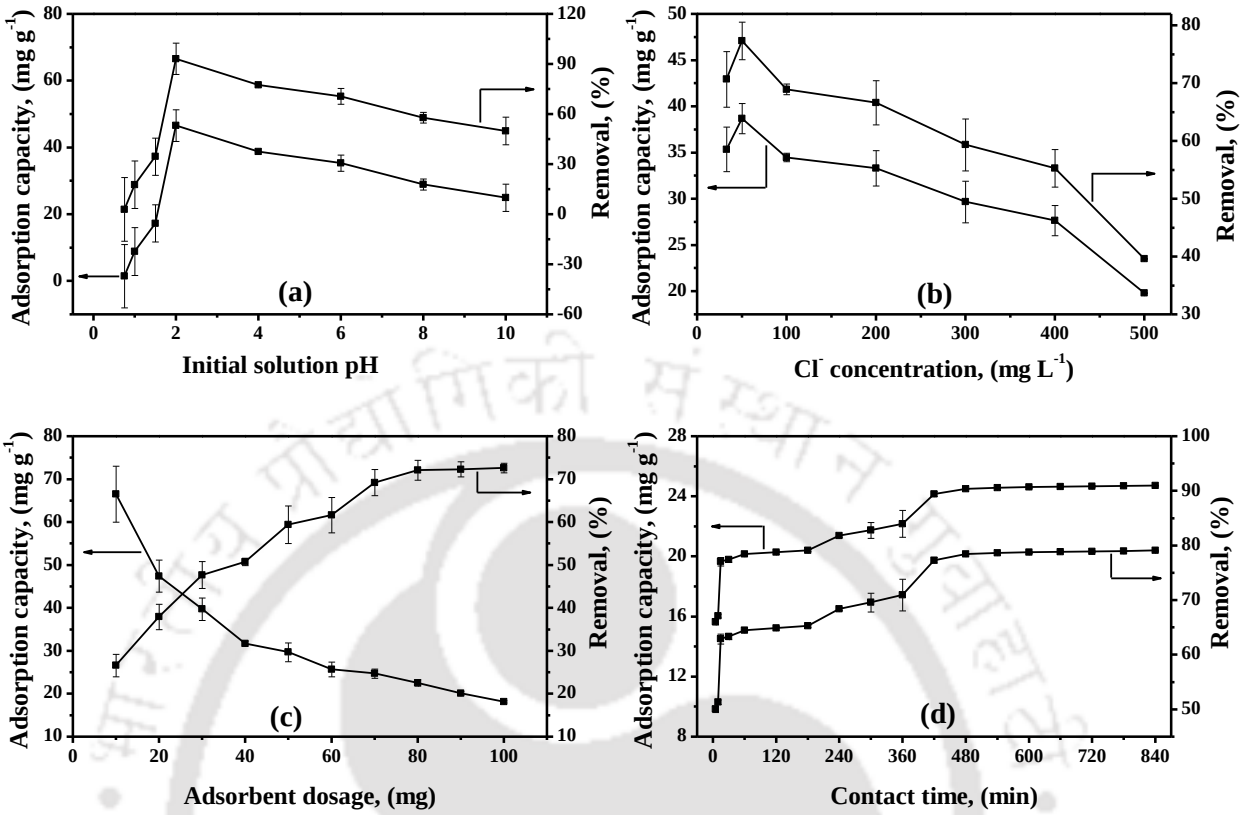

Fig. 3.3: Effect of (a) pH, (b) Chloride concentration, (c) Contact time and (d) Adsorbent dosage on Pd(II) adsorption characteristics.

In this regard, it is important to note that Pd(II) precipitated at a pH of 6 in the absence of Na_2EDTA, and hence control experiments using aqueous solutions have not been carried out. The literature indicates maximum Pd(II) removal of 94% for an optimal pH of 2, fixed choice of 360 min contact time, and 100 mg L^{-1} Pd(II) concentration (Sharififard et al. 2013). The literature data could not yield an appropriate conclusion in the context of dosage influencing adsorption characteristics and solution chemistry complexity. This is due to a lack of optimality data associated to adsorbent dosage in the literature.

The Pd speciation characteristics of EDTA-ELP solution for variant pH and Cl^- concentration have been summarized in section 3.2. As conveyed, in the entire range, Pd(II) primarily exists as

$PdEDTA^{2-}$, $PdCl_4^{2-}$, $PdCl_3^-$, $PdCl_2$ (aq), $PdCl^+$, $Pd(NH_3)_4^{2+}$, and $Pd(NH_3)_3^{2+}$. However, for low pH range (1−6) and high chloride concentration, Pd(II) mostly exists in $PdEDTA^{2-}$ form. At pH 7-10, $Pd(NH_3)_4^{2+}$ exists as predominant species. At low pH, the protonation effect will be dominant, i.e., the significantly higher influence of H^+ exists for $–NH_2$ groups (Fujiwara et al. 2007, Ramesh et al. 2008, Zhou et al. 2009). Therefore, for such cases, $–NH_3^+$ groups will become prominent on the chitosan. These groups will have an affinity to attract $Pd(EDTA)^{-2}$ and thereby enhance adsorption between at lower pH (2–6). These analyses have been depicted in Eq. 3.1. For higher pH, no protonation occurs, and Cl^- tends to eliminate one H^+ from $−NH_2$, and thereby, the negatively charged −NH group would have the affinity to attract and adsorb $Pd(NH_3)_4^{+2}$ group. Thus, it is apparent that lower pH favours better adsorption of the said groups ($Pd(EDTA)^{-2}$) (Eq. 3.1). Based on this hypothesis, it has been inferred that Pd(II) adsorption on chitosan is possibly due to electrostatic attraction and ion-exchange in the ELP solutions, where in the electrostatic interaction between protonated amine groups on the chitosan and noble metal ions is according to the following reaction (Eq. 3.1).

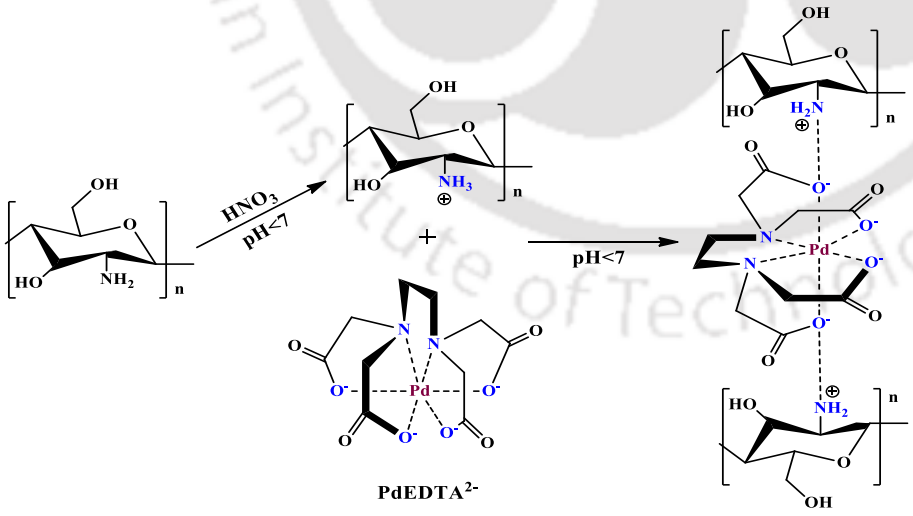

(3.1)

Fig. 3.3b presents the effect of chloride ions (Cl^-) on the chitosan adsorbent performance. For the case study, pH, contact time, adsorbent dosage, and Pd(II) concentration have been chosen as 6,

720 min, 1 g L^{-1}, and 50 mg L^{-1}, respectively. As shown, maximum adsorption capacity (35.35 mg g^{-1}) and removal (70.69%) have been obtained for an optimal Cl^- concentration of 33 mg L^{-1}.

Fig. 3.3c illustrates the effect of adsorbent dosage on the Pd(II) adsorption characteristics of the chitosan−ELP system for a fixed choice of pH, Cl^- concentration, initial Pd(II) solution concentration, and contact time of 6, 33 mg L^{-1}, 50 mg L^{-1}, and 720 min, respectively. For the maximum adsorbent dosage of 1.6 g L^{-1}, the best results have been obtained (22.53 mg g^{-1} adsorption capacity and 72.1% removal %). The enhancement in Pd(II) removal efficiency with adsorbent dosage was due to the enhancement in the number of the active sites available for Pd(II) adsorption. Simultaneously, the metal uptake reduced due to the reduction of metal ions available per unit gram of adsorbent. Hence, with increasing adsorbent dosage, higher removal, and lower capacity is expected, which is in agreement with the results obtained in this work. The literature confirms 93% Pd(II) removal for the highest adsorbent dosage of 10 g L^{-1} for a fixed choice of contact time (360 min), pH (2), and Pd(II) concentration (100 mg L^{-1}) (Sharififard et al. 2013). Once again, it can be observed that in comparison with the literature, lower removal efficiency values have been obtained. This is due to variations in the adsorbent dosage in this work (1.6 g L^{-1}) with respect to literature data (10 g L^{-1}). In other words, it is very likely that the solution chemistry complexity of synthetic ELP solutions did not facilitate stronger inhibition effect for Pd(II) adsorption on chitosan.

The Pd(II) adsorption characteristics of the chitosan-ELP system with respect to contact time have been depicted in Fig. 3.3d. For the case study, batch adsorption process parameters have been taken as 1.6 g L^{-1}, 33 mg L^{-1}, 50 mg L^{-1} and 6 for adsorbent dosage, Cl^- concentration, Pd(II) concentration, and pH, respectively. The figure affirms that the Pd(II) rate of adsorption is rapid up to 420 min. Also, the figure conveys that the maximum time of 540 min is required to achieve

equilibrium and obtain a maximum adsorption capacity and removal efficiency of 24.59 mg g^{-1} and 78.68%, respectively. The literature conveys upon 90% maximum Pd(II) removal for an optimal contact time of 200 min, and fixed choice of adsorbent loading, pH, and Pd(II) concentration value of 6 g L^{-1}, 2 and 100 mg L^{-1}, respectively (Sharififard et al. 2013). It is well known that as adsorbent dosage increases, metal uptake decreases, and removal % increases. The case considered in this work corresponds to a lower dosage than that reported in the literature. Therefore, it is very likely that solution chemistry complexity did not significantly influence Pd(II) adsorption characteristics.

Figs. 3.4a and 3.4b illustrate the effect of Pd(II) solution concentration and temperature on the adsorption characteristics of Pd(II) from synthetic ELP solutions without CTAB surfactant. These experiments were carried out for 50−300 mg L^{-1} Pd(II) solution concentration and 298-333 K temperature and for fixed choices of other parameters such as pH (6), Cl^- concentration (33 mg L^{-1}), adsorbent dosage (1.6 g L^{-1}) and contact time (540 min). As shown in the figure, at 298 K, the Pd(II) metal uptake and removal efficiency varied from 24.44−74.69 mg g^{-1} and 78.21−39.83%, respectively. Thus, higher concentrations didn't favour adsorption, as affirmed from the theory. The effect of temperature on the Pd(II) adsorption characteristics is in agreement with the theoretical insight, i.e., lower % removal values have been obtained at a higher temperature (70.55–33.50 % at 333 K) than those obtained at a lower temperature (78.21–39.83 % at 298 K).

3.4.2 Effect of CTAB on Pd(II) uptake

Experimental investigations were conducted for fixed choice of Pd solution concentration (50 mg L^{-1}), temperature (298 K), pH (6), Cl^- concentration (33 mg L^{-1}), adsorbent dosage (1.6 g L^{-1}), and contact time (540 min) but for variant CTAB surfactant concentration (1−4 CMC). Fig. 3.4c summarizes the obtained adsorption characteristics for variant CTAB surfactant concentration. For

1-4 CMC CTAB concentration variation, the Pd(II) metal uptake and removal efficiency varied from 24.94−25.48 mg g^{-1} and 81.55−78.81 %, respectively. These values are marginally higher than those obtained with synthetic ELP solutions that did not contain CTAB surfactant. The possible reasons for such marginal enhancement are due to the potential role of CTAB in altering surface characteristics to favour adsorption (Rajesh 2015, Nagireddi et al. 2017). In other words, the inclusion of CTAB in synthetic ELP solutions is favourable for Pd(II) adsorption, and this is a promising feature of the chitosan-ELP system adsorption characteristics.

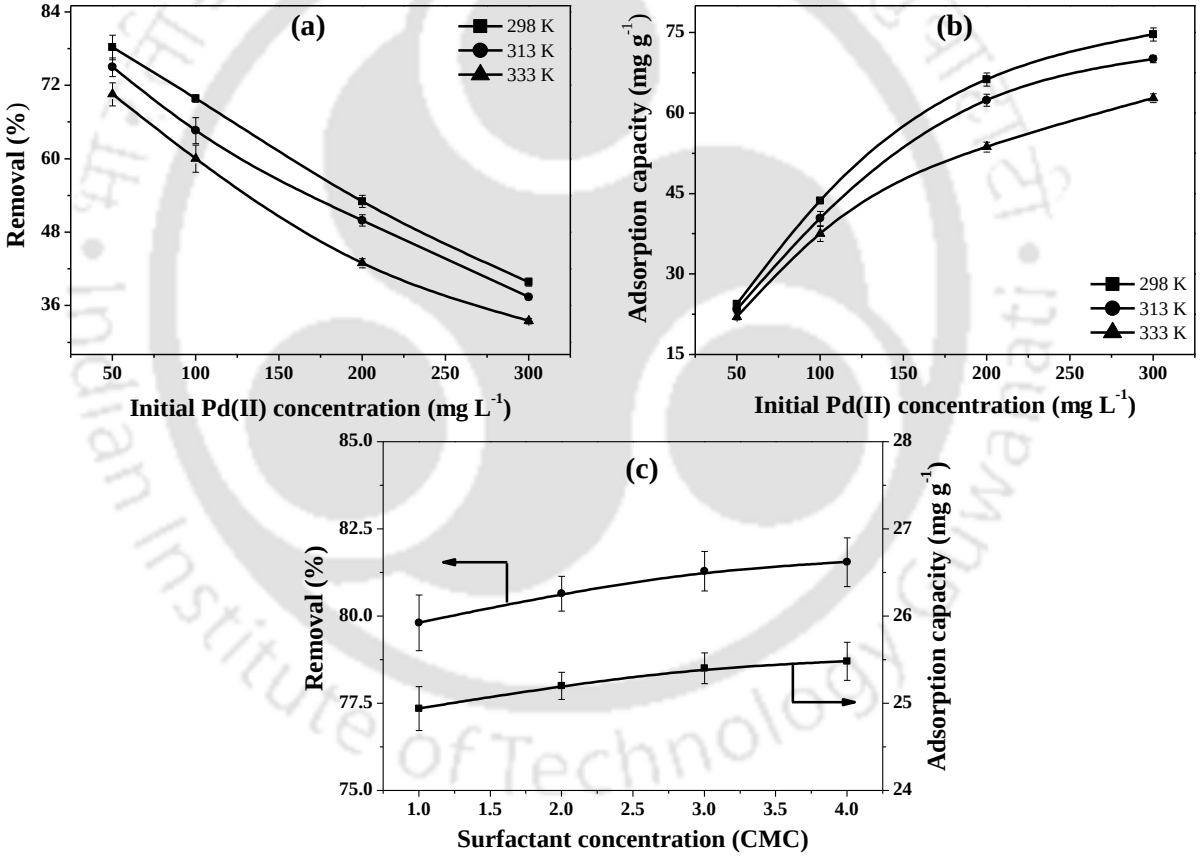

Fig. 3.4: Effect of temperature on (a) Pd(II) removal efficiency (b) Adsorption capacity for various initial Pd(II) concentration cases and (c) Effect of surfactant concentration on adsorption characteristics of chitosan.

3.4.3 Equilibrium, kinetic and thermodynamic model parameters

The fitness plots for alternate kinetic models have been presented in Figs. 3.5a−3.5c. Relevant parameters obtained from the fitness plots are summarized in Table 3.1. As presented, only for the pseudo-second-order model, the regression coefficient value was higher than 0.95. Further, the evaluated adsorption capacity based on the pseudo-second-order model was in agreement with the measured adsorption capacity. Therefore, pseudo-second-order model has been inferred to be the best fit to represent the kinetics of Pd(II) adsorption from synthetic ELP solutions onto chitosan adsorbent, which is based on the assumption that the rate limiting step could be the chemisorption involving valency forces through sharing or exchange of electrons with the N atom of adsorbent. The fitness of the pseudo-second-order model is also justified with the FTIR analysis of Pd(II) adsorbed chitosan that inferred strong Pd(II) chemical interaction with the prevalent functional groups of the chitosan. Also, Fig. 3.5c conveys that the intra-particle diffusion plot indicates the multi-linear plot in three distinct phases, and the fit plot did not meet the graph at its origin. Hence, intra-particle diffusion does not exist as a rate-limiting step Pd(II) adsorption process. Similar model fitness has been indicated for the Pd(II) adsorption kinetics of chitosan, chitosan-coated activated carbon, glutaraldehyde cross-linked chitosan, L-lycine modified cross-linked chitosan, glycine modified cross-linked chitosan and thiourea modified chitosan microspheres (Ruiz et al. 2000, Fujiwara et al. 2007, Ramesh et al. 2008, Zhou et al. 2009).

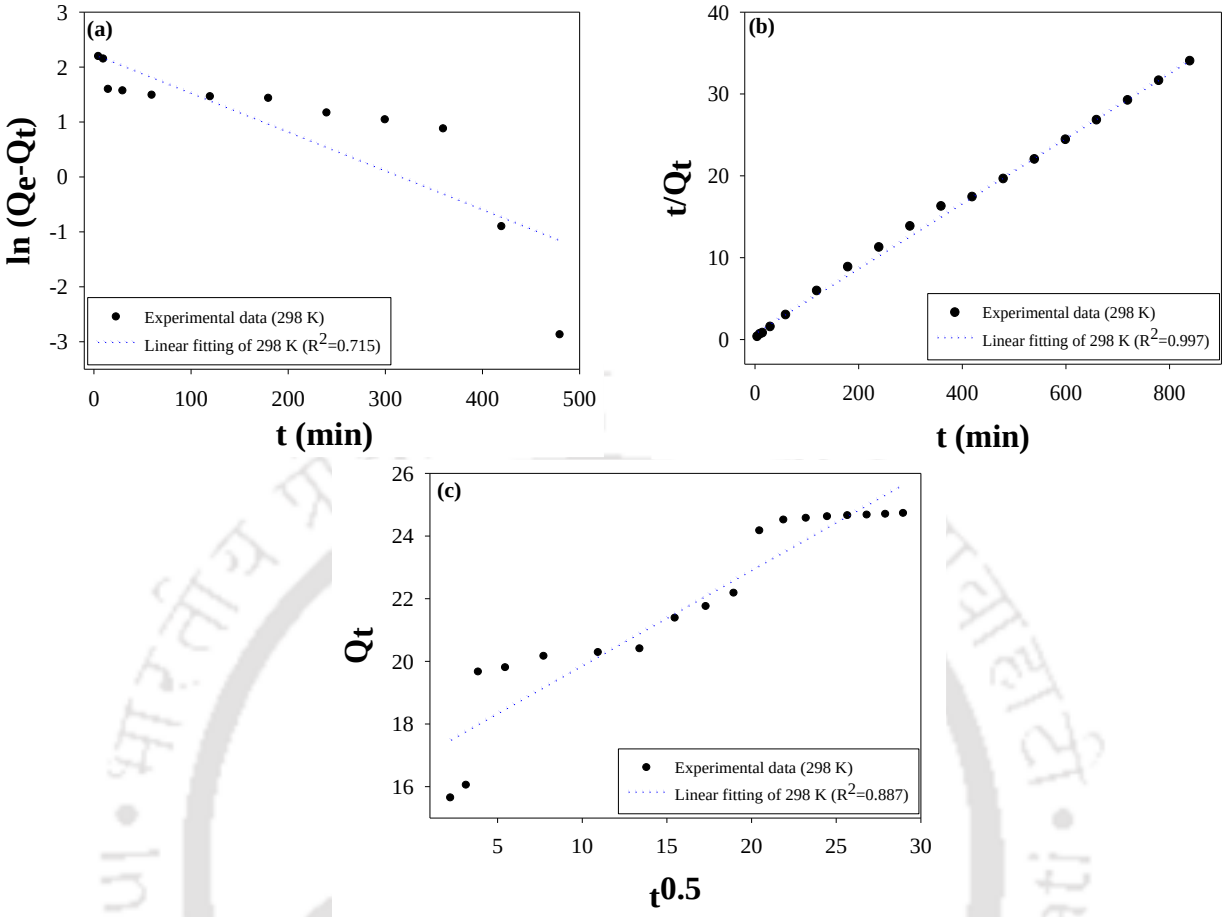

Fig. 3.5: Fitness of alternate Pd(II) adsorption kinetic models: (a) Pseudo-first order kinetic model, (b) Pseudo-second order kinetic model, and (c) Intra-particle Diffusion model.

Table 3.1: Regressed kinetic parameters to represent Pd(II) adsorption kinetics of the chitosan-ELP system.

Type of model	Experimental capacity (Q_{exp}, mg g^{-1})	Q_e (mg g^{-1})	K_1 (min^{-1})	K_2 (g mg^{-1} min^{-1})	K_{id} (min mg g^{-1})	C	R^2
Pseudo-first-order model		9.34	-7×10^{-3}	-	-	-	0.715
Pseudo-second-order model	24.56	25.64	-	0.019	-	-	0.997
Intra-particle diffusion model		-	-	-	0.304	16.82	0.887

Figs. 3.6a and 3.6b respectively present the fitness plots of Langmuir and Freundlich isotherm models to represent measured Pd(II) equilibrium adsorption data. Relevant model parameters and the coefficient of correlation (R^2) have been presented in Table 3.2. The figure and Table confirm that the Langmuir isotherm model best fits with the measured batch equilibrium data. Table 3.2 confirms upon a R_L value of 0-1 to affirm upon favourable adsorption of Pd(II) from synthetic ELP solutions using chitosan adsorbent.

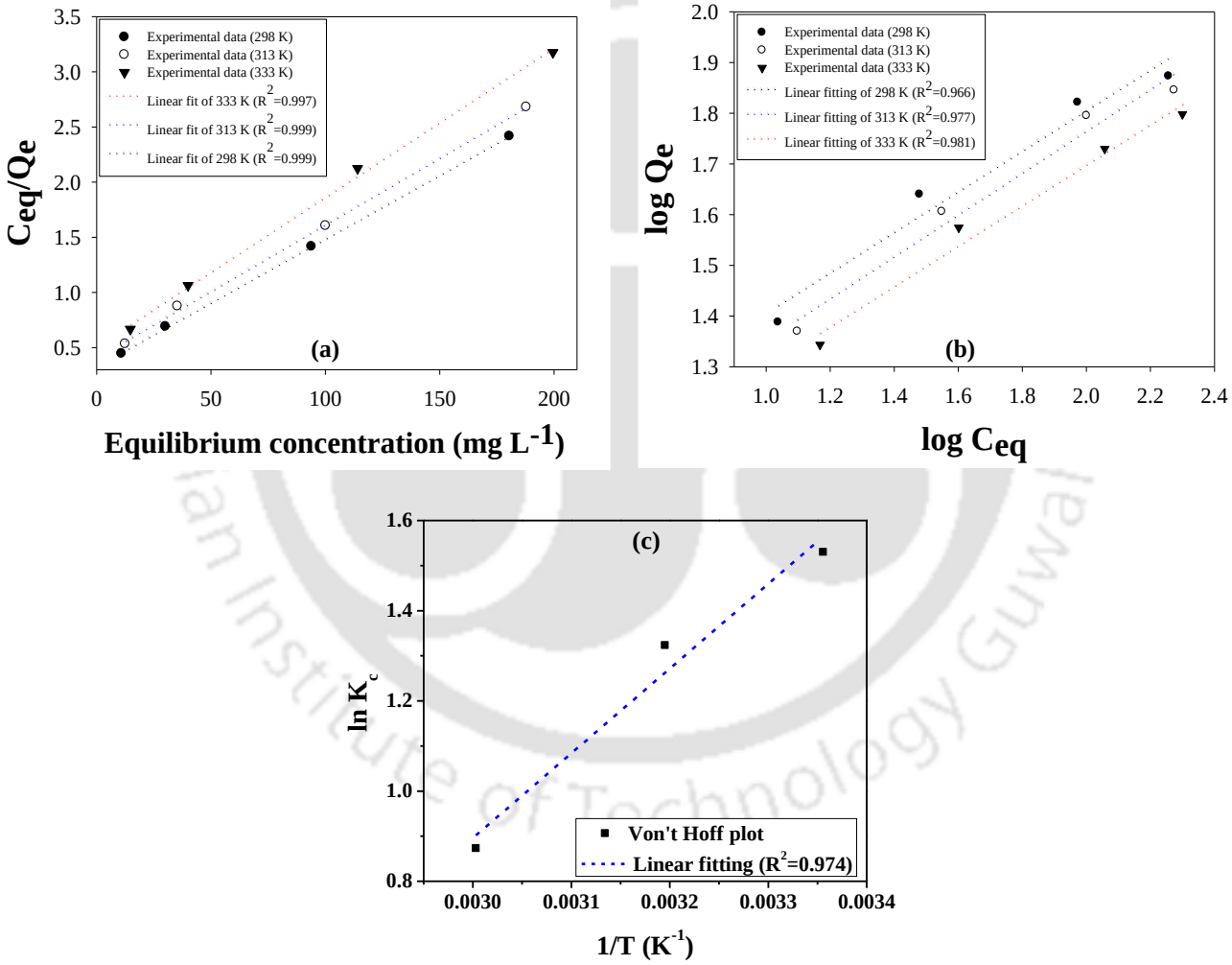

Fig. 3.6: Fitness of alternate models to represent Pd(II) equilibrium and adsorption thermodynamics: (a) Langmuir model (b) Freundlich model and (c) Van't Hoff model.

Table 3.2: Regressed equilibrium parameters to represent Pd(II) adsorption equilibrium of chitosan-ELP system.

Temperature (K)	Langmuir parameters				Freundlich parameters		
	Q_o (mg g^{-1})	b (L mg^{-1})	R^2	R_L	K_f	n	R^2
298	90.91	0.033	0.999	0.102-0.446	10.14	2.506	0.966
313	83.33	0.029	0.999	0.102-0.405	8.71	2.427	0.977
333	76.92	0.026	0.997	0.116-0.439	7.94	2.513	0.981

Fig. 3.6c depicts the thermodynamic behaviour of the adsorption process, and Table 3.3 summarizes relevant parameters obtained for the Vant Hoff's model. The table affirms negative ΔG° values to indicate upon spontaneous Pd(II) adsorption and negative ΔH° values to affirm upon exothermic adsorption process.

Table 3.3: Regressed thermodynamic parameters for Pd(II) adsorption equilibrium of the chitosan-ELP system.

Temperature (K)	K_c	ΔH^o (kJ mol^{-1})	ΔS^o (J K^{-1} mol^{-1})	ΔG^o (kJ mol^{-1})	R^2
298	2.40	-15.61	-39.39	-3.875	0.974
313	2.99			-3.284	
333	3.59			-2.496	

Comparative assessments of obtained results with those presented in the relevant literature are summarized in Table 3.4. As summarized, only one literature refers to adsorption characteristics of Pd(II) using chitosan, and this literature refers to aqueous solutions (Sharififard et al. 2013). All other materials refer to chelating resins, which are more complex materials in comparison to chitosan in the context of their natural abundance. While the removal% for the literature reported chitosan (Sharififard et al. 2013) was 93% for an adsorbent dosage of 10 g L−1, the removal

efficiency for the synthetic ELP–chitosan system in this work has been 78.68% for an adsorbent dosage of 1.6 g L−1. Thus, it is apparent that the obtained results in this work are comparable with those reported in the literature and, the solution complexity did not have a strong influence on the Pd(II) adsorption characteristics of the chitosan-ELP system.

Table 3.4: Efficacy of Pd(II) adsorption and desorption efficiencies of chitosan with respect to the best available data in the literature.

Adsorbent name	Contaminants	Adsorption			Desorption		Source
		Adsorbent dose ($g\ L^{-1}$)	pH	Adsorption capacity ($mg\ g^{-1}$)	Eluent	Desorption (%)	
L-lysine modified cross-linked chitosan	Pd(II) Au(III) Pt(VI)	3.33	2	109.47	0.7 M Thiourea–2 M HCl	99.98	Fujiwara et al. 2007
Thiourea modified chitosan microspheres	Pd(II) Pt(VI)	3.33	2	112.4	0.5 M EDTA–0.5 M H_2SO_4	98.38	Zhou et al. 2009
Glutaraldehyde cross-linked chitosan	Pd(II)	0.15	2	180	-	-	Ruiz et al. 2000
Glycine modified cross-linked chitosan	Pd(II) Au(III) Pt(VI)	3.33	2	120.39	0.7 M Thiourea–2 M HCl	98.27	Ramesh et al. 2008
Chitosan	Pd(II) Pt(VI)	10	2	62.5	-	-	Sharififard et al. 2013
Activated carbon coated with chitosan				43.48	-		
Ethylenediamine modified magnetic chitosan nanoparticles	Pd(II) Pt(VI)	0.5	2	138	0.4 M HNO_3–1.0 M Thiourea	97.3	Zhou et al. 2010
chitosan	Pd(II) Na_2EDTA NH_4OH	1.6	6	90.91	2 N NaOH	6.31	Present work

3.5 Characterization of chitosan adsorbent

3.5.1 Surface area analysis

The surface area and total pore volume of the chitosan was obtained as 8.212 m^2g^{-1} and 1.222x10^{-2} cc g^{-1}, respectively.

3.5.2 Thermogravimetric analysis

Figs. 3.7a and 3.7b depict the TGA and DSC profiles for chitosan. As shown in Fig. 3.7a, significant weight loss (14%) occurred for chitosan below 150 °C due to free water loss. However, the weight remained fairly constant up to 248 °C, and after this temperature, significant weight loss occurred up to 750 °C (69% total weight loss). On the other hand, Fig. 3.7b conveys that the glass transition temperature is 305 °C, and this confirms the crystallinity of chitosan. The crystallinity of chitosan has been further analysed using XRD studies, whose results are presented in the following paragraph.

3.5.3 Crystallinity analysis

The X-ray diffraction pattern of chitosan has been depicted in Fig. 3.7c. For the chitosan, in agreement with the available literature, a sharp diffraction peak exists at 19.85^o to affirm upon high crystallinity (Tripathi et al. 2009, Ge et al. 2012, Saita et al. 2012). The higher degree of crystallinity in chitosan is due to the formation of strong inter and intra-molecular hydrogen bonds with abundant hydroxyl and amino groups (Saita et al. 2012). Further, regularity in the chitosan molecular structure also contributes to its high degree of crystallinity.

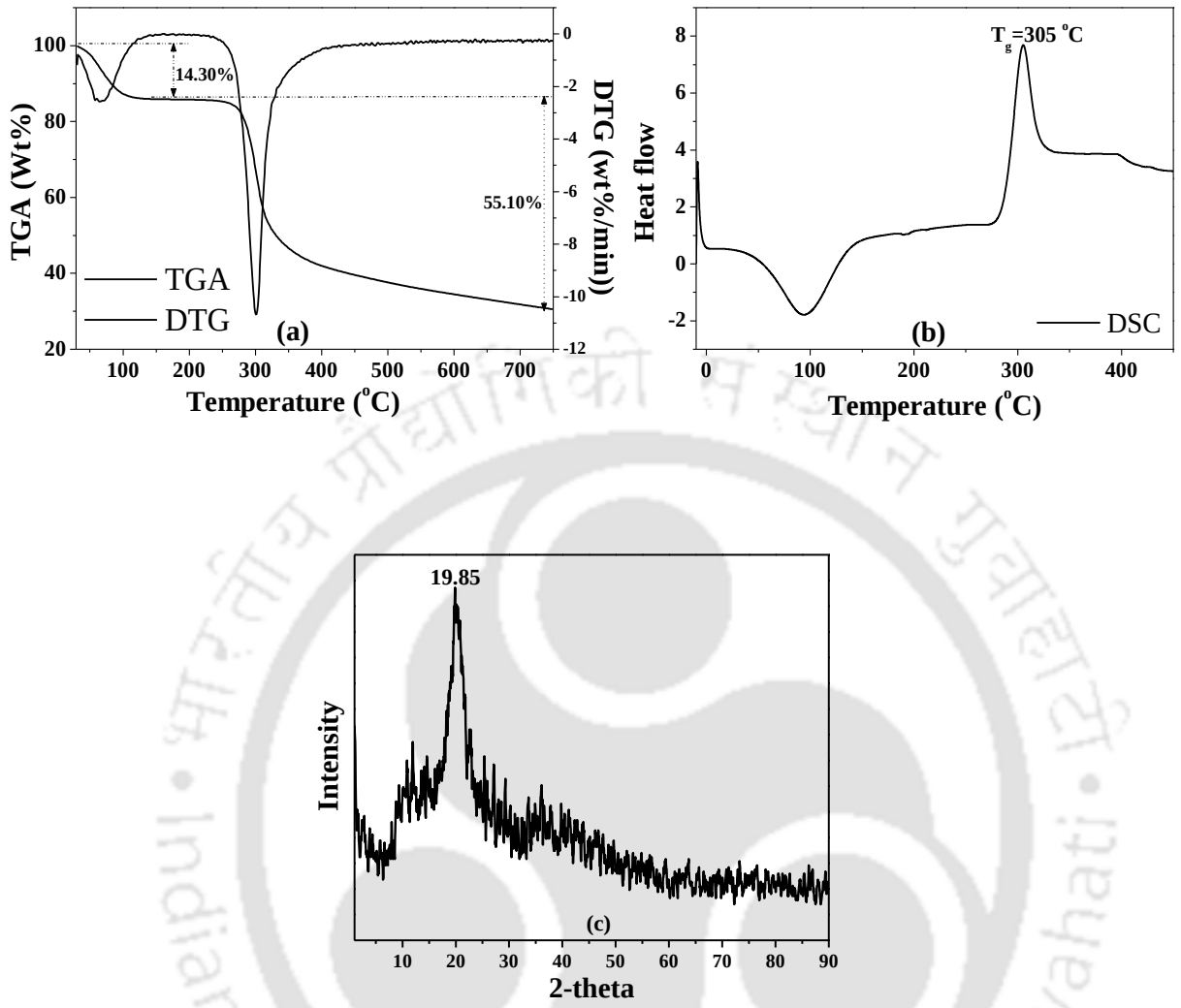

Fig. 3.7: Surface characterization diagrams of chitosan: (a) TGA and DTG plot, (b) DSC plot (c) X-ray diffractogram.

3.5.4 FTIR spectra

The FTIR spectra confirm the existence of various functional groups in both raw and Pd(II) loaded chitosan (Fig. 3.8). The peak depicted at 3436 cm^{-1} has been attributed to stretching vibrations of hydroxyl (−OH) and amine ($-NH_2$) groups. It also conveys the overlapping of intermolecular hydrogen bonds with one another. The existence of one amine spike around 3436 cm^{-1}

wavenumber confirms that a secondary amine group exists in the chitosan. A peak appearing at 1654 cm^{-1} affirms carbonyl group stretching vibration of amide I and a strong peak at 1660 cm^{-1} wavenumber affirm amide II group. A spectral peak at 1154 cm^{-1} affirms –CH vibration. Peak at 1078 cm^{-1} wavenumber confirms –CONH- group. The FTIR spectra of Pd(II) loaded chitosan indicate a significant peak shift from 1654 to 1639 cm^{-1} and 1078 to 1068 cm^{-1}. This may be due to the affinity or binding of Pd(II) with the $–NH_2$ group (Zakaria et al. 2012).

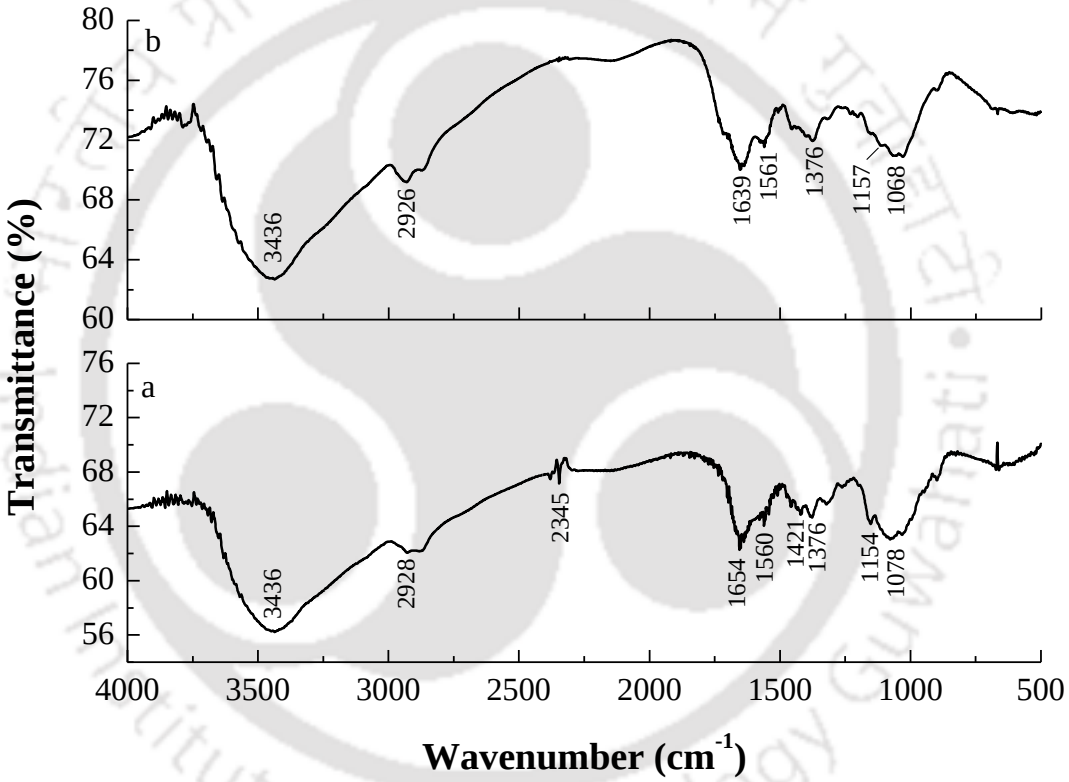

Fig. 3.8: FTIR spectra of (a) Raw and (b) Pd(II) loaded chitosan.

3.5.5 CHNS analysis

The elemental analysis of the chitosan also supplements FTIR data and confirms upon the presence of nitrogen groups in the chitosan structure. As per the CHNS elemental analysis data, chitosan contains 8.40% nitrogen, 41.98% carbon, and 6.76% hydrogen atoms in its structure.

3.5.6 EDX spectra

The FESEM spectra of chitosan obtained before and after Pd(II) adsorption have been depicted in Fig. 3.9. Figs. 3.9a and 3.9b depict the FESEM micrograph and EDX spectra of fresh chitosan samples. The presence of C (56.3 %), O (40.9 %), and N (2.7 %) are evident from this figure. It can also be seen that the chitosan surface became smooth after Pd(II) adsorption from synthetic ELP solutions (Figs. 3.9a and 3.9c). A significant amount of Pd can be found on the chitosan surface (Fig. 3.9d) after adsorption from synthetic ELP solutions.

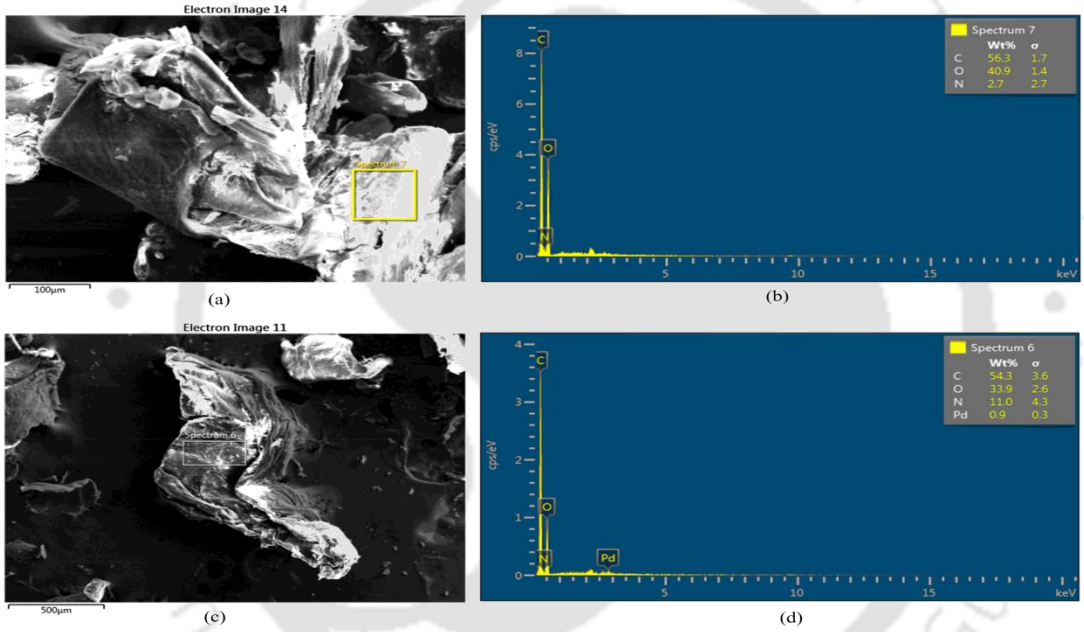

Fig. 3.9: (a) FESEM micrograph and (b) EDX spectra of chitosan; (c) FESEM micrograph and (d) EDX spectra of Pd(II) loaded chitosan.

3.6 Pd(II) desorption characteristics of chitosan

Desorption studies were carried out to recover Pd(II) ions that were adsorbed onto chitosan. Based on the results obtained from batch adsorption studies, the Pd(II) loaded chitosan had an average capacity of 21.23 mg g^{-1}. The maximum desorption percentage was obtained for 2 N NaOH eluent

as only 6.31% for chitosan owing to Pd(II) chemisorption. Table 3.5 presents the desorption efficiencies of Pd(II) onto different concentrations of the eluent. These desorption values are not at all satisfactory from the perspective of Pd(II) recovery and reuse. Hence, irreversible chemisorption seems to be significant for Pd(II) adsorption onto chitosan.

Table 3.5: Summary of evaluated Pd(II) desorption efficiencies for various eluents and chitosan-ELP system.

Desorption eluent	Desorption efficiency (%)
0.1M NaOH	0.99
0.3M NaOH	1.40
0.5M NaOH	2.66
1M NaOH	3.50
2M NaOH	6.31

3.7 Summary

Speciation studies affirmed the existence of $PdEDTA^{-2}$groups at optimal pH and its potential to effectively bind with existent free amine groups in chitosan structure. The batch adsorption study conveyed that the optimal batch adsorption parameters refer to 6 pH, 33 mg L^{-1} chloride ion concentration, 1.6 g L^{-1} adsorbent dosage, 540 min contact time, and 25 °C adsorption temperature. Langmuir isotherm and pseudo-second-order kinetic model have been evaluated to fit well with measured Pd(II) equilibrium and kinetic data. The inclusion of CTAB as an additive in the synthetic ELP solutions enhanced adsorption characteristics marginally and conveyed upon a contributory role of CTAB surfactant to influence Pd(II) adsorption characteristics. In summary,

complexity in solution chemistry has been evaluated to not significantly undermine Pd(II) adsorption onto chitosan adsorbent.

Chapter 4:

Efficacy of Commercial Resins for Pd(II) Removal, Recovery and Reuse

Chapter 4

Efficacy of Commercial Resins for Pd(II) Removal, Recovery, and Reuse

Section 4.1 summarizes the background for the conducted work. Section 4.2 elaborates upon Pd(II) batch adsorption characteristics of commercial resins. Section 4.3 details with respect to equilibrium, kinetic, and thermodynamic model fitness for measured data. Section 4.4 presents surface characterization results for fresh and Pd-loaded resins. Sections 4.5 and 4.6 detail upon the desorption characteristics of commercial resins and efficacy of the commercial resins, respectively. Finally, the summary is presented in section 4.7.

4.1 Introduction

Prior to this work, only one literature by our research group addressed Pd(II) adsorption characteristics from synthetic electroless solutions using a commercial resin. Several other investigations for palladium recovery targeted adsorption characteristics for aqueous solutions. Hence, the combinatorial role of stabilizer and liquor ammonia to influence the adsorption characteristics of palladium for several inexpensive commercial resins has not received any attention and is the central objective of this work. Further, desorption characteristics with simple and cheaper eluents have not been investigated. With these limitations in the literature, this work addresses the adsorption characteristics of palladium on commercial resins using synthetic electroless plating solutions. A deeper perspective of this work is to also examine upon the role of EDTA in influencing the adsorption characteristics of palladium from electroless plating solutions.

Surface characterization studies have been carried out using Fourier transform infrared (FTIR) spectral analysis and Field Emission Scanning Microscopy equipped energy dispersive X-Ray analysis (FESEM-EDX). For optimized pH, adsorbent dosage, and contact time, adsorption experiments were conducted for a wider range of Pd(II) solution concentrations (50–300 mg L^{-1}). The specific influence of various additives such as Na_2EDTA (stabilizer) and liquor ammonia (NH_3) on Pd(II) adsorption characteristics of commercial resins were addressed.

4.2 Batch adsorption characteristics

Based on adsorption studies conducted at specified combinations of contact time (720 min), adsorbent dosage (1 g L^{-1}) and initial Pd(II) concentration (50 mg L^{-1}), Figs.4.1a−4.1c depict pH optimality plots associated to Pd(II) adsorption on Amberlyst A21, Amberlite IRA 958 and Dowex MSA, respectively. Thereby, based on optimal removal efficiency and adsorption capacity, optimal pH has been evaluated to be 4 for both Dowex MSA and Amberlite IRA 958 resins and, 2 for Amberlyst A21 resin. Corresponding Pd(II) batch adsorption data are 74.58%, 37.28 mg g^{-1} for Amberlite IRA 958, and 86.57%, 43.29 mg g^{-1} for Dowex MSA and, 75.85% and 37.92 mg g^{-1} for Amberlyst A21 resins.

Speciation based analysis of pH optimality for the resins are being presented as follows. In synthetic ELP solutions, Pd(II) can exist as $PdEDTA^{2-}$, $PdCl_4^{2-}$, $PdCl_3^{-}$, $PdCl_2$ (aq), $PdCl^{+}$, $Pd(NH_3)_4^{2+}$ and $Pd(NH_3)_3^{2+}$ (Ge et al. 2012, Nagireddi et al. 2017). In the lower pH range of 1-6, only $PdEDTA^{-2}$ exists, and at higher pH, Pd exists as $Pd(NH_3)_4^{2+}$. Since both resins exhibited optimal performance at 4 pH, and stronger interaction between $PdEDTA^{-2}$ and prevalent NH_3^{+} groups in the resin are expected.

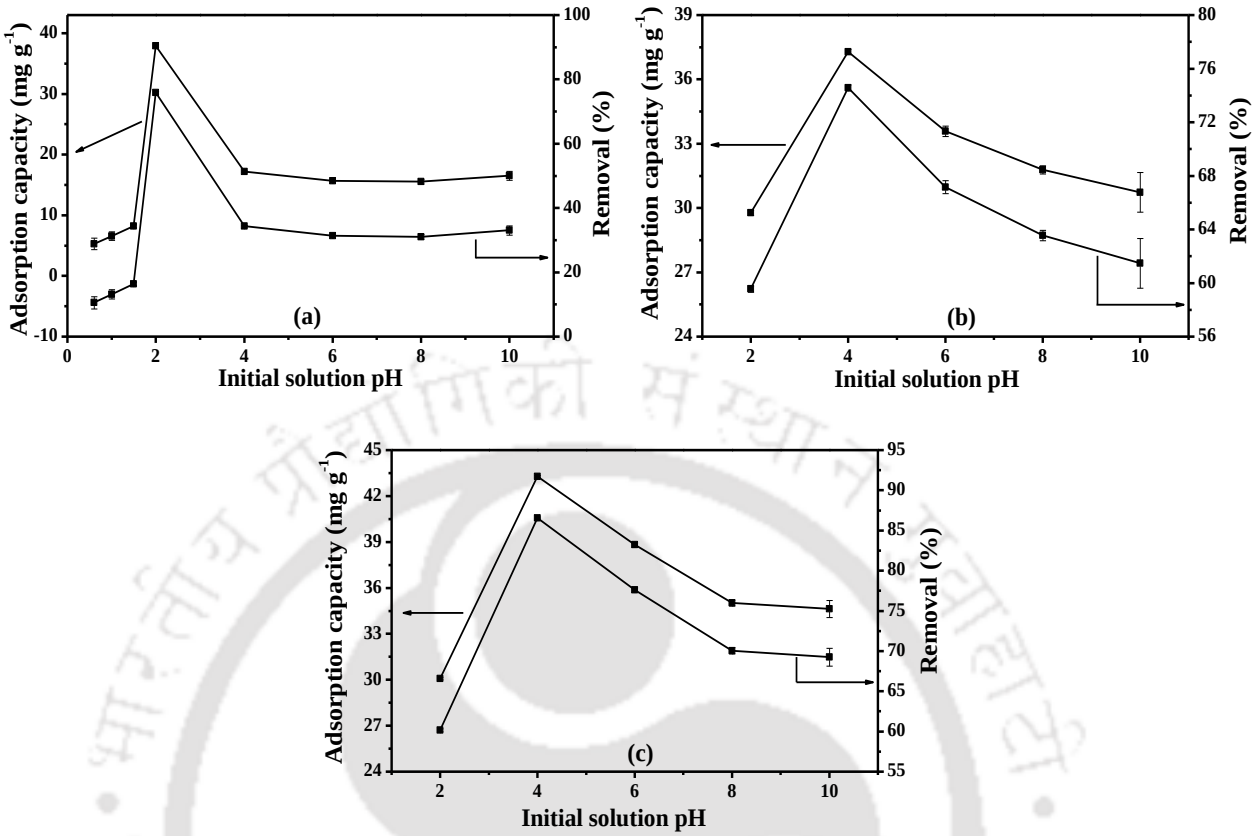

Fig. 4.1: Effect of initial solution pH on Pd(II) adsorption characteristics of (a) Amberlyst A21, (b) Amberlite IRA958, and (c) Dowex Marathon MSA resins.

The lower pH range facilitates protonation of $–NH_2$ groups, and due to this reason, the resin exhibits greater affinity to prevalent species ($PdEDTA^{-2}$) and hence higher adsorption capacities. Thus, speciation is in good agreement with solution chemistry complexity associated with pH and respective abundance of species and relevant functional group interactions. Thereby, resin Pd(II) adsorption mechanism can be deduced. Further characterization studies using FESEM and EDX instruments need to supplement the above-summarized speciation analysis. This will be addressed in a later section of the chapter. Based on protonation of amine groups to form a complex with OH^- ions that exist in the $PdEDTA^{-2}$ complex, the Pd(II) adsorption mechanism for the optimal pH value of 4 and lower pH range is illustrated as shown below (Eqs 4.1−4.3):

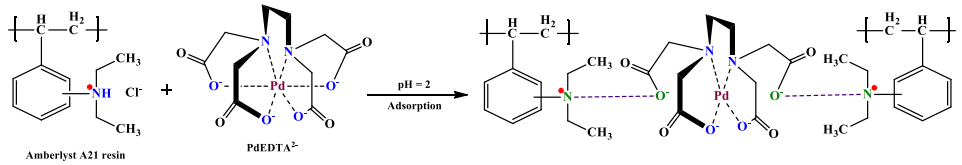

(4.1)

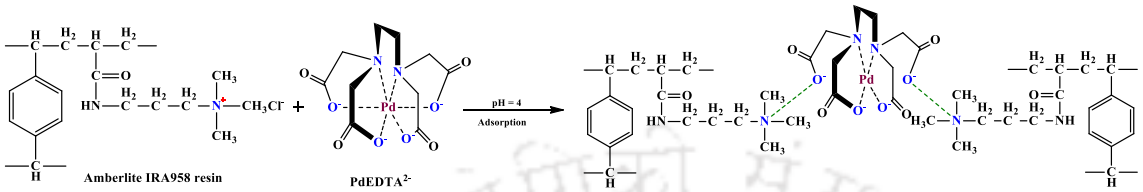

(4.2)

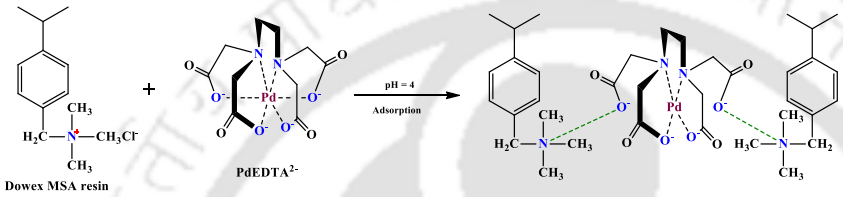

(4.3)

Based on adsorption studies conducted for specified combinations of pH (4 for Dowex MSA and Amberlite IRA 958 and, 2 for Amberlyst A21), contact time (720 min) and initial Pd (II) concentration (50 mg L^{-1}), Figs.4.2a−4.2c depict adsorbent dosage optimality plots associated to Pd(II) adsorption on Amberlyst A21, Amberlite IRA 958 and Dowex MSA, respectively. Thereby, based on optimal removal efficiency and adsorption capacity, the optimal adsorbent dosage has been evaluated as 1.6 g L^{-1} for Amberlite IRA958 and Amberlyst A21, and 1.4 g L^{-1} for Dowex MSA resins, respectively. Corresponding Pd(II) batch adsorption data are 87.79%, 27.44 mg g^{-1} for Amberlite IRA 958, 81.98%, 25.62 mg g^{-1} for Amberlyst A21 and 92.29%, 32.96 mg g^{-1} for Dowex MSA resins. The enhancement in Pd(II) removal efficiency with adsorbent dosage was due to the enhancement in the number of the active sites available for Pd(II) adsorption. Simultaneously, the metal uptake reduced due to the reduction of metal ions available per unit gram of adsorbent.

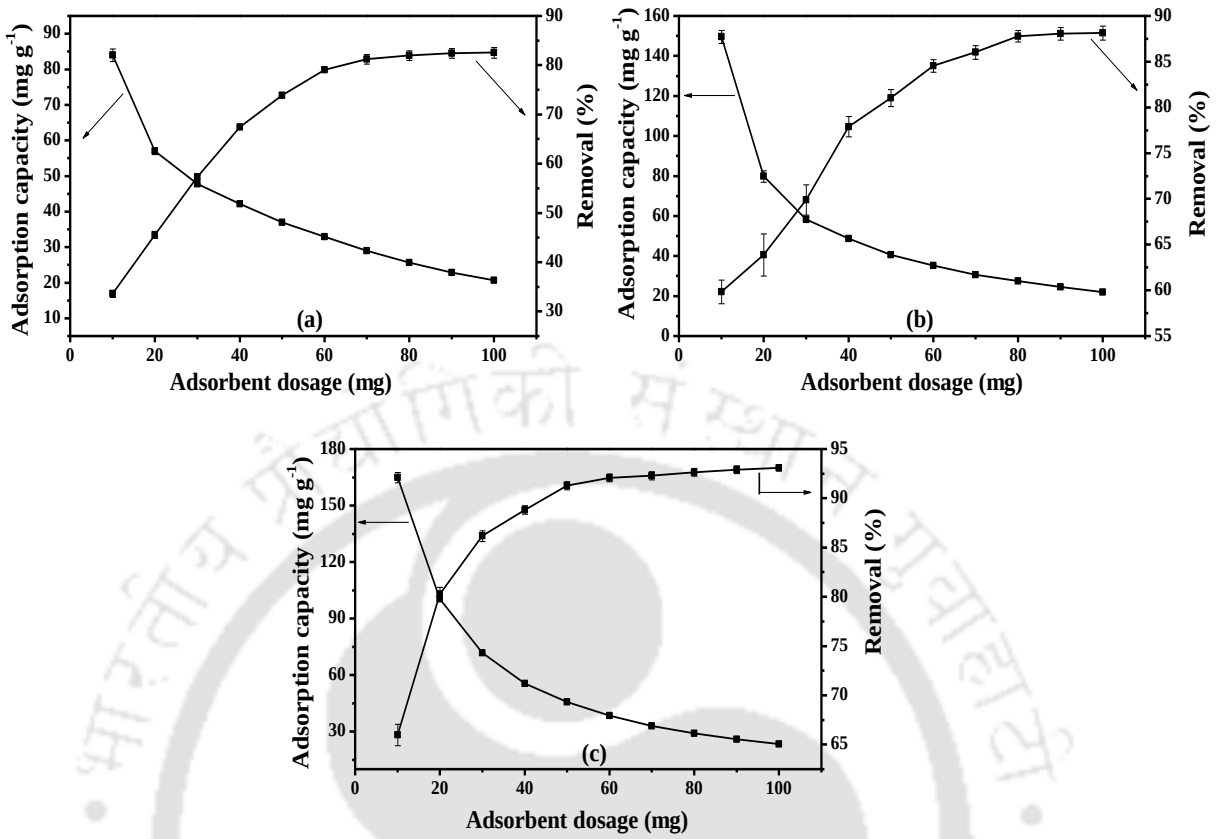

Fig. 4.2: Effect of adsorbent dosage on Pd(II) adsorption characteristics of (a) Amberlyst A21, (b) Amberlite IRA958, and (c) Dowex Marathon MSA resins.

Based on adsorption studies conducted at optimized resin dosage, pH values, and 50 mg L^{-1} initial Pd(II) concentration, Figs.4.3a−4.3c depicts contact time optimality plots associated to Pd(II) adsorption on Amberlyst A21, Amberlite IRA 958 and Dowex MSA, respectively. Optimal contact time values have been evaluated as 840, 720, and 780 min, respectively for the resins at which maximum adsorption capacity (31.56, 26.55, and 24.62 mg g^{-1}, respectively) was obtained. Correspondingly, metal removal % obtained were 88.37, 84.97, and 78.78%.

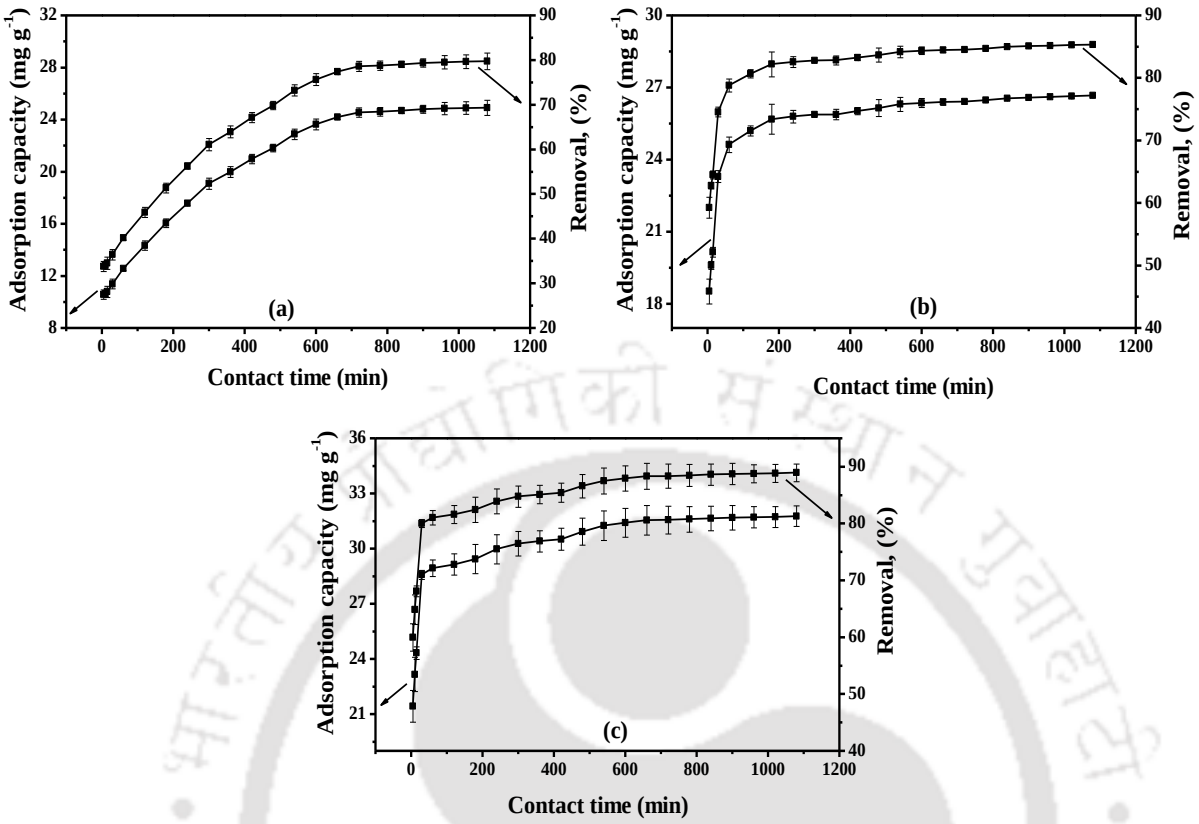

Fig. 4.3: Effect of contact time on Pd(II) adsorption characteristics of (a) Amberlyst A21, (b) Amberlite IRA958, and (c) Dowex Marathon MSA resins.

The effect of Pd(II) concentration (50-300 mg L^{-1}) and temperature (298-333 K) on the Pd(II) adsorption characteristics of commercial resins is illustrated in Figs. 4.4a−4.4f. These experiments were conducted for optimized combinations of adsorption process parameters (pH, dosage, and contact time). Both resins exhibit enhanced metal removal % and adsorption capacity values at higher Pd concentrations (78.78−44.3% and 24.62−83.06 mg g^{-1} for Amberlyst A21 resin and 82.57-57.33% and 25.80-107.50 mg g^{-1} for Amberlite IRA958 and, 88.02-64.49% and 31.44-138.19 mg g^{-1} for Dowex MSA). In agreement with theoretical insights, both resins exhibit lower % removal at the higher temperature (59.10–41.51, 73.50–48.07 and

60.90–33.48%, respectively at 333 K) in comparison those obtained at a lower temperature (82.57–57.33, 88.02–64.49 and 78.78−44.3 % at 298 K).

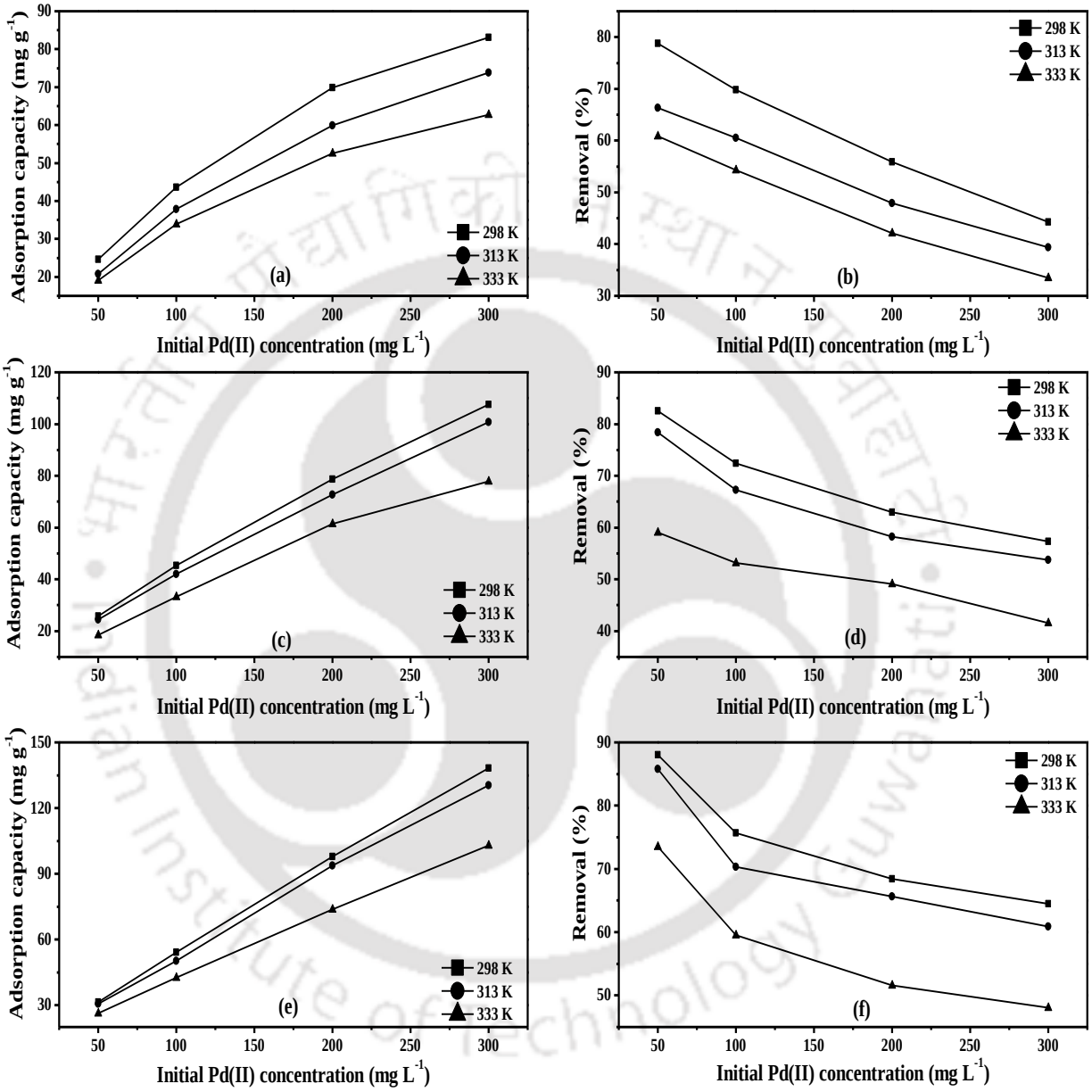

Fig. 4.4: Effect of temperature on Pd(II) adsorption characteristics of Amberlyst A21 (a & b), Amberlite IRA 958 (c & d) and Dowex MSA (e & f) commercial resins.

4.3 Equilibrium, kinetic and thermodynamic model fitness

Figs. 4.5a-4.5c depicts fitness plots for various kinetic models. Table 4.1 summarizes the associated parameters of these fitness plots. Among all models for all resins, the figures and table infer that the pseudo-second-order kinetic model fits well with a regression coefficient value greater than 0.95.

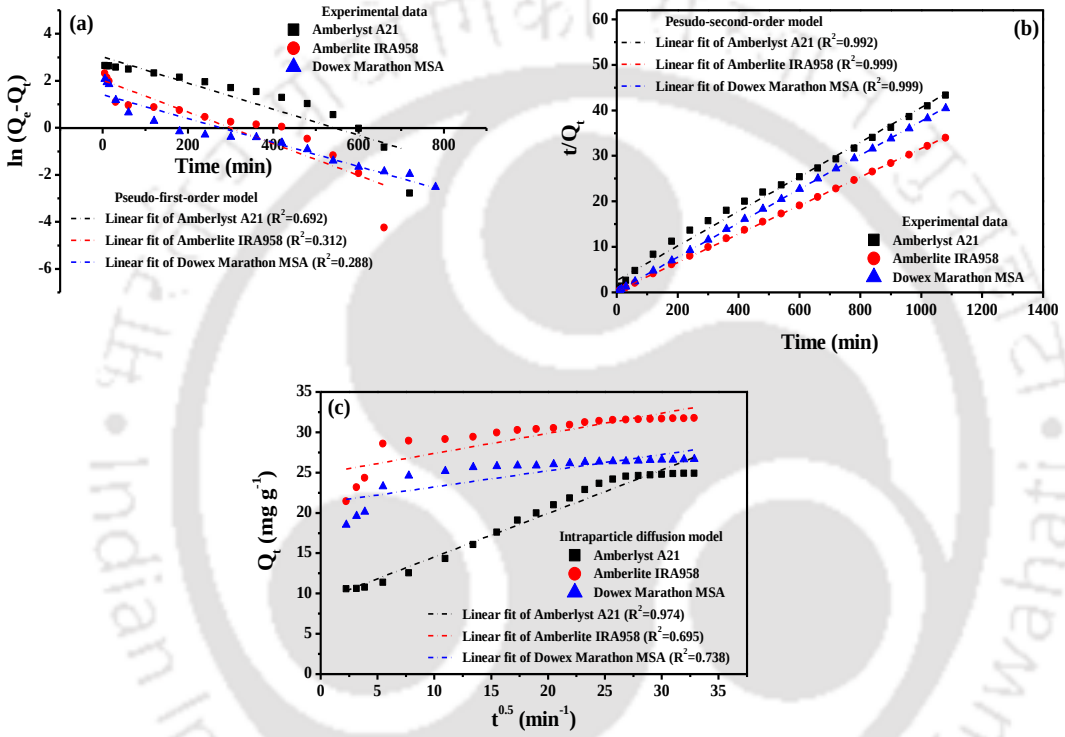

Fig. 4.5: Fitness plots of (a) Pseudo-first order, (b) Pseudo-second order, and (c) Intra-particle diffusion models to represent Pd(II) adsorption kinetics of commercial resins.

Pd(II) adsorption onto three adsorbents followed the pseudo-second-order kinetic model (Fig. 4.5b), which is based on the assumption that the rate-limiting step may be chemisorption involving valency forces through sharing or exchange of electrons with the N atom of all three adsorbents. The fitness of pseudo-second-order model is also justified with the FTIR analysis of

Pd(II) adsorbed commercial resin that inferred strong Pd(II) chemical interaction with the prevalent functional groups of the commercial resins.

Intraparticle diffusion model was also applied to adsorption data in order to analyze whether the intraparticle diffusion mechanism was also involved or not in the Pd(II) adsorption process. A plot of q_t versus $t^{0.5}$ produced a straight line ($R^2 = 0.690$-0.980, Fig. 4.5c). However, the graph didn't pass through the origin, indicating that intraparticle diffusion was involved initially due to faster Pd(II) adsorption on active sites, which cannot be regarded as the rate limiting step.

Figs. 4.6a and 4.6b depict corresponding fitness plots for Langmuir and Freundlich isotherm models, respectively. Table 4.2 summarizes all relevant fitness plot parameters. The Figures and Table convey the best fitness of Freundlich isotherm for Dowex MSA and Amberlite IRA 958, and Langmuir isotherm for Amberlyst A21 to represent measured Pd(II) adsorption characteristics. Also, Table 4.2 affirms R_L value in the range of 0-1. This indicates that for all resins, the chosen adsorbent-adsorbate system is favourable for Pd(II) recovery.

Table 4.1: Regressed kinetic parameters to represent Pd(II) adsorption kinetics of commercial resins.

Experimental capacity (Q_{exp}, mg g^{-1})	Pseudo-first order model			Pseudo-second order model			Intra-particle Diffusion model		
	Q_e (mg g^{-1})	K_1 (min^{-1})	R^2	Q_e (mg g^{-1})	K_2 (g mg^{-1} min^{-1})	R^2	K_{id} (min mg g^{-1})	C	R^2
Amberlyst A21									
24.62	15.23	6.91×10^{-3}	0.692	26.32	5.50×10^{-4}	0.992	0.539	9.14	0.974
Amberlite IRA958									
26.55	5.19	4.38×10^{-3}	0.312	26.74	5.31×10^{-3}	0.999	0.201	21.21	0.695
Dowex Marathon MSA									
31.56	12.92	4.84×10^{-3}	0.288	31.95	3.12×10^{-3}	0.999	0.250	24.87	0.738

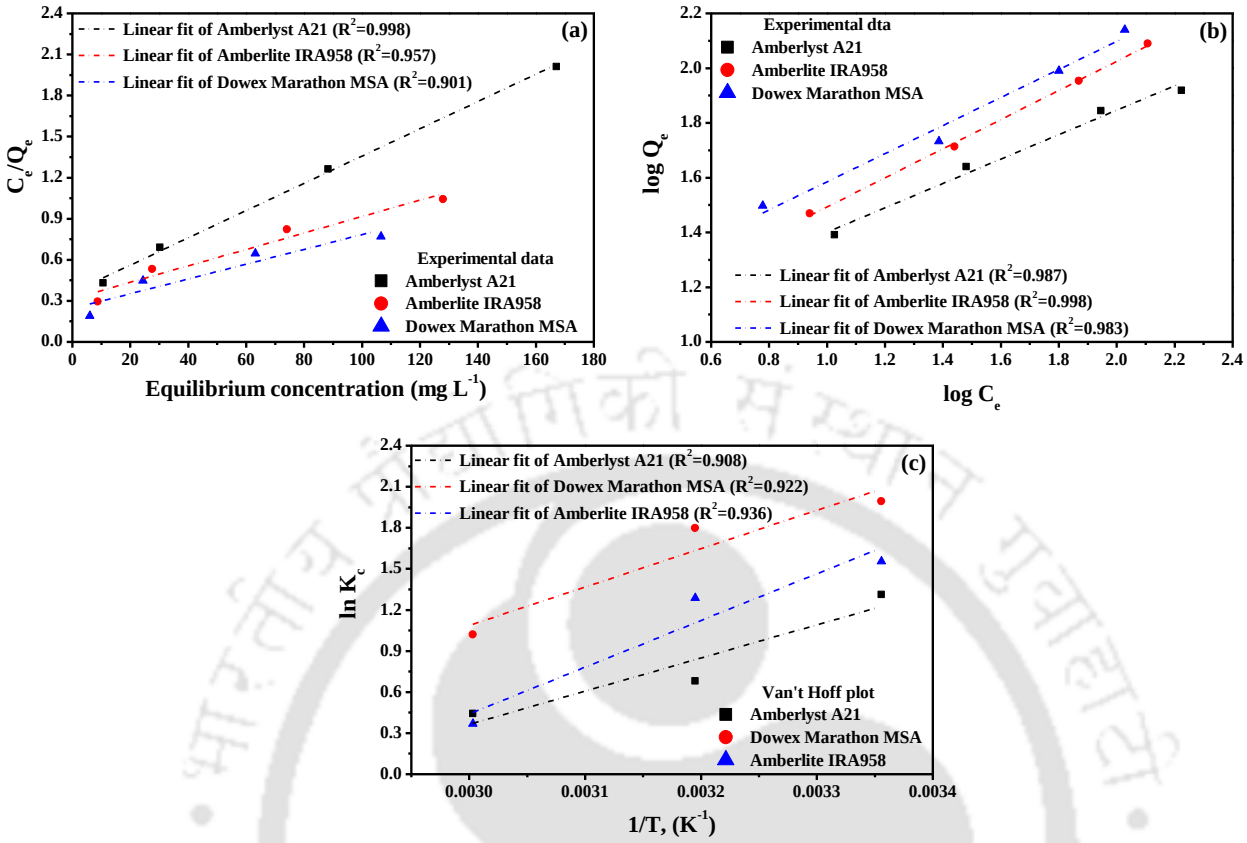

Fig. 4.6: Fitness plots of (a) Langmuir equilibrium, (b) Freundlich equilibrium, and (c) Van't Hoff thermodynamic models for Pd(II) adsorption with commercial resins.

Table 4.2: Regressed model parameters to represent Pd(II) adsorption equilibrium data of commercial resins.

Temperature (K)	Langmuir parameters				Freundlich parameters		
	Q_o (mg g^{-1})	b (L mg^{-1})	R^2	R_L	K_f	n	R^2
Amberlyst A21 resin							
298	100	0.028	0.998	0.419-0.108	8.99	2.247	0.987
313	99.01	0.016	0.998	0.564-0.177	4.97	1.890	0.983
333	83.33	0.015	0.999	0.571-0.182	4.39	1.949	0.981
Amberlite IRA958							
298	166.67	0.019	0.957	0.512-0.149	9.15	1.879	0.998
313	163.93	0.015	0.940	0.575-0.184	7.28	1.805	0.996
333	161.29	0.007	0.984	0.738-0.320	2.70	1.456	0.992
Dowex Marathon MSA							
298	185.16	0.022	0.901	0.475-0.131	11.81	1.949	0.983
313	181.82	0.018	0.865	0.529-0.158	10.23	1.927	0.967
333	149.25	0.012	0.906	0.626-0.218	5.98	1.808	0.988

Fig. 4.6c and Table 4.3 present relevant thermodynamic parametric findings, which affirm negative combinations of ΔG° and ΔH° values due to spontaneous and exothermic nature of Pd(II) adsorption.

Table 4.3: Regressed thermodynamic model parameters for Pd(II) adsorption using commercial resins.

Temperature (K)	K_c	ΔH° (kJ mol^{-1})	ΔS° (J K^{-1} mol^{-1})	ΔG° (kJ mol^{-1})	R^2
Amberlyst A21 resin					
298	3.71			-3.035	
313	1.97	-20.15	-57.42	-2.174	0.908
333	1.56			-1.025	
Amberlite IRA958					
298	4.74			-4.098	
313	3.62	-28.37	-81.44	-2.877	0.936
333	1.45			-1.248	
Dowex Marathon MSA					
298	7.35			-5.164	
313	6.04	-23.31	-60.89	-4.251	0.922
333	2.77			-3.033	

A comparative assessment of obtained results with those presented in the relevant literatures has been summarized in Table 4.4. For Amberlyst A21 resin, significantly better results were obtained in comparison with the literature data. The literature refers to adsorption capacities of 0.029–0.012 mg g^{-1} for 1.0 M NaCl with 100 mg L^{-1} Pd(II) solutions prepared with 0.1–2.0 M HCl media (Hubicki and Wołowicz 2009). In this work, for the synthetic ELP solution, higher metal uptake values of 24.62–83.06 mg g^{-1} were obtained for 50–300 mg L^{-1} Pd(II) solution concentration. Thus, it can be inferred that additives such as disodium EDTA and NH_4OH didn't detrimentally influence the adsorption characteristics of the Amberlyst A21 resin. For comparison purposes, no relevant literature data is available for Amberlite IRA958 and Dowex Marathon MSA resins and aqueous/chloride based Pd(II) solutions.

Table 4.4: Efficacy of Pd(II) adsorption and desorption characteristics of commercial resins with respect to the best available data in the literature.

Adsorbent name	Type of Solution	pH	Metal ion concentration (mg L^{-1})	Adsorption capacity (mg g^{-1})	Desorption (%)	Reference
Amberlyst A21	ELP	2 (Optimal)	50-300	100	59.66[#]	Present study
Amberlite IRA958		4 (Optimal)		166.67	66.80[#]	
Dowex MSA				185.16	68.08[#]	
Lewatit TP-214	ELP	8 (Optimal)	50-300	172.41	66.95[#]	Nagireddi et al. 2018
Lewatit MonoPlus TP-220	Acidic	-	100-1000	10-99.95	-	Wołowicz and Hubicki 2012
Amberlyst A29	Chloride	0-8	100	0.023-0.006	-	Hubicki and Wołowicz 2009
Amberlyst A21				0.029-0.012		
Duolite GT-73	Chloride and Chloride-nitrate	0-7	195	19.5-35.46	>99.9	Hubicki et al. 2007
				21.27-31.9		
Lewatit TP-214		0-14		171.9-205.6		
				285.4-306.7		
Purolite A-400TL	Aqueous	0-14	100-1000	404.15	-	Wołowicz and Hubicki 2014

[#] With 50 mg L^{-1} initial Pd(II) solution concentration

4.4 Characterization of commercial resins

4.4.1 FTIR spectra

Fourier transform infrared (FTIR) spectroscopy was conducted for raw and Pd(II) loaded Dowex marathon MSA, Amberlite IRA958, and Amberlyst A21 commercial resins in the wavelength range of 400–4000cm^{-1}. Figs. 4.7 and 4.8 depict the FTIR spectra of Dowex MSA and Amberlite IRA958 resins, respectively. For both anion exchanging resins, very significant and broader band of −OH stretching vibration exists in the higher frequency region (3400−3200 cm^{-1}). For pure Dowex MSA resin, few peaks exist about 3021 and 2928 cm^{-1}. These correspond to symmetric or asymmetric stretching vibrations of the C−H bonds ((3021 cm^{-1} υ_{as}(C–H)) and $–CH_2$ groups

(2928 cm^{-1} $\upsilon_{as}(-CH_2)$) associated to the cross-linked polystyrene matrix of the anion exchanging resins.

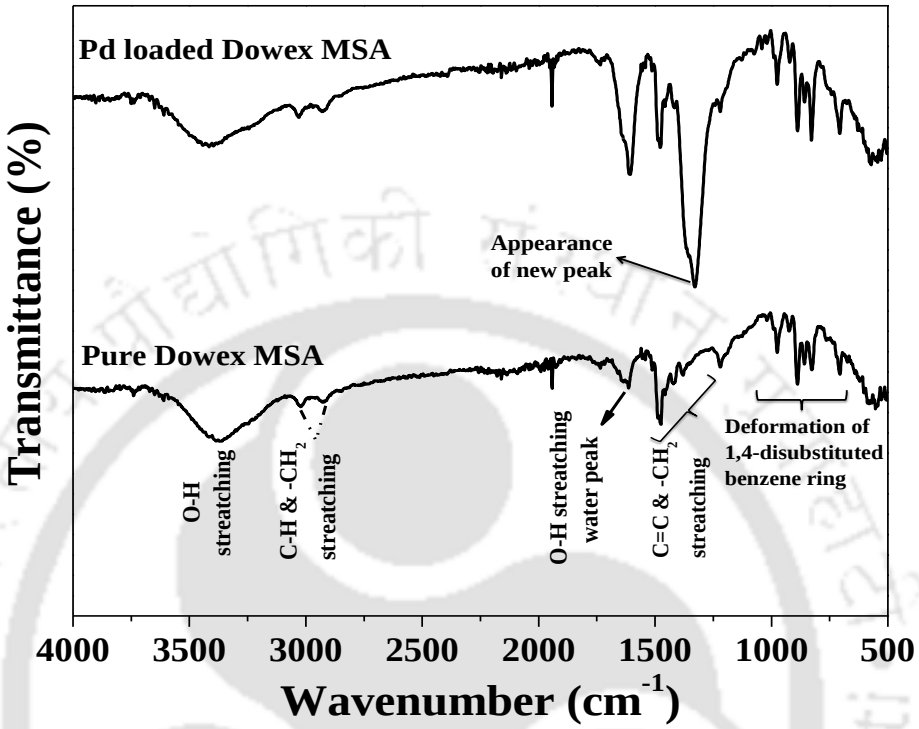

Fig. 4.7: FTIR spectra of raw and Pd(II) loaded Dowex Marathon MSA resins.

Further, it is well known that –OH group vibrations arise due to pertinent water molecules in the resin, and hence these can be observed at 1641 cm^{-1} (δ(O–H)). The asymmetric, stretching vibrations of carbon-carbon bonds in the ring (υ_{as}(C=C)) and asymmetric, scissoring vibrations of methylene groups ($\delta_{as}(-CH_2)$) exist at frequencies of 1473, 1419, 1381 cm^{-1}. The deformation vibrations of 1,4−disubstituted benzene ring associated to styrene–divinylbenzene matrix(S–DVB) of the resin can be affirmed in the 975−823 cm^{-1} wavenumber range(Socrates 2001, Nska et al. 2008, Nski et al. 2008).

Similar functional group fitness with prevalent peaks can be observed for the Amberlite IRA 958 resin (Fig. 4.8). For the fresh resin, asymmetric stretching of alkane ($\upsilon_{as}(-CH_2)$) was observed at

a frequency of 2940 cm^{-1}. Also, peaks appearing in the frequency range of 1651−1595, 1460−1326, and 1262 cm^{-1} have been assigned to C−C stretching, C−H deformation, and C−N stretching bonds, respectively.

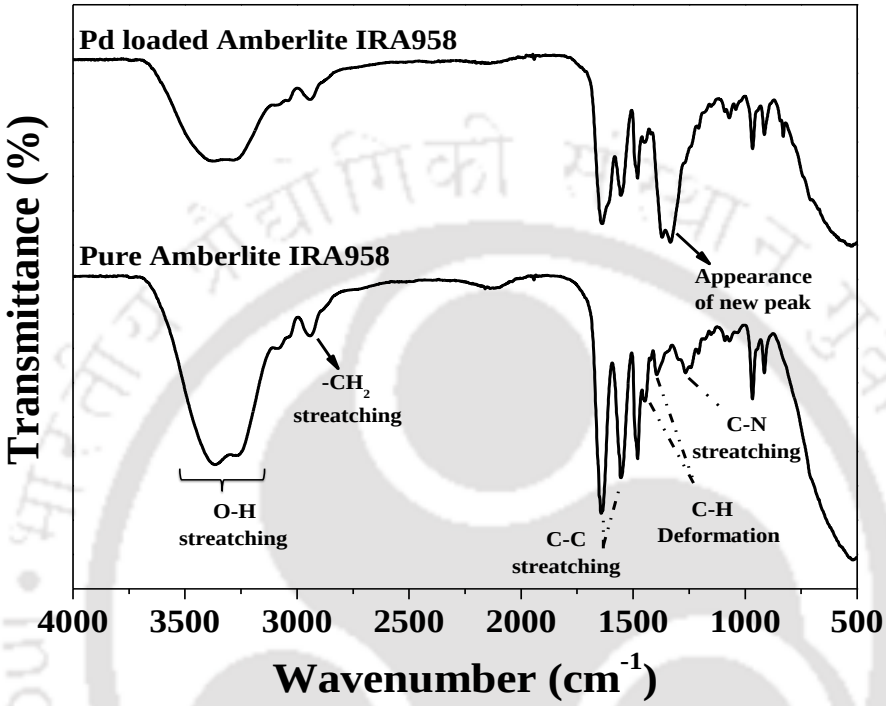

Fig. 4.8: FTIR spectra of raw and Pd(II) loaded Amberlite IRA958 resins.

Further, peaks corresponding to ($–N^{+}(CH_3)$) functional group of Amberlite IRA 958 can be observed at a frequency of 1480 cm^{-1}, whose intensity reduced for the Pd loaded resin. For the Pd loaded resins, new peaks appeared at 1327 and 1334 cm^{-1} for Dowex MSA and Amberlite IRA958 resins, respectively. These peaks have been assigned to the interaction of relevant Pd species with the pertinent functional groups of the resin.

Fig. 4.9 illustrates the FTIR spectral profiles of fresh and Pd-loaded for Amberlyst A21 resin. For fresh Amberlyst A21, the C−H stretching vibrations of alkane was observed at a wavelength range of 3000-2850 cm^{-1}. At a frequency of 1360-1080 cm^{-1}, C−N stretching vibrations of amine

has been observed. Subsequently, at 1680-1620, 1600-1400, and 1000-675 cm^{-1} frequencies, C=C stretching vibrations of conjugated alkene, aromatic stretching vibrations of C=C and =C−H bending vibrations of alkene were observed, respectively.

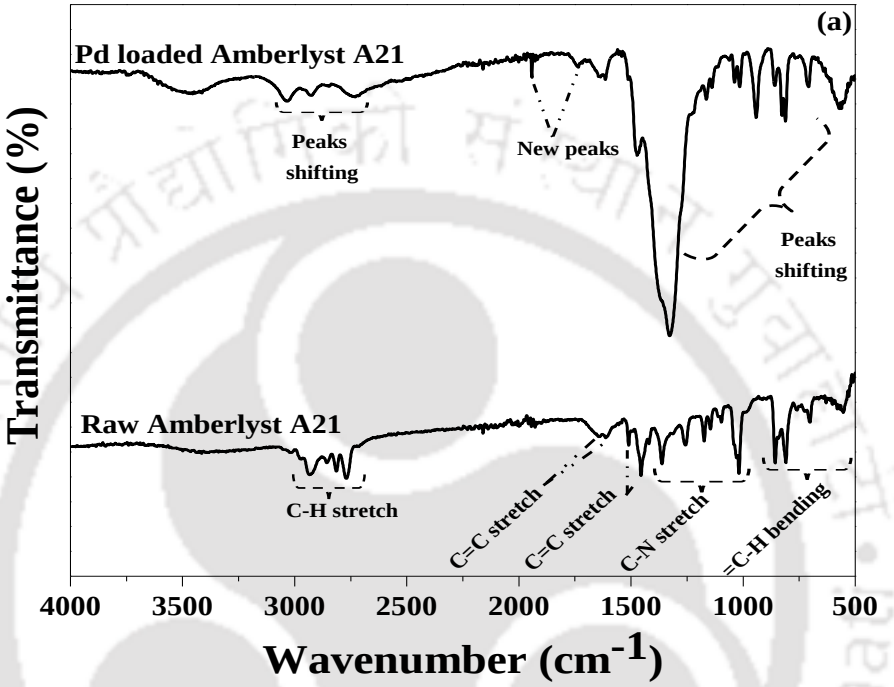

Fig. 4.9: FTIR spectra of raw and Pd(II) loaded Amberlyst A21 resins.

However, for Pd(II)-loaded Amberlyst A21, a significant shift in the spectral peaks were observed in 3000-2850, 1680-1620, 1600-1400, 1360-1080 and 1000-675 cm^{-1} wavelength range. For the Pd(II)-loaded resin, new peaks can be observed at 1945 and 1738 cm^{-1}, and this is due to the affinity or bonding of Pd(II) with the –NH group (Boucher and Katz 1967, Belver et al. 2003).

4.4.2 EDX spectra

EDX spectra obtained for pure and Pd(II) loaded Amberlyst A21 (a, b), Amberlite IRA 958 (c, d), and Dowex Marathon MSA (e, f) resins are depicted in Figs. 4.10a−4.10f.

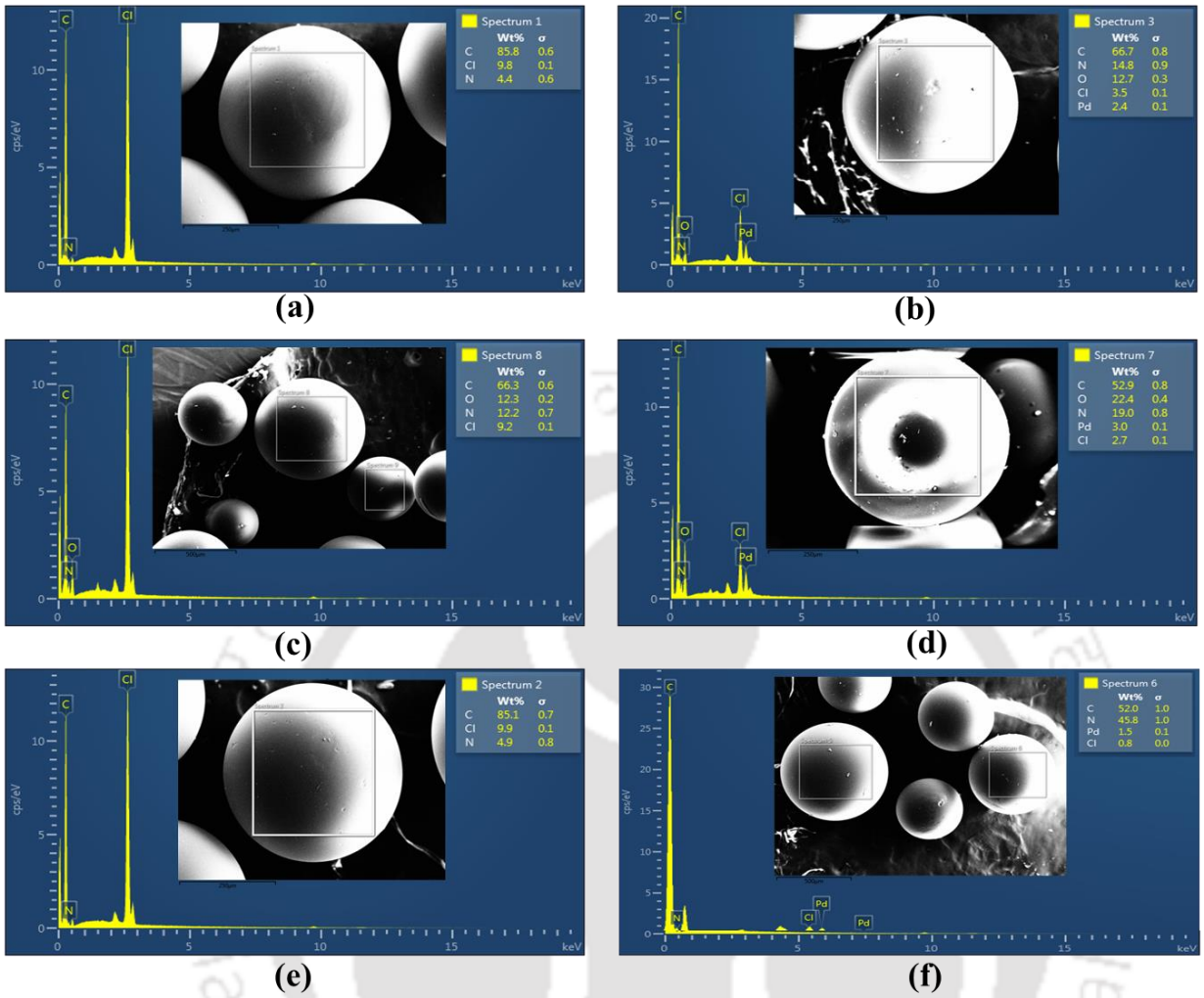

Fig. 4.10: EDX spectra of raw and Pd(II) loaded resins: (a-b) Amberlyst A21, (c-d) Amberlite IRA958 and (e-f) Dowex Marathon MSA resins.

The EDX spectra of Amberlyst A21 (Fig. 4.10a) confirm the presence of C (85.8 atomic weight %), Cl (9.8 atomic weight %), and N (4.4 atomic weight %). For Amberlite IRA958 pure resin, the composition refers to C (66.3%), O (12.3%), N (12.2%), and Cl (9.2%). On the other hand, for the pure Dowex MSA sample, the elemental composition refers to C (85.1%), Cl (9.9%), and N (4.9%). The Pd loaded resins refer to a significant presence of Pd element (2.4% for Amberlyst A21, 3.0% for Amberlite IRA 958, and 1.5% for Dowex Marathon MSA after Pd(II) adsorption with synthetic ELP).

4.5 Batch desorption characteristics of commercial resins

For an initial Pd(II) solution concentration of 50 mg L^{-1} for Dowex MSA and Amberlite IRA958 and 100 mg L^{-1} for Amberlyst A21, the adsorption experiments with commercial resins indicated an average capacity of 40.23, 40.21 and 85.94 mg g^{-1} for Dowex MSA, Amberlite IRA958, and Amberlyst A21 resins, respectively. Using 2 N KOH eluent, these spent resins (for Amberlite IRA958 and Dowex MSA) provided maximum desorption of 66.80 and 68.09%, respectively and, 59.66% for Amberlyst A21 resin (with 0.1N NaOH eluent). For other eluent concentrations, the obtained desorption characteristics have been presented in Table 4.5. Thus, it is apparent that reasonable desorption based recovery has been obtained with eluents prepared with common acids and bases, and the chosen resins are competent for Pd(II) reuse applications.

4.6 Efficacy of commercial resins

Table 4.6 summarizes the optimal adsorption-desorption characteristics of alternate commercial resins that have been investigated in this work. The table conveys interesting insights. Firstly, when the cost competitiveness of alternate resins is ignored, Dowex Marathon MSA (containing nitrogen functional groups) performed best but not with respect to equilibrium contacting time. For a similar basis, among sulfur and sulfur-nitrogen containing functional groups, Lewatit TP214 performed the best with faster Pd(II) adsorptive kinetics(Nagireddi et al. 2018). In this regard, it is interesting to note that the nitrogen functional groups containing commercial resins (Dowex MSA) performed better than the resin (in terms of adsorption and desorption capacity) with sulfur and sulfur-nitrogen functional groups (LewatitTP214). Therefore, the conventional norm that sulfur-nitrogen functional groups containing commercial resins outplay nitrogen functional groups has been proven to be illogical in the present study. Secondly, when cost

effectiveness of alternate resins is being considered, Amberlyst A21 can be regarded to be the most effective among all resins, despite exhibiting poorer Pd adsorption capacity and higher optimal contact time. Thirdly, all commercial resins indicated similar desorption characteristics, and this is interesting from the perspective of similar irreversible adsorption characteristics of the commercial resins.

Table 4.5: Summary of evaluated Pd(II) desorption efficiencies for various combinations of commercial resins and eluents.

Desorption Eluent	Desorption efficiency (%)			Desorption Eluent	Desorption efficiency (%)			Desorption Eluent	Desorption efficiency (%)	
	Amberlyst A21	Dowex MSA	Amberlite IRA958		Amberlyst A21	Dowex MSA	Amberlite IRA958		Dowex MSA	Amberlite IRA958
0.1M NaOH	59.66	5.03	5.52	0.1M KOH	58.77	4.52	6.84	0.1M HCl	64.95	62.34
0.3M NaOH	58.12	38.20	15.90	0.3M KOH	57.83	33.01	17.58	0.3M HCl	62.18	59.23
0.5M NaOH	57.40	58.72	32.33	0.5M KOH	57.36	57.45	27.44	0.5M HCl	62.00	51.35
1M NaOH	57.26	59.50	63.23	1M KOH	56.02	64.07	63.74	1M HCl	61.88	30.62
2M NaOH	57.21	60.39	65.83	2M KOH	55.19	68.08	66.80	2M HCl	61.64	24.52

Table 4.6: Comparative assessment of performance and cost efficacy parameters of alternate commercial resins.

Resin	Functional groups containing	Optimal batch adsorption-desorption characteristics*				Cost ($/100g)	Reference
		Dosage (g L^{-1})	Time (min)	Adsorption capacity (mg g^{-1})	Desorption (%)		
Lewatit TP214	S, N	2	300	115.47	66.24	59.71	Nagireddi et al. 2018
Amberlyst A21	N	1.6	780	83.06	66.95	10.14	This work
Amberlite IRA958	N,O	1.6	840	107.50	66.80	22.86	
Dowex Marathon MSA	N	1.4	720	138.19	68.09	41.69	

* 300 mg L^{-1} Pd(II) initial solution concentration

4.7 Summary

Several inferences can be deduced from the experimental and modelling investigations carried out in this work to evaluate the efficacy of commercial resins for Pd(II) recovery and reuse from synthetic electroless plating solutions. Firstly, Amerblite IRA958, Dowex MSA, and Amberlyst A21 commercial resins provided promising adsorptive as well as desorptive performance for Pd(II) recovery and reuse from synthetic ELP solutions, without indicating the strong inhibitory role of Na_2EDTA and NH_4OH additives of the chosen adsorbate system. Secondly, amongst the resins considered in this work, Dowex MSA provided better performance with lower contact time (720 mins) and lower adsorbent dosage (1.4 g L^{-1}) but is expensive. Thirdly, non-homogeneous adsorptive patterns and pseudo-second-order kinetic model have been affirmed in the spontaneous and exothermic Pd(II) adsorption process with the commercial resins. Fourthly,

speciation facilitated upon the evaluation of Pd(II) adsorption mechanism with the available resin functional groups and pertinent species at optimal pH.

Fifthly, among four commercial resins (three commercial resins considered in this work and one resin studied previously) that contain S-N/N/N-O containing functional groups, with appreciable adsorption and desorption characteristic (65-70% removal), Dowex MSA can be inferred to be the best adsorbent for the studied application. Also, free amine groups (in nitrogen functional groups containing resins) have been evaluated to have a significant role in influencing Pd(II) binding and chelation behaviour during adsorption and desorption. Finally, when cost efficacy is being considered, among all four commercial resins (containing either N or N-O or S-N functional groups), Amberlyst A21 has been proven to be most effective despite exhibiting poorer adsorption kinetics and adsorption capacity. Thus, the acid-base theory based generalized rule of thumb has been proven to be ineffective in identifying the most competent commercial resin. In summary, the combinatorial optimality of process parameters, performance characteristics, and commercial resin cost has been verified as a better guideline for the identification of the most efficient commercial resin for Pd(II) recovery and reuse. Such a guideline is superlative to the acid-base theory based general rule of thumb. This guideline is anticipated to serve as a generic guideline to benchmark relevant research associated to adsorption based noble metal recovery and reuse using commercial and synthetic chelating/ion-exchange resins.

Chapter 5:

Pd(II) Adsorption and Desorption Characteristics of Nitrogen Functionalized Chitosan Derivatives

Chapter 5

Pd(II) Adsorption and Desorption Characteristics of Nitrogen Functionalized Chitosan Derivatives

The chapter summarizes experimental and theoretical findings associated to Pd(II) adsorption and desorption characteristics of nitrogen functionalized adsorbents, namely melamine cross-linked chitosan (CH-ME) and triethylenetetramine cross-linked chitosan (CH-TETA) derivatives. Section 5.1 presents relevant background followed by the solubility resistance of derivatives in section 5.2. Section 5.3 briefly accounts for adsorption characteristics. Thereafter, section 5.4 presents Pd(II) desorption characteristics of spent nitrogen functionalized chitosan derivatives using various inexpensive eluents. Section 5.5 briefly describes the findings associated to surface characterizations of raw and Pd loaded derivatives. Finally, a summary of the findings is presented in section 5.6.

5.1 Background

Prior to this work, the nitrogen and sulfur functionalized adsorbents evaluated for Pd(II) recovery and reuse from synthetic ELP solutions are glutaraldehyde cross-linked chitosan derivative and Lewatit TP214 resin. However, many such resins have been evaluated for Pd(II) recovery from aqueous solutions. Therefore, the emphasis of the conducted research examined the role of liquor ammonia and stabilizer (Na_2EDTA) to influence Pd(II) adsorption characteristics for CH-ME and CH-TETA derivatives. Further, simple eluent based desorption was targeted for these chitosan derivatives.

The Pd(II) adsorption characteristics were evaluated for optimal combinations of pH, contact time, adsorbent dosage, and initial Pd(II) concentrations. Surface characterizations were conducted using Fourier Transform-Infrared Spectrophotometer (FTIR), Braummer-Emmet-Teller (BET), X-ray diffractometer (XRD), Thermo Gravimetric Analyser (TGA) and Field Emission Scanning Microscopy equipped energy dispersive X-Ray analyser (FESEM-EDX). For optimized pH, adsorbent dosage, and contact time, adsorption experiments were conducted for a wider range of Pd(II) solution concentrations (50–300 mg L^{-1}). The specific influence of various additives such as Na_2EDTA (stabilizer) and liquor ammonia (NH_3) on Pd(II) adsorption characteristics of nitrogen functionalized chitosan derivatives were addressed.

5.2 Solubility resistance of CH-ME and CH-TETA derivatives

For both resins, the weight loss % has been evaluated to be approximately 1% for both 1M HNO_3 and 1M NaOH solutions. This confirms that the CH-ME and CH-TETA derivatives are stable in the entire pH range (0.5−10). Therefore, this pH range has been considered to evaluate pH optimality for optimal adsorbent performance during batch adsorption studies.

5.3 Pd(II) adsorption characteristics of CH-ME and CH-TETA derivatives

5.3.1 Effect of adsorption parameters on batch adsorption characteristics

Figs. 5.1a and 5.1b illustrate the effect of pH on the Pd(II) adsorptive performance of CH-ME and CH-TETA derivatives, respectively. For both cases, the experiments were conducted at 720 min contact time, 1 g L^{-1} adsorbent dosage, and 50 mg L^{-1} initial Pd(II) concentration, which were set based on few trails and prior experience. For a variation in initial solution pH from 0.5 to 10, the adsorption capacity of CH-ME enhanced from 28.07 mg g^{-1} (pH 0.5) to 36.38 mg g^{-1} (2 pH)

followed by a steady decline to 28.32 mg g^{-1} (pH 10). Corresponding metal removal varied from 56.14–72.76 % (pH 0.5−2) and thereafter declined to 56.64 % (pH 10). For the CH-TETA, the adsorption capacity values varied from 31.85−41.25 and 41.25−32.88 mg g^{-1} for corresponding pH variations from pH 0.5−2 and pH 2−10, respectively. Therefore, the figures illustrate that the optimal removal efficiency and adsorption capacity were obtained at pH 2. There are 72.76% and 36.36 mg g^{-1} for CH-ME and 82.50% and 41.25 mg g^{-1} for CH-TETA derivatives.

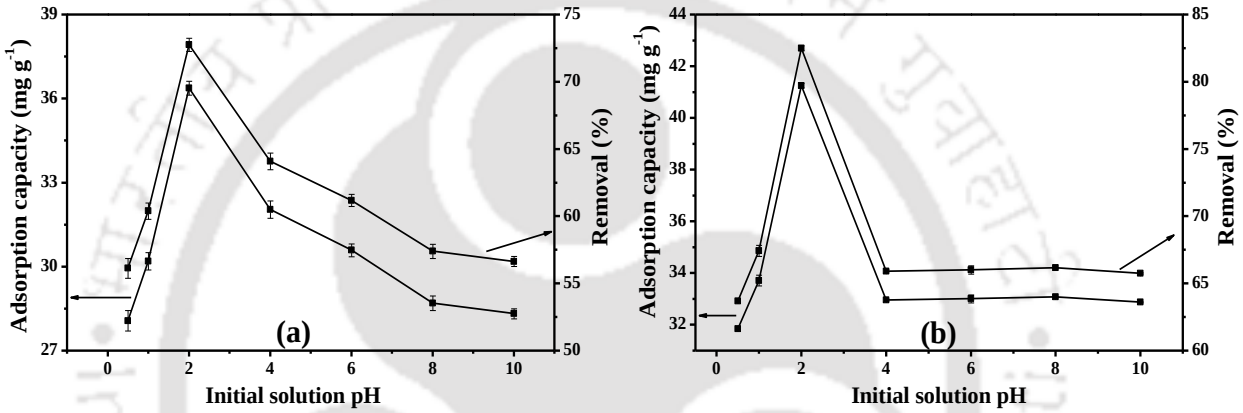

Fig. 5.1: Effect of pH on Pd (II) adsorption characteristics of (a) CH-ME and (b) CH-TETA derivatives.

For low pH range (1−6) and high chloride concentration (33−500 g L^{-1}), Pd(II) mostly exists in $PdEDTA^{2-}$ form and protonation effect will be dominant, i.e., significantly higher influence of H^+ will be prevalent on $–NH_2$ groups (Fujiwara et al. 2007, Ramesh et al. 2008, Zhou et al. 2009). Therefore, $–NH_3^+$ groups exist significantly on the CH-ME and CH-TETA derivatives. These abundant groups will have a stronger affinity to attract $Pd(EDTA)^{-2}$ and therefore facilitate significant adsorption at a pH of 2. Based on this hypothesis, it can be inferred that Pd(II) adsorption on CH-ME and CH-TETA derivatives is very likely to occur due to electrostatic attraction and ion-exchange in the ELP solutions, where in the electrostatic interaction between

protonated amine groups on the CH-ME and CH-TETA derivatives and noble metal ions is according to the following reactions (Eqs. 5.1 and 5.2):

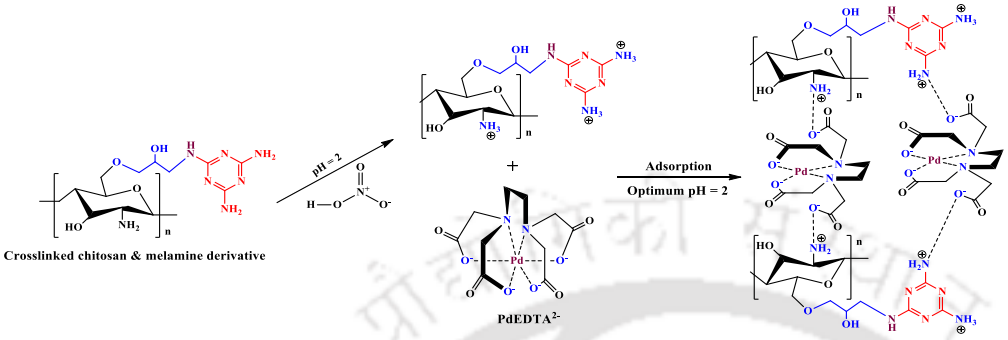

(5.1)

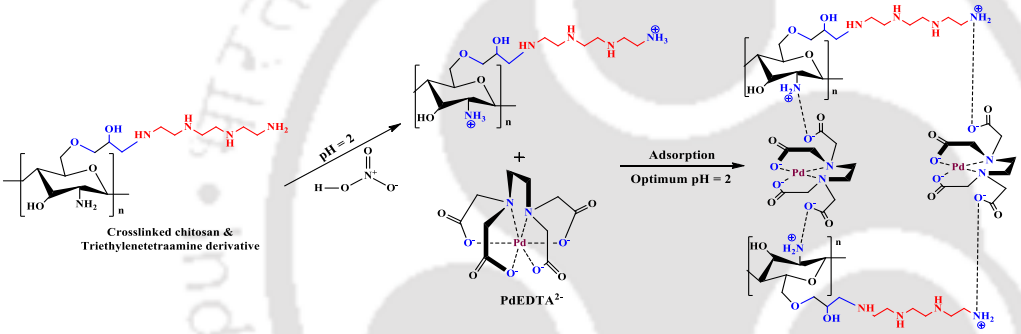

(5.2)

As shown, for both cases of CH-ME and CH-TETA, for an optimal pH of 2, the $PdEDTA^{-2}$ gets functionally bonded to protonated -NH_2 groups prevalent in the resin structure.

Figs. 5.2a and 5.2b illustrate the variation in % removal and adsorption capacity (mg g^{-1}) with adsorbent dosage for both CH-AZ and CH-TETA derivatives. These data were obtained at pH 2 for CH-ME and CH-TETA, 720 min contact time, and 50 mg L^{-1} Pd(II) initial concentration. As shown, for CH-ME derivative, the adsorption capacity reduced from 141.06 to 19.71 mg $g^{-1}$and removal % increased from 56.43 to 78.88 % for a variation in adsorbent dosage from 10 to 100 mg. Similarly, for CH-TETA derivative, the corresponding adsorption capacity reduced from 162.26 to 20.92 mg g^{-1}, and removal % increased from 64.90 to 83.70 %. Based on the trends, the

maximum removal % of 78.79 and 82.49 and relevant adsorptive capacities of 21.89 and 41.25 mg g^{-1} were obtained at an optimal equilibrium dosage of 1.8 and 1 g L^{-1} for the CH-ME and CH-TETA derivatives, respectively. The enhancement in Pd(II) removal efficiency with adsorbent dosage was due to the enhancement in the number of the active sites available for Pd(II) adsorption. Simultaneously, the metal uptake reduced due to the reduction of metal ions available per unit gram of adsorbent.

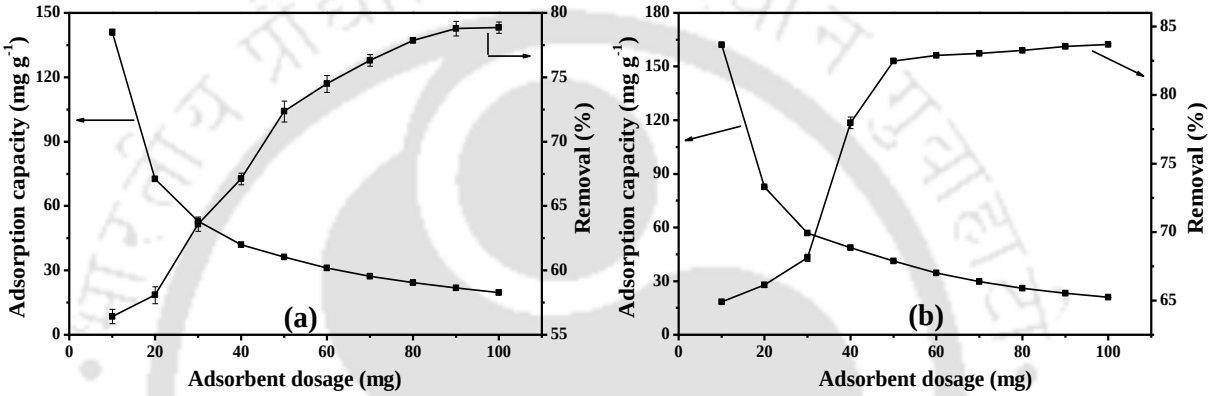

Fig. 5.2: Effect of adsorbent dosage on Pd(II) adsorption characteristics of (a) CH-ME and (b) CH- TETA derivatives.

Figs. 5.3a and 5.3b depict Pd(II) adsorptive performance of CH-ME and CH- TETA derivatives for a variation in contact time. These experiments were conducted at pH 2, 1.8, and 1 g L^{-1} dosage of CH-ME and CH- TETA derivatives, respectively along with 50 mg L^{-1} initial Pd(II) concentration. As shown, for CH-ME derivative, the adsorption process is rapid from 5 to 840 min and reaches equilibrium at 840 min. Similarly, for CH-TETA derivative, the adsorption process is rapid from 5 to 300 min and reaches saturation at 300 min. Based on the profiles, the maximum adsorption capacity was obtained at 840 (22.22 mg g^{-1}) and 300 min (40.76 mg g^{-1}) with corresponding metal removal % of 79.98 and 81.52 for CH-ME and CH- TETA derivatives, respectively.

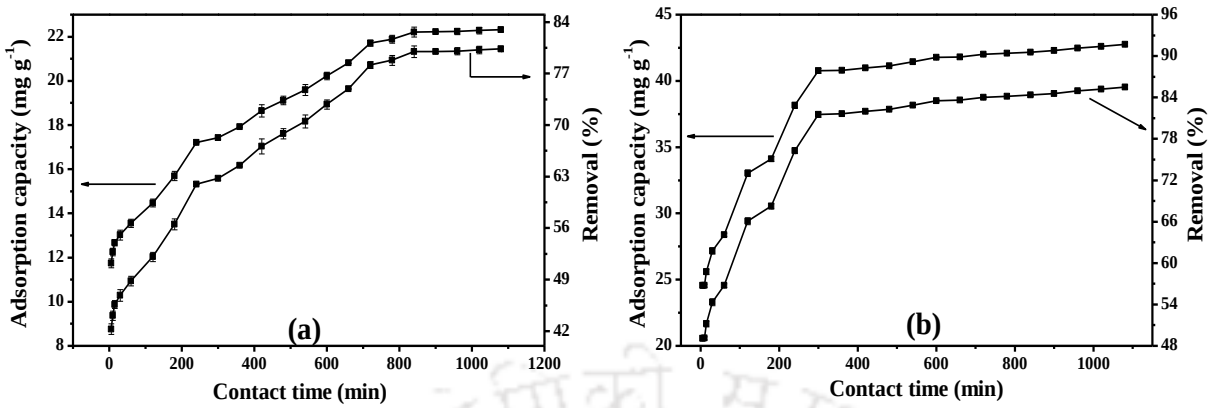

Fig. 5.3: Effect of contact time on Pd(II) adsorption characteristics of (a) CH-ME and (b) CH-TETA derivatives.

Figs. 5.4a−5.4d present the effect of initial Pd(II) concentration and temperature on the adsorptive performance of CH-ME and CH- TETA derivatives with synthetic ELP solution. These experimental investigations were conducted for 50−300 mg L^{-1}Pd(II) solution concentration and 298−333 K temperature and for fixed choice of pH 2, 1.8 g L^{-1} (CH-ME derivative) and 1 g L^{-1} (CH- TETA derivative) adsorbent dosage, and 840 min (CH-ME derivative) and 300 min (CH-TETA derivative) contact time. At 298 K, the Pd(II) capacity and removal % varied from 22.64−85.58, 40.89−117.08 mg g^{-1} and 81.50−51.35, 87.05−39.03 %, for CH-ME and CH- TETA derivatives, respectively. Thus, higher concentrations detrimentally influenced metal removal %. This is in agreement with theoretical insights. The temperature effect on noble metal adsorptive characteristics for both resins is in agreement with the theoretical insight i.e., lower % removal values have been obtained at higher temperature (70.04-45.14 % and 81.78–29.23 % at 333 K for a variation in initial solution concentration from 50−300 mg L^{-1}) than those obtained at lower temperature (81.50-51.35 % and 87.05–39.03 % at 298 K for a variation in initial solution concentration from 50−300 mg L^{-1}) for CH-ME and CH- TETA derivatives, respectively.

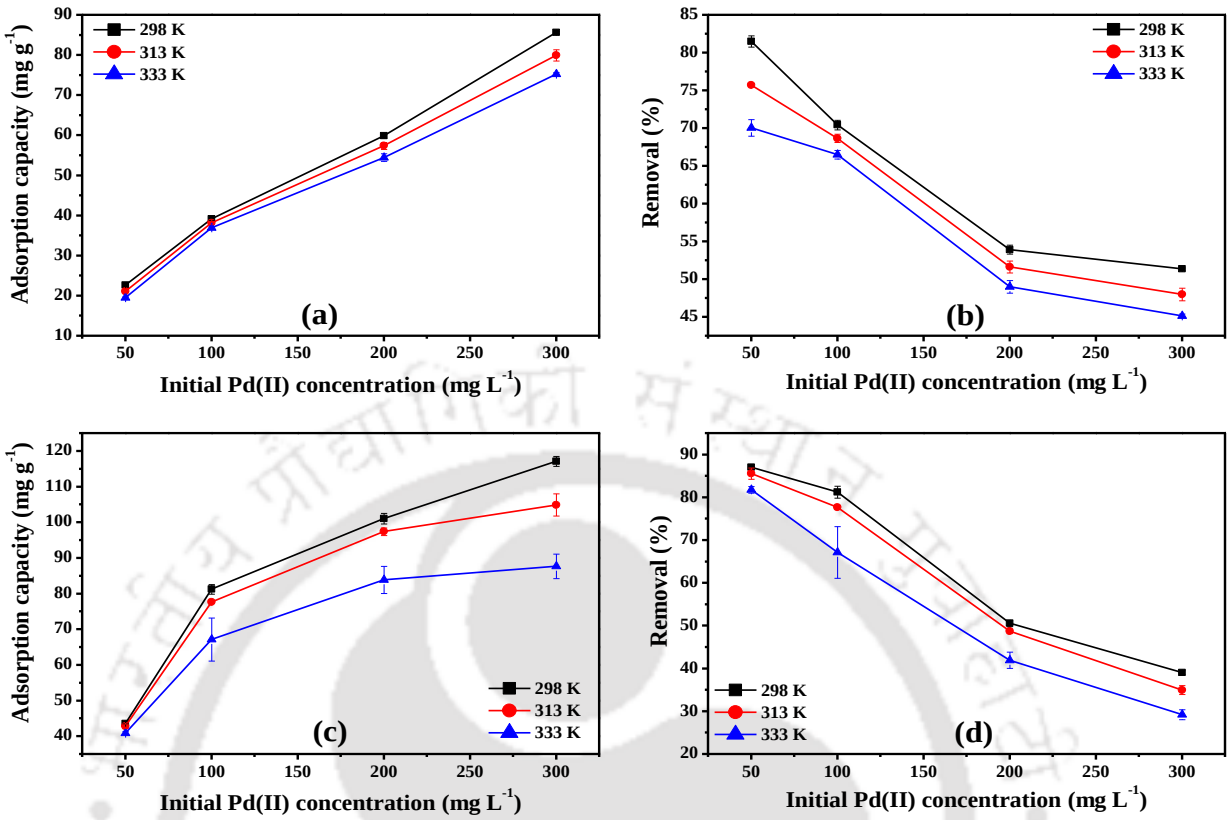

Fig. 5.4: Effect of temperature and initial Pd(II) concentration on adsorption capacity (a, c) and removal % (b, d) for CH-ME (a, b) and CH-TETA (c, d) derivatives.

5.3.2 Equilibrium, kinetic and thermodynamic model parameters

The fitness plots for the kinetic models (pseudo-first-order, pseudo-second-order, and intraparticle diffusion) have been presented in Figs. 5.5a−5.5c. Relevant parameters obtained from the fitness plots are summarized in Table 5.1. As indicated in the table, for both cases, the best fitness corresponds to the pseudo-second-order model for which a regression coefficient greater than 0.95 has been obtained. Further, the model based adsorption capacity was in agreement with the adsorption capacity determined from experimental data. Therefore, pseudo-second-order model has been inferred to be the best fit to represent the kinetics of Pd(II) adsorption from synthetic ELP

solutions onto both CH-ME and CH-TETA derivatives, which is based on the assumption that the rate limiting step may be chemisorption involving valency forces through sharing or exchange of electrons with the N atom of all three adsorbents. The fitness of the pseudo-second-order model is also justified with the FTIR analysis of Pd(II) adsorbed functionalized chitosan resins that inferred strong Pd(II) chemical interaction with the prevalent functional groups of the functionalized chitosan derivatives.

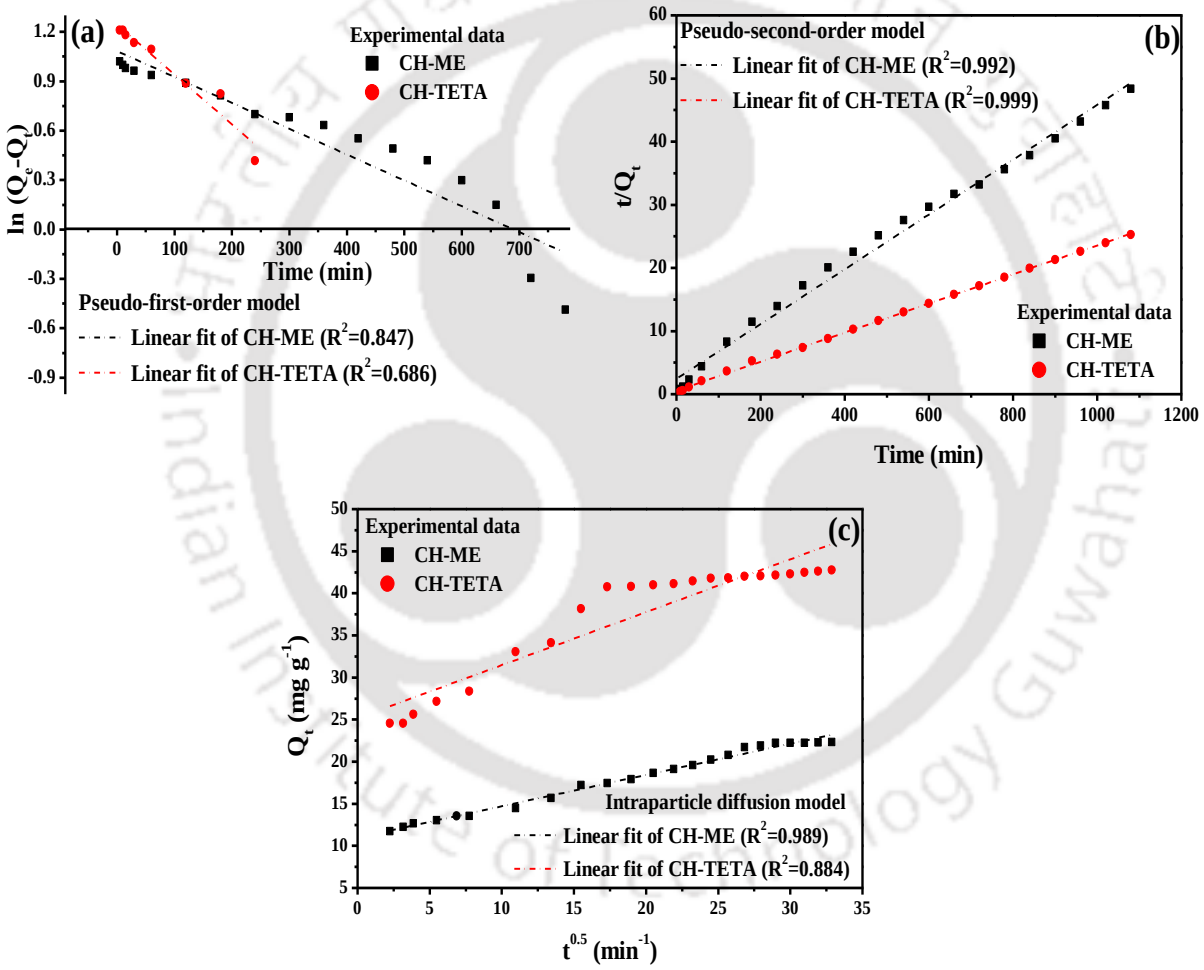

Fig. 5.5: Fitness plots of (a) Pseudo-first order, (b) Pseudo-second order, and (c) Intra-particle diffusion models to represent Pd(II) adsorption kinetics of CH-ME and CH-TETA derivatives.

The intraparticle diffusion model was also applied to adsorption data in order to assess whether the intraparticle diffusion mechanism was also involved or not in the Pd(II) adsorption process in addition to the pseudo-second-order model. A plot of q_t versus $t^{0.5}$ produced a straight line ($R^2 = 0.880$-0.990, Fig. 5.5c). However, the graph didn't pass through the origin, indicating that intraparticle diffusion was involved initially due to faster Pd(II) adsorption on active sites, which cannot be regarded as the rate-limiting step.

Table 5.1: Regressed kinetic parameters to represent Pd(II) adsorption kinetics of CH-ME and CH-TETA derivatives.

Experimental capacity (Q_{exp}, mg g^{-1})	Pseudo-first order model			Pseudo-second order model			Intra particle Diffusion model		
	Q_e (mg g^{-1})	K_1 (min^{-1})	R^2	Q_e (mg g^{-1})	K_2 (g mg^{-1} min^{-1})	R^2	K_{id} (min mg g^{-1})	C	R^2
CH-ME									
22.22	9.82	2.80×10^{-3}	0.686	23.04	7.80×10^{-4}	0.991	0.371	10.9	0.989
CH-TETA									
40.76	8.20	2.80×10^{-3}	0.686	43.48	9.90×10^{-4}	0.999	0.629	25.2	0.884

For both derivatives, the corresponding fitness plots for Langmuir and Freundlich equilibrium models are depicted in Figs. 5.6a and 5.6b, respectively. Table 5.2 summarizes relevant model parameters and the regression coefficient (R^2).

Table 5.2: Regressed model parameters to represent Pd(II) adsorption equilibrium data of CH-ME and CH-TETA derivatives.

Temperature (K)	Langmuir parameters				Freundlich parameters		
	Q_o (mg g^{-1})	b (L mg^{-1})	R^2	R_L	K_f	n	R^2
CH-ME							
298	104.17	0.022	0.931	0.475-0.131	8.08	2.168	0.988
313	101.01	0.019	0.954	0.516-0.151	6.31	2.009	0.985
333	99.01	0.016	0.959	0.559-0.175	5.02	5.018	0.971
CH-TETA							
298	121.95	0.079	0.995	0.041-0.202	30.08	3.713	0.892
313	109.89	0.091	0.999	0.035-0.180	29.09	3.883	0.891
333	92.59	0.084	0.999	0.038-0.193	25.80	4.140	0.934

The illustrated figures and table confirm best fitness of Freundlich and Langmuir models for CH-ME and CH-TETA derivatives, respectively to represent measured batch equilibrium data. For both cases, Table 5.2 confirms a R_L value of 0−1, and this value range conveys that the ELP-modified chitosan derivatives system is favourable for adsorption based Pd(II) recovery.

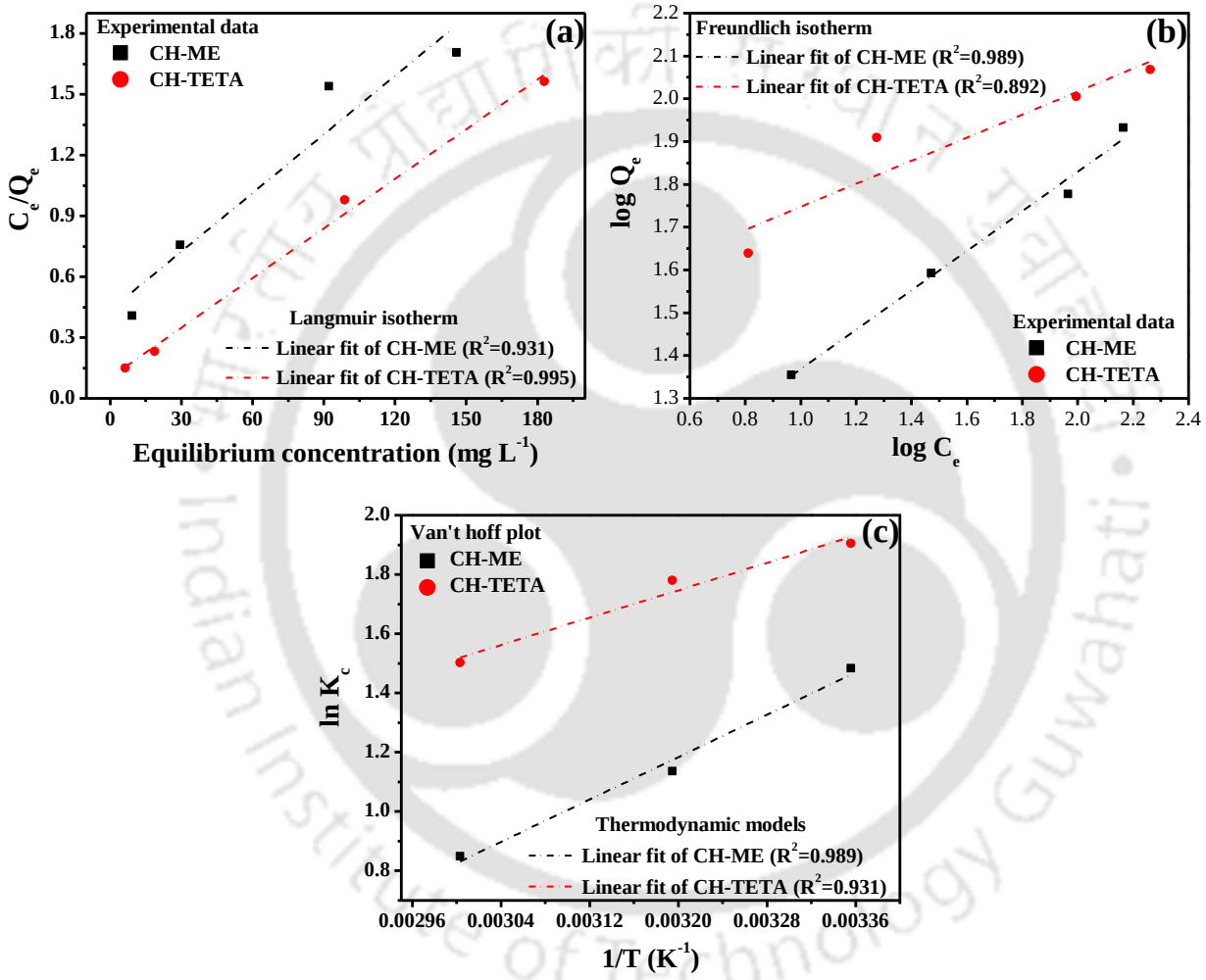

Fig. 5.6: Fitness plots of (a) Langmuir equilibrium, (b) Freundlich equilibrium, and (c) Van't Hoff thermodynamic models for Pd(II) adsorption with CH-ME and CH-TETA derivatives.

For both derivatives, Fig. 5.6c depicts the thermodynamic behaviour of the Pd(II) adsorption process, and Table 5.3 summarizes relevant parameters obtained for the Van't Hoff's model. For

the said cases, the table confirms negative ΔG° and negative ΔH° values, and these infer spontaneous and exothermic Pd(II) adsorption, respectively.

Table 5.3: Regressed thermodynamic model parameters for Pd(II) adsorption using CH-ME and CH-TETA derivatives.

Temperature (K)	K_c	ΔH° (kJ mol^{-1})	ΔS° (J K^{-1} mol^{-1})	ΔG° (kJ mol^{-1})	R^2
CH-TETA					
298	4.41			-3.622	
313	3.12	-14.86	-37.70	-3.056	0.989
333	2.34			-2.303	
CH-AZ					
298	6.72			-4.774	
313	5.93	-9.60	-16.19	-4.531	0.973
333	4.49			-4.207	

5.4 Desorption characteristics of Pd(II) loaded CH-ME and CH-TETA derivatives

Pd(II) desorption studies were conducted for both CH-ME and CH-TETA derivatives to recover Pd(II) using media prepared with various eluents. For both derivatives, after adsorption experiments, an average capacity of 16.95 and 38.57 mg g^{-1} was obtained for CH-ME and CH-TETA derivatives, respectively. Based on desorption experiments and mass balance, maximum desorption % was obtained as 59.82 (with 2M H_2SO_4) and 39.68 % (with 2M HCl eluent) for CH-ME and CH-TETA derivatives, respectively. Table 5.4 summarizes the Pd(II) desorption efficiencies for various eluent concentrations. Reasonable desorption % was obtained for other eluent systems prepared with common acids and bases. Considering the solution complexity of ELP solutions and deployed eluent systems, the obtained desorption data with simple eluents can be inferred to be reasonably satisfactory from the perspective of Pd(II) recovery and reuse.

Based on the explanation provided in section 1.3.3, most researchers used complex and expensive eluents such as EDTA, Thiourea, EDTA-H_2SO_4, Thiourea–HCl, and KCN–NaOH to recover Pd(II) from spent adsorbents, which are expensive, toxic and non-sustainable in industrial scale adsorption based recovery and reuse systems and methodologies. Such eluents will have functional interactions and can enable the achievement of 99% desorption removal efficiencies. However, the recovered Pd(II) cannot be reused due to complex chemistry associated to the formation of relevant stable species. Hence, we considered simple acids and bases as eluents to minimize the complexity and cost of the process. Considering these issues, the CH-ME derivative has been reported to provide good desorption characteristics despite indicating a moderately higher desorption efficiency value of about 58%.

Table 5.4: Summary of evaluated Pd(II) desorption efficiencies for various combinations of eluents and CH-ME/CH-TETA derivatives.

Desorption Eluent	Desorption efficiency (%)		Desorp-tion Eluent	Desorption efficiency (%)		Desorp-tion Eluent	Desorption efficiency (%)		Desorption Eluent	Desorption efficiency (%)	
	CH-TETA	CH-ME		CH-TETA	CH-ME		CH-TETA	CH-ME		CH-TETA	CH-ME
0.1M NaOH	27.74	31.45	0.1M KOH	31.74	38.51	0.1M HCl	36.38	41.19	0.1M H_2SO_4	29.08	46.41
0.5M NaOH	23.52	19.19	0.5M KOH	18.52	24.09	0.5M HCl	37.52	45.08	0.5M H_2SO_4	35.04	52.26
1M NaOH	21.49	15.61	1M KOH	15.49	24.04	1M HCl	37.62	46.49	1M H_2SO_4	36.08	56.54
2M NaOH	15.45	14.59	2M KOH	10.45	21.06	2M HCl	39.68	49.68	2M H_2SO_4	37.67	59.82

The experimental findings with respect to optimality of adsorption parameters, adsorption, and desorption characteristics of CH-ME and CH-TETA derivatives have been compared with the best available literature for most relevant adsorbate (electroless plating solutions) and adsorbent

systems (chitosan, chitosan-derivatives, and commercial resins). A summary of these findings is presented in Table 5.5. For electroless plating adsorbate systems, data of our research group is the only relevant data to compare adsorbent performance, as other relevant literature focused only on aqueous acidic solutions. Based on data summarized in the table, the following can be inferred:

a) From Pd(II) removal perspective and for synthetic ELP solutions, among chitosan derivatives, CH-TETA performed similar to the glutaraldehyde cross-linked chitosan in terms of adsorption capacity (121.95 mg g^{-1} for 50-300 mg L^{-1} initial Pd(II) solution concentration range compared to 166.67 mg g^{-1} for 50-500 mg L^{-1} initial Pd(II) solution concentration range). However, the CH-ME derivative was marginally poor with respect to glutaraldehyde cross-linked chitosan (104.17 mg g^{-1} for 50-300 mg L^{-1} initial Pd(II) solution concentration range compared to 166.67 mg g^{-1} for 50-500 mg L^{-1} initial Pd(II) solution concentration range). Hence, the performance of CH-ME and CH-TETA derivatives is comparable with glutaraldehyde cross-linked chitosan resin for both adsorption and desorption characteristics. Both these resins studied in this work performed excellent in terms of Pd removal but satisfactory in terms of Pd recovery and reuse.

b) From Pd(II) recovery and reuse perspective and for synthetic ELP solution, the CH-ME derivative performed excellent (59.82 compared to 42.35 desorption %). However, the performance of CH-TETA is marginally poor (39.68 compared to 42.35 desorption %). In addition, the desorption efficiency is significantly better than that of chitosan. Hence, from Pd(II) recovery and reuse perspective, CH-ME is the best among CH-ME, CH-TETA, and glutaraldehyde cross-linked chitosan.

c) All other literature data cannot be compared to obtained data in this work, as these literature target Pd(II) recovery from acidic solutions and expensive eluents.

Table 5.5: Efficacy of Pd(II) adsorption and desorption characteristics of CH-ME and CH-TETA derivatives with nitrogen functionalized adsorbents reported in the literature.

Adsorbent name	Pd(II) concentration (mg L^{-1})	Adsorbent dose (g L^{-1})	pH	Adsorption capacity (mg g^{-1})	Eluent	Desorption (%)	Reference
Melamine cross-linked chitosan	50-300	1.8	2	104.17	2M H_2SO_4	59.82*	Present study
Triethylenetetramine cross-linked chitosan		1		121.95	2M HCl	39.68*	
Glutaraldehyde cross-linked chitosan	50-500	0.6	8	166.67	0.1M HCl	42.35*	Nagireddi et al. 2017
Ethylenediamine modified magnetic chitosan nanoparticles	60	0.5	2	138	0.4M H_2SO_4−1.0M Thiourea	90.5	Zhou et al. 2010
L-lysine modified cross-linked chitosan	400	0.1	2	109.47	0.7M Thiourea–2M HCl	99.98	Fujiwara et al. 2007
Glycine modified cross-linked chitosan	500	3.33	2	120.39	0.7M thiourea–2M HCl	98.27	Ramesh et al. 2008

* All desorption studies were conducted at Pd(II) concentration of 50 mg L^{-1}.

5.5 Surface characterizations of raw and Pd(II) loaded derivatives

5.5.1 FTIR spectra

The FTIR spectra confirm upon the existence of various functional groups both in raw, modified, and Pd loaded modified chitosan (Figs. 5.7 and 5.8). For raw chitosan, the peak appeared at 3436 cm^{-1} has been attributed to stretching vibrations of hydroxyl (−OH) and amine ($-NH_2$) groups. It also conveys the overlapping of intermolecular hydrogen bonds with one another. The existence of one amine spike around 3436 cm^{-1} wavenumber confirms that a secondary amine group in the chitosan. A peak appearing at 1654 cm^{-1} affirms carbonyl group stretching vibration of amide I. Spectral peak at 1154 cm^{-1} is affirming –CH vibration. Peak at 1078 cm^{-1} wavenumber is confirming –CONH- group.

The FTIR spectra of CH-ME (Fig. 5.7) convey significantly new peaks at 1564 cm^{-1} and in between 1460-1220 cm^{-1}. These have been attributed to stretching vibrations of N-H and C-N-C groups, respectively (Lambert et al. 1976, Silverstein et al. 1991) and thereby infer definite cross-linking of melamine onto chitosan backbone. The interactions of Pd ions with primary amine groups in the structure of CH-ME was confirmed by the shift in the peak from 3436 to 3293 cm^{-1} and the disappearance of peak at 1564 cm^{-1}.

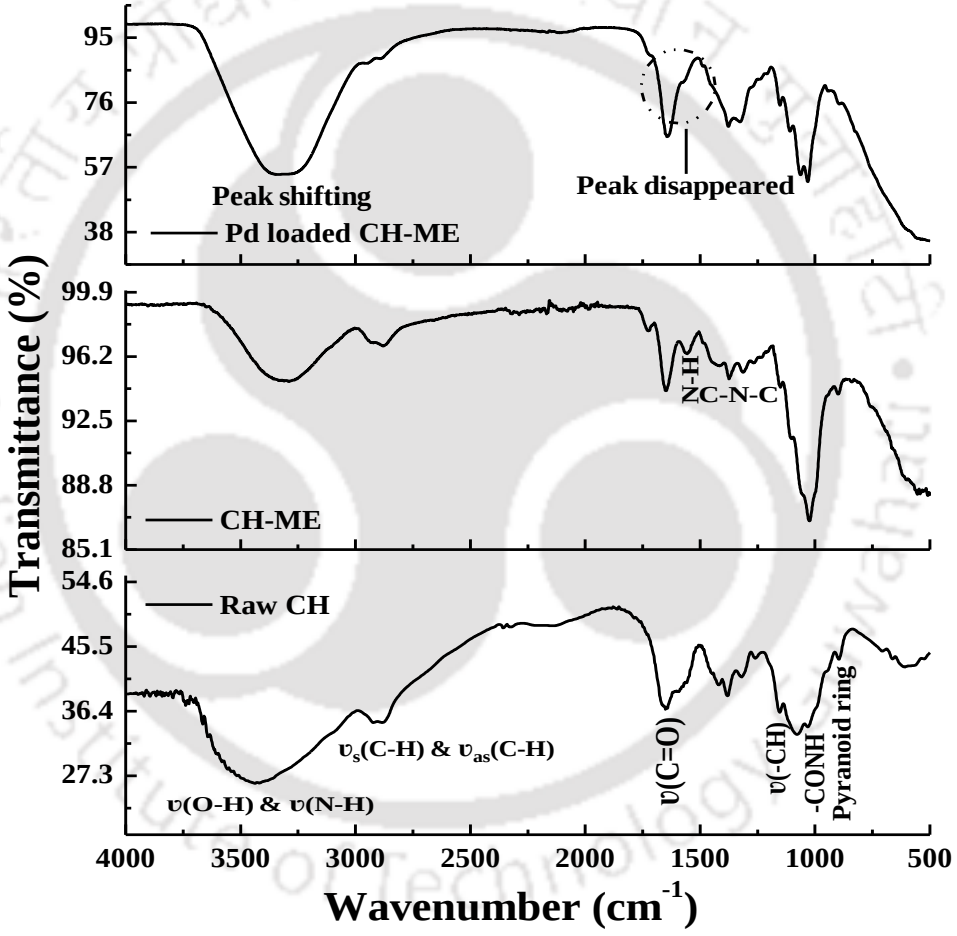

Fig. 5.7: FTIR spectra of (a) Raw chitosan, (b) CH-ME, and (c) Pd(II) loaded CH-ME derivative.

New peaks appeared in the wavenumber range of 1470 to 1220 cm^{-1}. These are attributed to stretching vibrations of C-N-C (Fig. 5.8) and thereby confirm definite cross-linking of triethylenetetramine onto the structure of chitosan (Tang et al. 2007, Kuang et al. 2013). The interactions of Pd(II) ions with primary amine groups in the structure of CH-TETA were confirmed through the shift in the peak from 3436 to 3293 cm^{-1}.

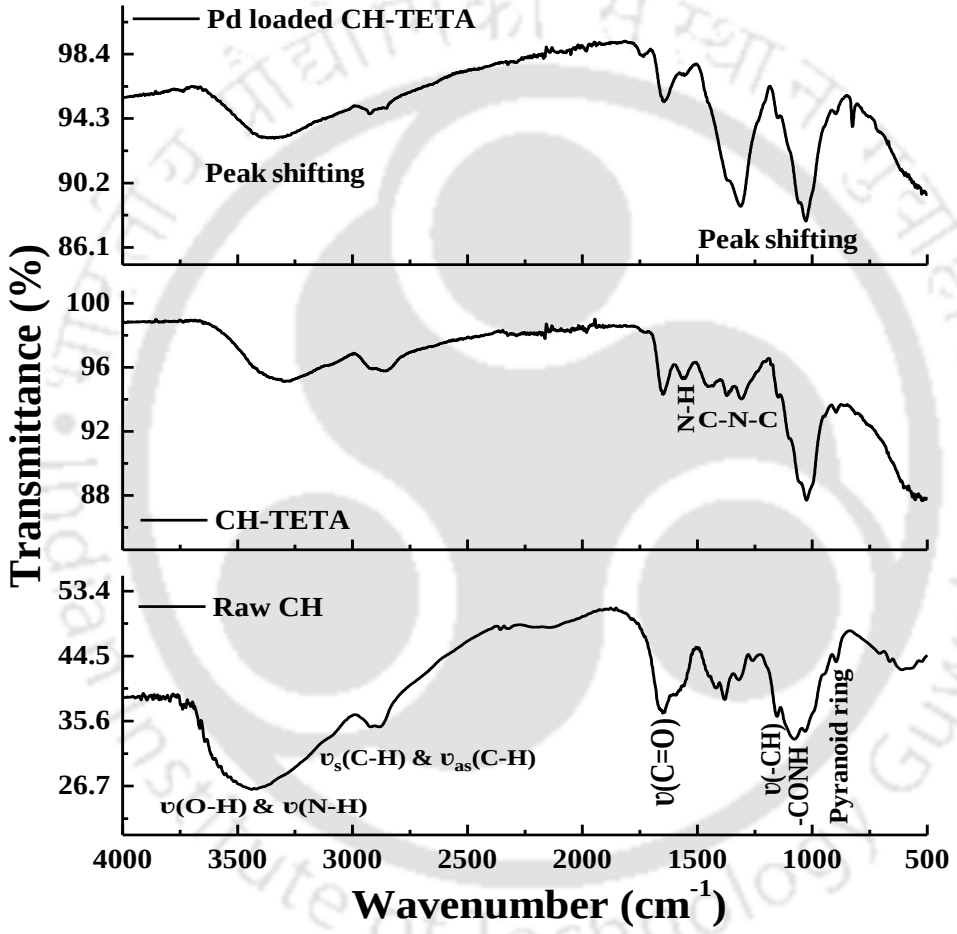

Fig. 5.8: FTIR spectra of (a) Raw chitosan, (b) CH-TETA, and (c) Pd(II) loaded CH-TETA derivative.

5.5.2 Surface area analysis

The BET surface area of raw chitosan is obtained as 8.212 m^2g^{-1}. For CH-ME and CH-TETA, the BET surface area was obtained as 10.16 m^2g^{-1} and 12.41 m^2g^{-1}, respectively. The enhancement in the surface area for both derivatives also affirms adequate modification of the chitosan structure.

5.5.3 Thermogravimetric analysis

The thermo-gravimetric analysis plots for chitosan and CH−TETA have been illustrated in Figs. 5.9a−5.9b, respectively. For chitosan, weight loss occurred in two stages. However, for the CH−TETA, weight loss occurred in three different stages. For both chitosan and CH-TETA, the first stage weight loss is due to the removal of physically adsorbed and fractional hydrogen-bonded water. This corresponds to 14% for raw chitosan at 194 °C and 11% for CH−TETA at 260 °C. The second stage is likely to occur due to the decomposition of the resins and would involve dehydration of saccharide rings, depolymerization, and decomposition of acetylated and deacetylated resins. The mass loss % for chitosan in the second stage is 55% at 750 °C. The corresponding value for CH−TETA is 61% at 440 °C. The third and final stage of mass loss for CH−TETA case refers to the contributions from the destruction of pyranose rings with ring-opening reactions and charring of chitosan at the higher temperature. Corresponding mass loss for the CH−TETA derivative during the stage is 6% at 750 °C. A comparative analysis of both TGA plots of chitosan and CH−TETA confirms marginally higher thermal stability than that of the raw material.

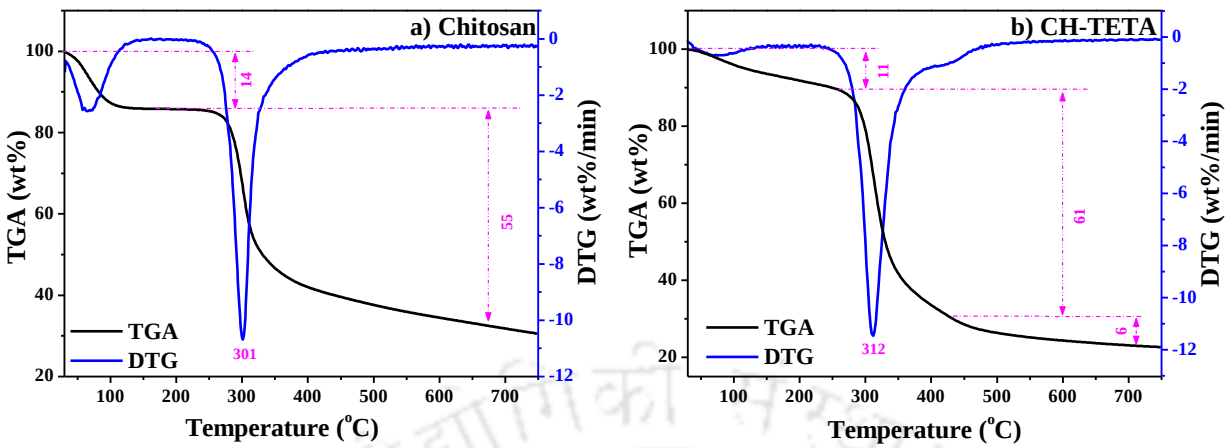

Fig. 5.9: TGA Spectra of (a) Raw chitosan and (b) CH−TETA derivative.

Similar to the CH-TETA, for CH-ME, the weight losses happened at three stages: (i) on the first stage, weight losses relating to the physically adsorbed, and fractional hydrogen-bonded water. The percent of weight loss at near 130 °C was 3.9. (ii) The second stage depicted 89.2% of CH-ME mass was lost when the temperature went up from 238 °C. This is may be caused by decomposition of the studied resins, including dehydration of the saccharide rings, depolymerization, and decomposition of the acetylated and deacetylated units of the resins. (iii) On the third stage, the mass of the studied resin dropped gradually and depicted 3.02%. This is ascribed to the further destruction of pyranose rings with ring-opening reaction and charing of chitosan at high temperature (Elwakeel et al. 2016).

5.5.4 Crystallinity analysis

The X-ray diffraction pattern of raw chitosan, CH−ME, and CH−TETA has been depicted in Figs. 5.10a and 5.10b. The XRD spectra of chitosan are in agreement with the available literature and depict broad and sharp peaks at 9.18 and 19.85° to affirm high crystallinity (Kanai et al. 2008, Ramesh et al. 2008, Zhou et al. 2009). This is due to the formation of strong inter and intra-molecular hydrogen bonds with abundant hydroxyl and amino groups (Zhou et al. 2009). In

addition, the regularity in the structure of chitosan also contributes to its higher degree of crystallinity. The XRD spectra of CH−ME derivative and indicates a lower degree of crystallinity and a greater degree of amorphous nature due to the modification with melamine. However, the same resin after Pd sorption become more amorphous because of complex form Pd availability on CH-ME surface. Similar patterns were obtained for CH-TETA derivative case as it shown in the Figs. 5.10b.

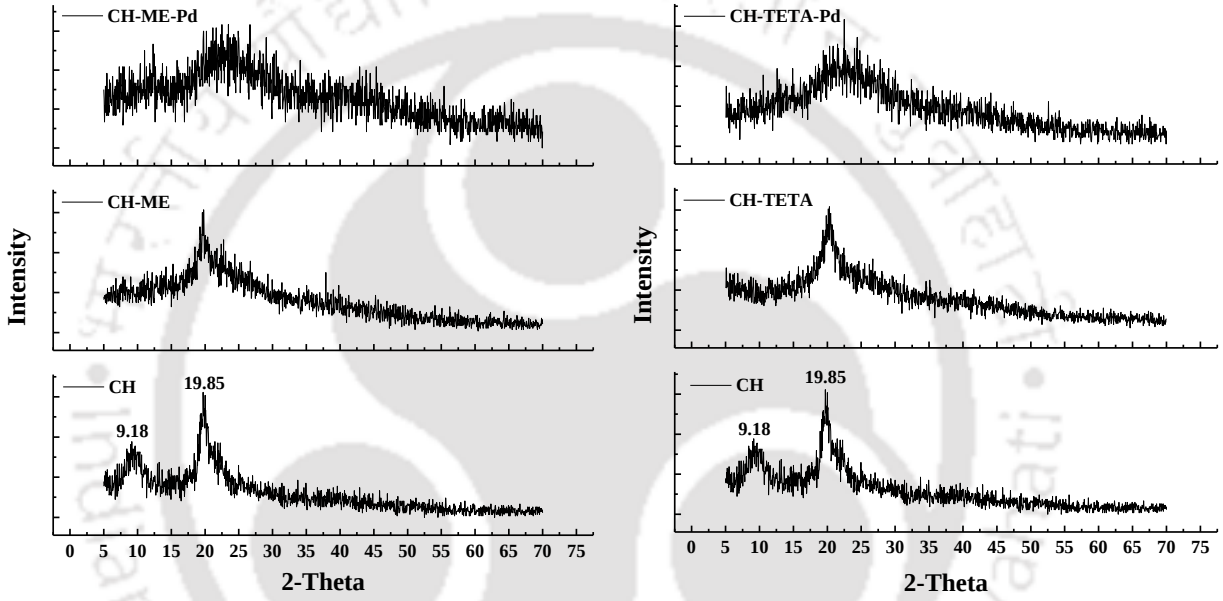

(a) (b)

Fig. 5.10: XRD spectra of (a) CH−ME and (b) CH-TETA derivatives.

5.5.5 EDX spectra

Figs. 5.11a−5.11d depict FESEM and EDX spectra of fresh and Pd(II)-loaded CH-ME and CH-TETA samples. Fig. 5.11a FESEM/EDX micrograph of CH-ME sample confirms existence of C (58.1 %), O (36.8 %), N (4.4 %) and Cl (0.7 %). The Pd(II)-loaded CH-ME sample confirmed the existence of a significant amount of Pd (2.1 %) on the adsorbent surface (Fig. 5.11b). The CH-TETA sample micrograph infers elemental composition as C (58.2 %), O (32.6 %), Cl (0.1 %) and

N (9.1 %) (Fig. 5.11c). The Pd(II)-loaded CH-TETA sample confirmed the existence of a significant amount of Pd (5.5 %) on the adsorbent surface (Fig. 5.11d).

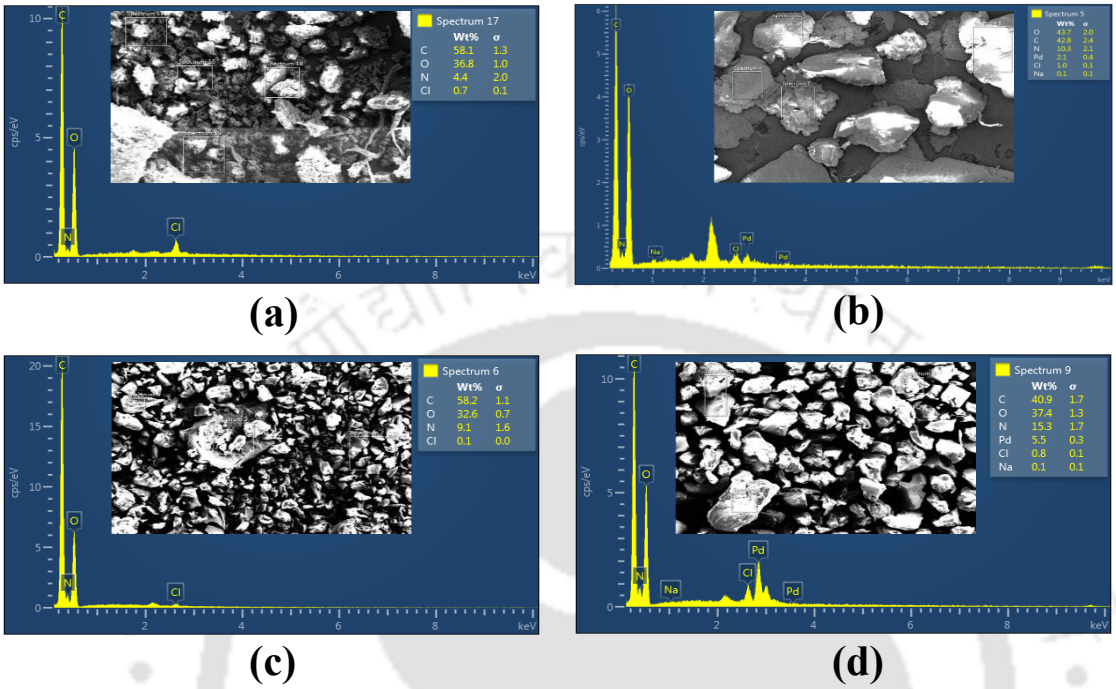

Fig. 5.11: FESEM and Energy dispersive X-Ray spectra of (a) CH-ME, (b) Pd(II)-loaded CH-ME, (c) CH-TETA and (d) Pd(II)-loaded CH-TETA.

5.6 Summary

Useful insights have been gained with respect to the Pd(II) adsorption and desorption characteristics of CH-ME and CH-TETA derivatives with synthetic ELP solutions. Firstly, the optimal Pd(II) batch adsorption parameters for CH-ME are pH of 2, a dosage of 1.8 g L^{-1}, and contact time of 840 min. Corresponding Pd(II) adsorption capacity and metal removal % of the resin are 22.64−85.58 mg g^{-1} and 81.50-51.35 %, respectively, in the initial Pd(II) solution concentration range of 50−300 mg L^{-1}. On the other hand, the optimal Pd(II) batch adsorption parameters for CH-TETA are pH of 2, a dosage of 1 g L^{-1}, and contact time of 300 min. Corresponding Pd(II) adsorption capacity and metal removal % of the resin are 43.53−117.08 mg

g^{-1} and 87.05-39.03 %, respectively, in the initial Pd(II) solution concentration range of 50−300 mg L^{-1}. Hence, compared to CH-TETA, CH-ME provided marginally lower removal efficiencies. However, CH-ME exhibited higher recovery characteristics in comparison with CH-TETA derivative. Secondly, the Pd(II) desorption characteristics are 39.68 and 59.82 % for CH-TETA and CH-ME, respectively. These indicate and confirm satisfactory but not excellent Pd(II) recovery and reuse characteristics. The higher contact time and better Pd(II) desorption characteristics of CH-ME can be targeted by suitable variation in functional group chemistry facilitated by stoichiometric and synthesis alterations. The surface analysis with FTIR, BET, TGA, XRD, and FESEM-EDX etc., are in good agreement with apparent functional interactions between various chemical species. From the perspective of Pd(II) recovery and reuse, compared to the glutaraldehyde cross-linked chitosan performance, CH-ME performed better but not CH-TETA. With respect to chitosan, all adsorbents exhibited excellent desorption characteristics and thereby confirming the greater role of chelating functional groups to improvise Pd(II) recovery and reuse from synthetic ELP solutions.

Chapter 6:

Pd(II) Adsorption and Desorption Characteristics of Sulfur and Nitrogen Functionalized Chitosan Derivatives

Pd(II) Adsorption and Desorption Characteristics of Sulfur and Nitrogen Functionalized Chitosan Derivatives

To further analyse the efficacy of sulphur and nitrogen functionalized chitosan derivatives in comparison with nitrogen functionalized chitosan derivatives, Pd(II) adsorptive and desorptive characteristics of said derivatives (thiosemicarbazide cross-linked chitosan (CH-TSC) and 3-amino-1,2,4-triazole-5-thiol cross-linked chitosan (CH-AZ)) were investigated. Section 6.2 briefly accounts for solubility resistances of the derivatives. Section 6.3 presents the results obtained for Pd(II) batch adsorption with the derivatives in terms of parametric optimality, functional groups interactions, and fitness of equilibrium, kinetic, and thermodynamic models. Section 6.4 presents the desorption characteristics of CH-TSC and CH-AZ derivatives. Section 6.5 presents the surface characterizations of CH-TSC and CH-AZ derivatives. Section 6.6 presents the efficacy and cost indices of all adsorbents tested in the thesis, followed by a summary of the findings in section 6.7.

6.1 Introduction

Prior to this work, sulfur and nitrogen functionalized chitosan derivatives were investigated for Pd(II) adsorption characteristics by few research groups that targeted thiol, amine and thiourea functionalization (Guibal et al. 2002, Atia 2005, Birinci et al. 2009, Butewicz et al. 2009, Zhou et al. 2009, Bratskaya et al. 2011). The authors deployed simple adsorption systems of aqueous solutions. On the other hand, CH-AZ and CH-TSC have been deployed for applications other than Pd(II) removal, recovery, and reuse. Thus, moderate complex solutions systems such as synthetic ELP solutions were not targeted for said derivatives. Further, desorption

characteristics were not targeted as well. Considering these limitations, Pd(II) adsorption and desorption characteristics were targeted for CH-TSC and CH-AZ derivatives with synthetic ELP solutions. Conducted surface characterizations with FTIR, BET, XRD, TGA, and FESEM-EDX. The specific role of Na_2EDTA (stabilizer) and liquor ammonia (NH_3) on Pd(II) removal and recovery characteristics was targeted in specific for said derivatives.

6.2 Solubility resistance of CH-TSC and CH−AZ derivatives

For both derivatives, the weight loss % has been evaluated to be approximately 1% for both HNO_3 (1M) and NaOH (1M) solutions. This confirms that the CH-TSC and CH−AZ derivatives are stable in the entire pH range (0.5−10). Therefore, this pH range has been considered to evaluate pH optimality for optimal adsorbent performance during batch adsorption studies.

6.3 Pd(II) adsorption characteristics of CH-TSC and CH-AZ derivatives

6.3.1 Effect of adsorption parameters on batch adsorption characteristics

For a fixed choice of other adsorption process parameters (720 min, 1 g L^{-1}, 298 K, and 50 mg L^{-1} for contact time, adsorbent dosage, temperature, and Pd(II) concentration), Fig. 6.1 depicts the variation of Pd(II) adsorption capacity and % removal profiles for a variation in pH. For a variation in initial solution pH from 0.5 to 10, the adsorption capacity of CH-TSC enhanced from 30.08 mg g^{-1} (pH 0.5) to 44.31 mg g^{-1} (pH 2) followed by a steady decline to 21.72 mg g^{-1} (pH 10). Corresponding metal removal varied from 60.17–88.62 % (pH 0.5−2) and thereafter declined to 43.44 % (pH 10). For the CH-AZ, the adsorption capacity values varied from 34.40−47.01and 47.01−31.81 mg g^{-1} for corresponding pH variation from pH 0.5−4 and pH 4−10, respectively. For a CH-TSC and CH-AZ derivative, the figure depicts an optimal pH

of 2 and 4, respectively. Corresponding optimal adsorption capacity values are 44.31 and 47.01 mg g^{-1}, respectively. Similarly, corresponding % removal values are 88.62 and 94.02%, respectively.

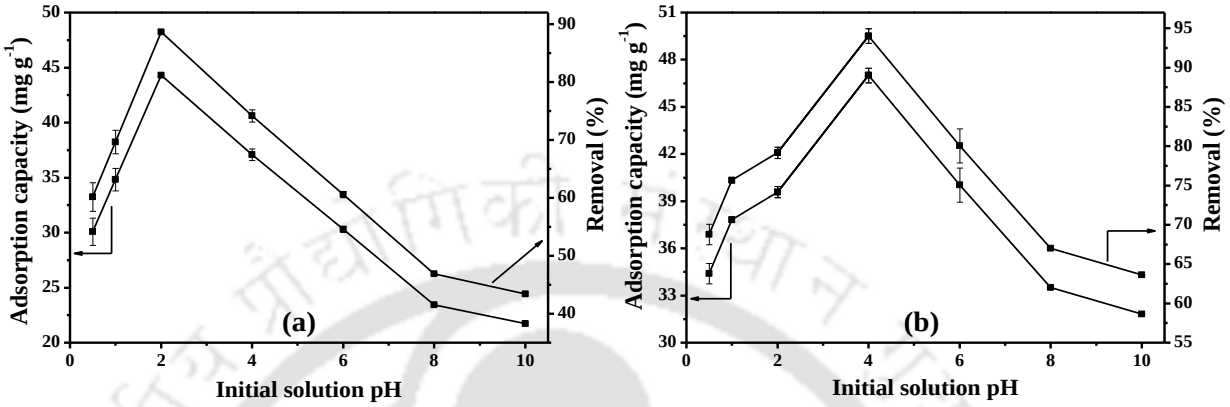

Fig. 6.1: Effect of initial solution pH on the Pd(II) adsorption characteristics of (a) CH-TSC and (b) CH-AZ derivatives.

The findings in chapter 3 convey that for raw chitosan, the optimal pH is 6 (70.69% removal) for a fixed choice of 720 min contact time, 1 g L^{-1} adsorbent dosage, and 50 mg L^{-1} Pd(II) concentration. Therefore, the existence of new functional groups (S and N) can be analysed to a strong influence on pH optimality and corresponding Pd(II) adsorption characteristics. In this context, it can be analysed that prior speciation analysis conducted by our research group affirmed that for lower pH range (1−6) and higher chloride concentration (33−500 mg L^{-1}), Pd exists mostly in $PdEDTA^{2-}$ form and hence protonation effect will be significant to enable higher H^+ influence on $–NH_2$ groups(Fujiwara et al. 2007, Ramesh et al. 2008, Zhou et al. 2009). Thus, at the optimal pH of 2 and 4, the existence of significant quantities of protonated amine groups ($–NH_3^+$) on the CH-TSC and CH−AZ derivatives, respectively, would enable higher affinity to bind $Pd(EDTA)^{-2}$ and thereby promote optimal adsorptive behaviour. Also, such an interaction mechanism may occur along with adduct formation (R-S—›$PdEDTA^{2-}$) (Kanai et al. 2008, Zhou et al. 2009). Thus, based on these hypotheses, Pd(II) adsorption on

CH-TSC and CH−AZ derivatives is very likely to occur due to electrostatic attraction and ion-exchange in the synthetic ELP solution. Corresponding electrostatic interaction between protonated amine groups on the CH-TSC and CH−AZ derivatives and noble metal species is expressed in the following reaction mechanisms (Eqs. 6.1 and 6.2):

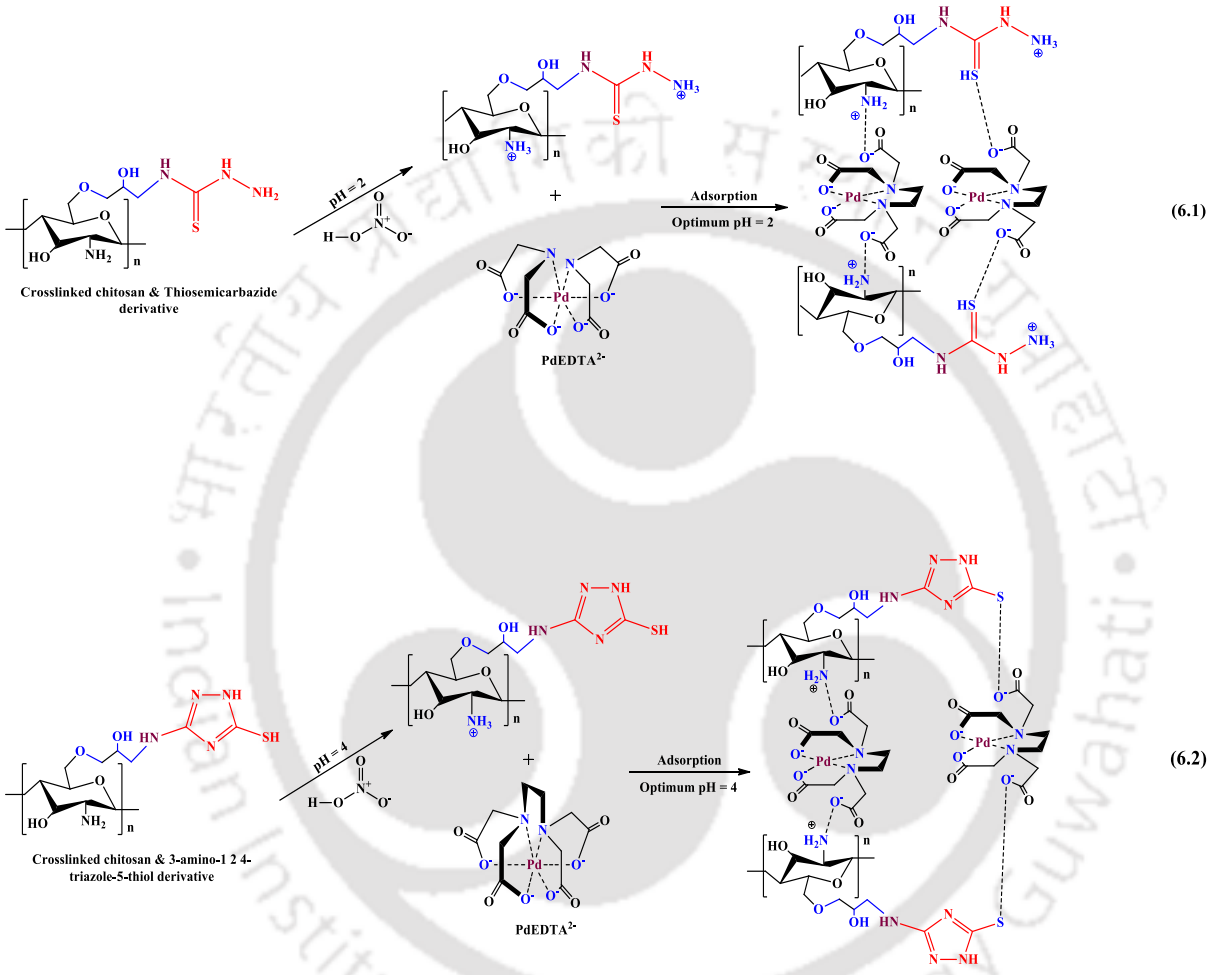

As shown in the above equations, at the optimal pH, the $PdEDTA^{-2}$ gets functionally bonded to protonated -NH_2 and thiol groups of the CH-TSC and CH-AZ.

The optimality of adsorbent dosage with respect to Pd(II) adsorption characteristics of CH-TSC and CH−AZ and ELP system is illustrated in Fig. 6.2. For the reported data, at an initial solution pH of 2 and 4 for CH-TSC and CH-AZ was used respectively. Corresponding fixed choice of adsorption process parameters refers to solution pH, initial Pd(II) solution

concentration and contact time of 4, 50 mg L^{-1}, and 720 min, respectively. As shown, for CH-TSC derivative, the adsorption capacity reduced from 128.79−24.30 mg g^{-1}, and removal % increased from 51.52−97.19 % for a variation in adsorbent dosage from 10−100 mg. Correspondingly, for CH-AZ derivative, the adsorption capacity reduced from 115.82−24.96 mg g^{-1}, and removal % increased from 46.33−99.85 %. For both cases, the optimal adsorbent dosage refers to the highest dosage (1.6 g L^{-1}) at which best adsorption characteristics have been obtained (30.28 and 31.19 mg g^{-1} adsorption capacity and, 96.88 and 99.82% removal % for CH-TSC and CH-AZ derivatives, respectively). The enhancement in Pd(II) removal efficiency with adsorbent dosage was due to the enhancement in the number of the active sites available for Pd(II) adsorption. Simultaneously, the metal uptake reduced due to the reduction of metal ions available per unit gram of adsorbent. The obtained trends are in good agreement with the findings reported in chapter 3 for raw chitosan. For the case, the optimal dosage obtained was 1.6 g L^{-1} (720 min contact time, pH 6, and 50 mg L^{-1} Pd concentration) for a maximum Pd(II) removal (72.1%). Compared to chitosan, higher removal efficiency has been obtained for the CH-TSC and CH-AZ derivatives. Due to the availability of newer functional groups in the chitosan structure.

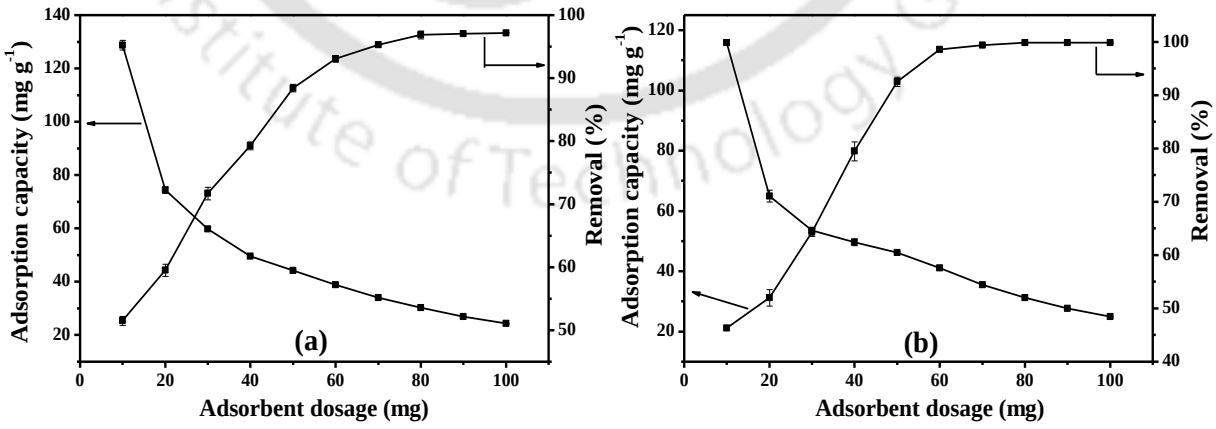

Fig. 6.2: Effect of adsorbent dosage on the Pd(II) adsorption characteristics of (a) CH-TSC and (b) CH-AZ derivatives.

Fig. 6.3 depicts the effect of contact time on the Pd(II) adsorption characteristics of CH-TSC and CH−AZ derivatives and the ELP system. For the reported data, other adsorption process parameters have been chosen as 1.6 g L^{-1} (adsorbent dosage), 50 mg L^{-1} (Pd(II) concentration), and pH of 2 (CH-TSC) and 4 (CH-AZ). As shown, for CH-TSC derivative, the adsorption process is rapid for the first 60 min. Later, Pd(II) adsorption occurred with a gradual increment up to 720 min at which it reached saturated. Similarly, for CH-AZ derivative, Pd(II) adsorption process is rapid from 5−120 min and reaches equilibrium at 120 min. Thus, based on the illustrations, it can be analysed that the system reaches equilibrium at 720 and 120 min for CH-TSC and CH-AZ, respectively. Corresponding optimal adsorption capacity and removal efficiencies are 30.27 mg g^{-1} and 96.85 % for CH-TSC and 30.96 mg g^{-1} and 99.12% for CH-AZ, respectively.

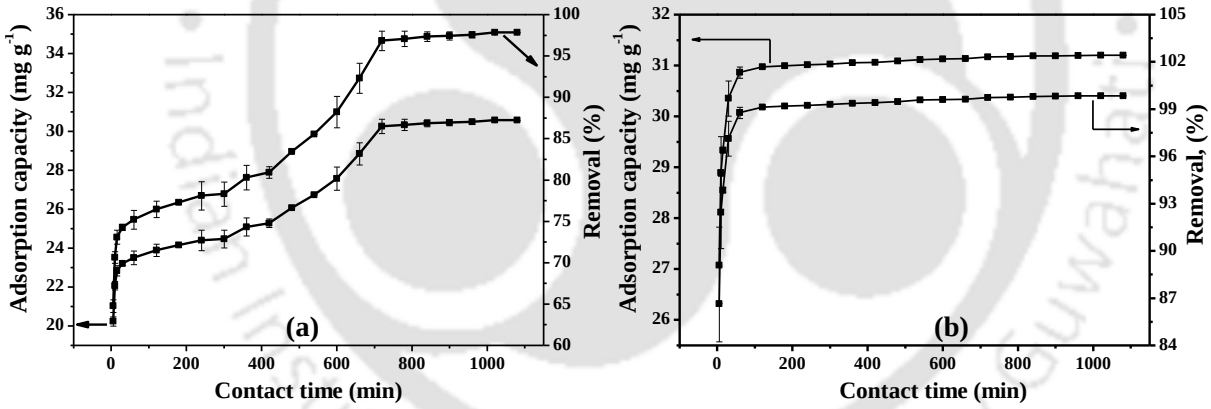

Fig. 6.3: Effect of contact time on the Pd(II) adsorption characteristics of (a) CH-TSC and (b) CH-AZ derivatives.

For comparison, it can be noted from the findings in chapter 3 that for chitosan, the optimal contact time is 540 min for a fixed choice of other adsorption parameters as 1.6 g L^{-1} adsorbent dosage, pH 6 and 50 mg L^{-1} Pd(II) concentration. For these conditions, the optimal characteristics refer to 78.68% Pd removal. The obtained trend is in agreement with the hypothesis that with increasing adsorbent dosage, metal uptake reduces, and % removal

increases. Thus, it is apparent that the functionalization of chitosan strongly influenced the optimality of contact time for both derivatives.

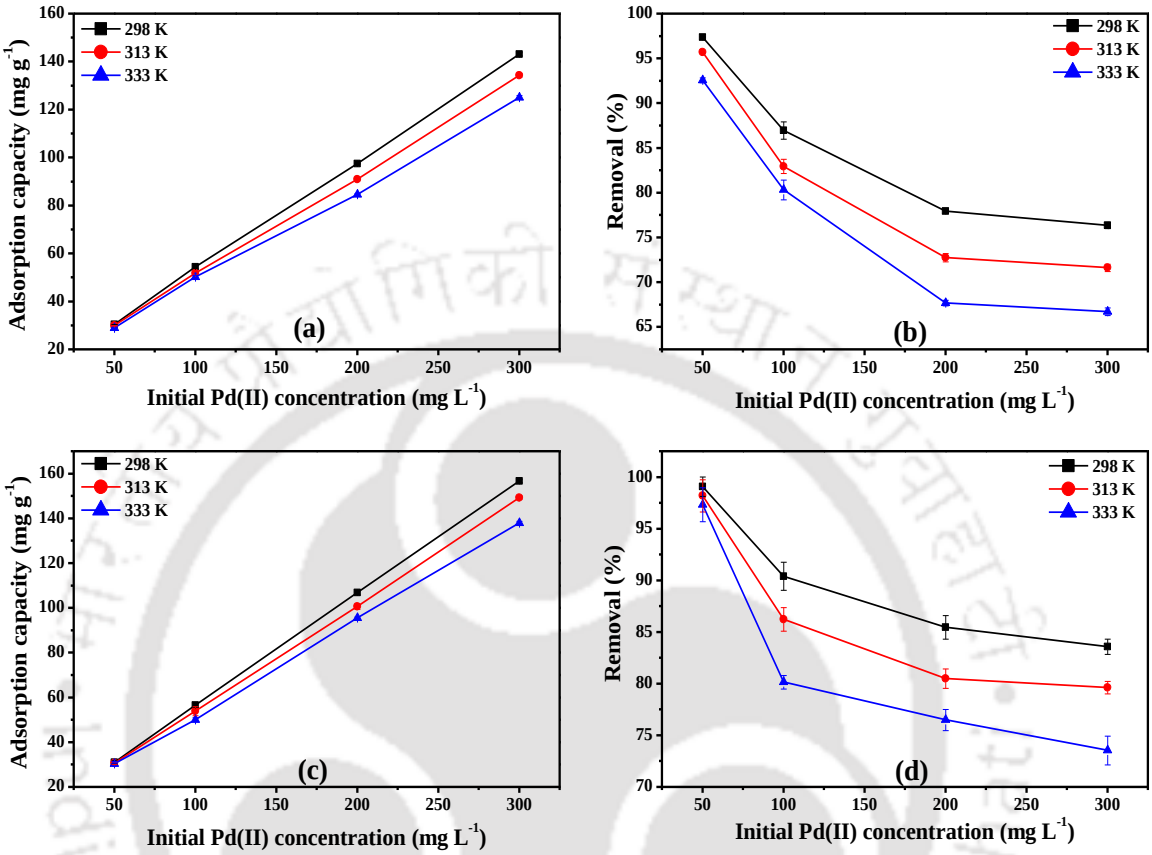

Fig. 6.4: Effect of temperature and initial Pd(II) concentration on adsorption capacity (a & c) and removal efficiency (b & d) of CH-TSC and CH−AZ derivatives, respectively.

For the Pd(II) solution concentration range of 50−300 mg L^{-1} and temperature range of 298−333 K and for a fixed choice of other parameters such as optimal pH (2 and 4), adsorbent dosage (1.6 g L^{-1}) and contact time (720 and 120 min), Figs. 6.4a − 6.4d depicts the dependence of adsorption characteristics on Pd concentration and temperature for CH-TSC and CH-AZ derivatives, respectively. The figure affirms that, for a corresponding variation in Pd solution concentration from 50-300 mg L^{-1}, the Pd metal uptake and removal efficiency vary from 30.43-143.17 and 30.96-156.72 mg g^{-1} and, 97.38-76.35 and 99.08−83.58% for CH-TSC and CH-AZ derivatives, respectively. Thus, higher Pd concentrations did not favour adsorption,

and this is in agreement with theoretical insights of the adsorption process. With a similar agreement with respect to theoretical insights, lower % removal values have been obtained at higher temperature (92.56-66.72 and 97.33–73.55 % at 333 K for CH-TSC and CH-AZ derivatives, respectively) than those obtained at lower temperature (97.38-76.35 and 99.08−83.58% at 298 K for CH-TSC and CH-AZ derivatives, respectively).

6.3.2. Equilibrium, kinetic and thermodynamic model parameters

Figs. 6.5a−6.5c and Table 6.1 respectively present fitness plots and relevant parameters of alternate kinetic models for the best representation of measured Pd(II) adsorption kinetics with CH-TSC, CH−AZ, and ELP system. Among all the models, only the pseudo-second-order model provided very good fitness (R^2 = 0.991 and 0.999 for CH-TSC and CH-AZ, respectively). Further, the pseudo-second-order model based adsorption capacity (31.25 mg g^{-1} for CH-TSC and 31.25 mg g^{-1} for CH-AZ) is also in agreement with the measured adsorption capacity (30.27 mg g^{-1} for CH-TSC and 30.96 mg g^{-1} for CH-AZ). Therefore, pseudo-second-order model has been inferred to be the best fit to represent the kinetics of Pd(II) adsorption from synthetic ELP solutions onto both CH-ME and CH-TETA derivatives, which is based on the assumption that the rate limiting step may be chemisorption involving valency forces through sharing or exchange of electrons with the N and S atoms of CH-TSC and CH-AZ derivatives. This is also confirmed by the FTIR analysis of the Pd(II) adsorbed CH-ME and CH-TETA derivatives that indicated strong chemical interactions of Pd(II) with relevant functional groups of the resins.

Fig. 6.5c infers that the plot fitness corresponds to a multi-linear plot in three distinct phases. Also, the plot did not meet the graph at the origin to affirm that the intra-particle diffusion model is not the sole rate-limiting step of Pd adsorption on to CH-TSC, CH−AZ for the ELP solution system. Similar fitness trends have been reported for the relevant data reported by our

research group for Lewatit TP-214, and glutaraldehyde cross-linked chitosan (Nagireddi et al. 2017, Nagireddi et al. 2018).

Table 6.1: Regressed kinetic parameters to represent Pd(II) adsorption kinetics of CH-TSC and CH-AZ derivatives.

Experimental capacity (Q_{exp}, mg g^{-1})	Pseudo-first order model			Pseudo-second order model			Intra-particle Diffusion model		
	Q_e (mg g^{-1})	K_1 (min^{-1})	R^2	Q_e (mg g^{-1})	K_2 (g mg^{-1} min^{-1})	R^2	K_{id} (min mg g^{-1})	C	R^2
CH-TSC									
30.27	9.18	-2.30×10^{-3}	0.915	31.25	7.60×10^{-4}	0.992	0.315	20.36	0.919
CH-AZ									
30.96	1.01	-2.30×10^{-5}	0.0003	31.25	2.46×10^{-2}	0.999	3.437	19.90	0.925

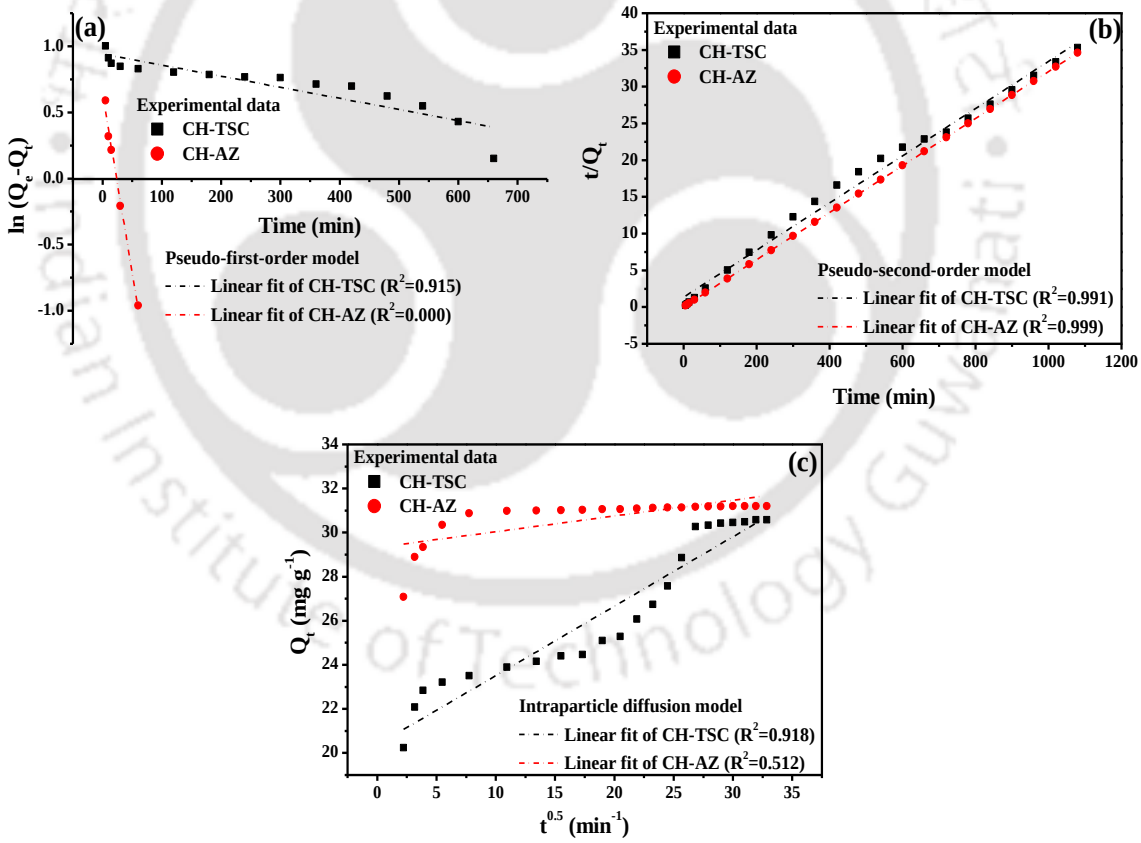

Fig. 6.5: Fitness plots of (a) Pseudo-first-order model, (b) Pseudo-second-order kinetic model, and (c) Intraparticle diffusion model to represent Pd(II) adsorption kinetic of CH-TSC and CH-AZ derivatives.

Figs 6.6a–b and Table 6.2 presents the fitness plots and relevant parameters of alternate equilibrium models, namely Langmuir and Freundlich isotherms. The figures and table affirm fitness of the Freundlich isotherm model to represent measured Pd(II) batch equilibrium adsorption data for both CH-TSC and CH-AZ derivatives. The R_L value reported in Table 2 is in the range of 0-1, and this concludes that the CH-TSC and CH−AZ adsorbents are favourable for Pd(II) adsorption from model electroless plating solutions.

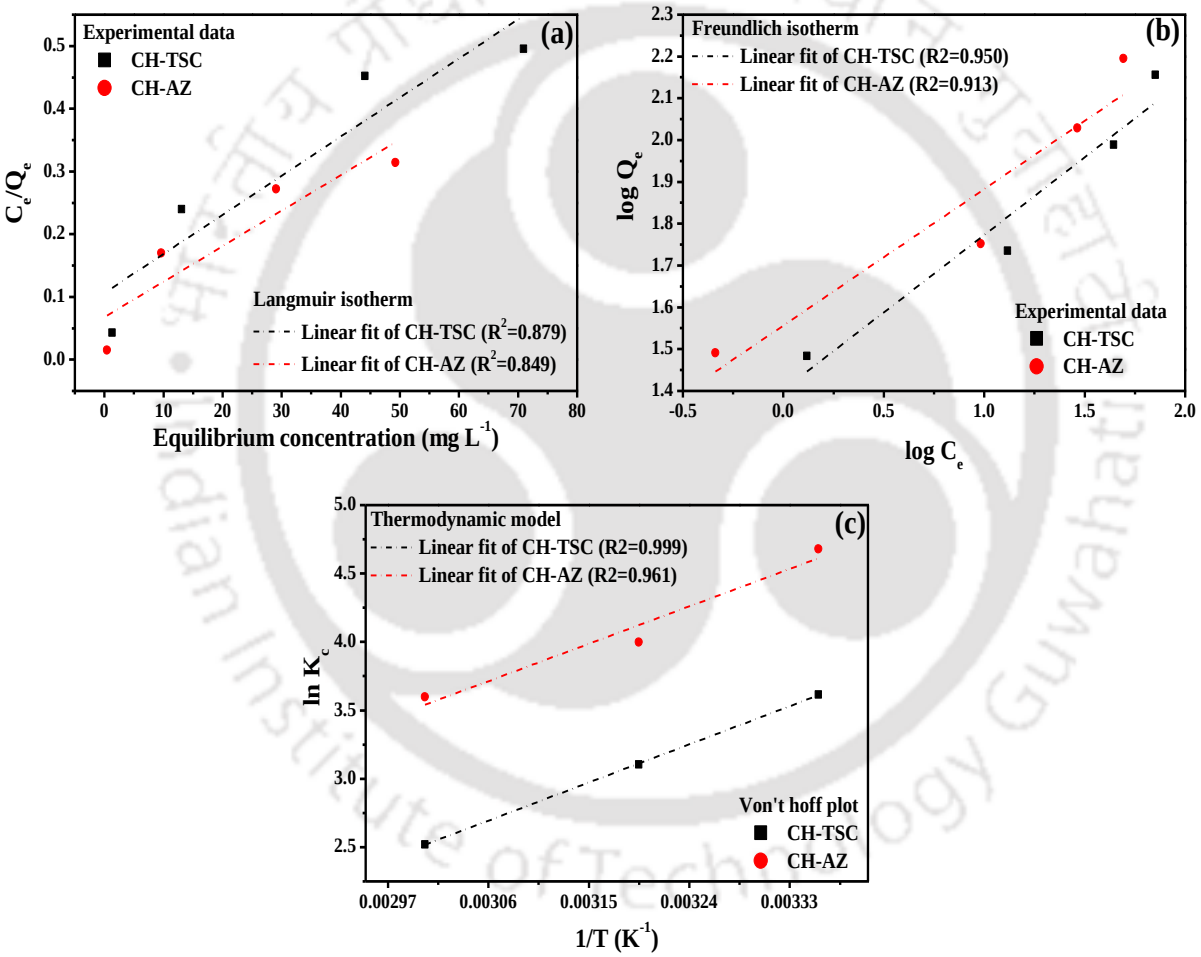

Fig. 6.6: Fitness of alternate models to represent equilibrium and thermodynamics data for CH-TSC and CH-AZ derivatives: (a) Langmuir model (b) Freundlich model and (c) Van't Hoff model.

Table 6.2: Regressed model parameters to represent Pd(II) adsorption equilibrium data of CH-TSC and CH-AZ derivatives.

Temperature (K)	Langmuir parameters				Freundlich parameters		
	Q_o (mg g^{-1})	b (L mg^{-1})	R^2	R_L	K_f	n	R^2
CH-TSC							
298	161.29	0.058	0.880	0.255-0.054	25.27	2.698	0.950
313	153.85	0.044	0.870	0.314-0.071	20.44	2.569	0.950
333	144.93	0.035	0.887	0.363-0.087	15.56	2.346	0.971
CH-AZ							
298	175.44	0.084	0.849	0.192-0.038	36.02	3.064	0.913
313	169.49	0.058	0.812	0.257-0.054	28.69	2.858	0.905
333	163.93	0.040	0.786	0.334-0.077	24.67	2.879	0.881

Fig. 6.6c depicts the fitness of Van't Hoff's equation to depict the thermodynamics of Pd(II) adsorption process. Corresponding thermodynamic parameters obtained from the plot are summarized in Table 6.3. The figure and table confirm spontaneous (negative ΔG° values) and exothermic (negative ΔH° values) Pd(II) adsorption from synthetic ELP solutions for both derivatives.

Table 6.3: Regressed thermodynamic model parameters for Pd(II) adsorption using CH-TSC and CH-AZ derivatives.

Temperature (K)	K_c	ΔH° (kJ mol^{-1})	ΔS° (J K^{-1} mol^{-1})	ΔG° (kJ mol^{-1})	R^2
CH-TSC					
298	37.14	-25.77	-56.46	-8.95	0.999
313	22.29			-8.10	
333	12.43			-6.97	
CH-AZ					
298	107.7	-25.26	-46.42	-11.43	0.961
313	54.56			-10.73	
333	36.48			-9.80	

6.4 Desorption characteristics of Pd(II) loaded CH-TSC and CH-AZ derivatives

The Pd-loaded CH-TSC and CH-AZ adsorbents have been prepared with 50 mg L^{-1} Pd(II) solution concentration. These adsorbents have been evaluated to possess a corresponding average adsorption capacity of 31.82 and 30.79 mg g^{-1}. For these adsorbents, Table 6.4 presents the desorption efficiency for various eluents (0.1−2 M NaOH, KOH, and HCl). Among all cases, the best desorption efficiency was obtained for 2M HCl (40.82% for CH-TSC and 45.03% for CH-AZ). Thus, the desorption efficiencies are not excellent from the perspective of Pd(II) reuse and irreversible chemisorption to be highly prevalent during Pd(II) adsorption onto CH-TSC and CH−AZ derivatives. Even for CH-TSC, the chemisorption is strong and indicative of difficulty to recover adsorbed Pd(II) from the adsorbent using simple eluents.

Table 6.4: Summary of evaluated Pd(II) desorption efficiencies for various combinations of eluents and CH-TSC/CH-AZ derivatives.

Desorption Eluent	Desorption efficiency (%)		Desorption Eluent	Desorption efficiency (%)		Desorption Eluent	Desorption efficiency (%)	
	CH-TSC	CH-AZ		CH-TSC	CH-AZ		CH-TSC	CH-AZ
0.1M NaOH	32.14	34.02	0.1M KOH	33.41	36.10	0.1M HCl	26.83	31.62
0.3M NaOH	29.25	31.64	0.3M KOH	32.04	35.71	0.3M HCl	28.24	34.91
0.5M NaOH	26.71	29.81	0.5M KOH	31.72	35.08	0.5M HCl	33.52	38.17
1M NaOH	22.18	25.14	1M KOH	28.84	33.85	1M HCl	37.23	40.45
2M NaOH	19.06	21.80	2M KOH	27.19	29.10	2M HCl	40.82	45.03

The experimentally measured optimal Pd(II) adsorption and desorption characteristics have been compared with the best available literature for nitrogen (glutaraldehyde cross-linked chitosan), and nitrogen and sulfur (Lewatit TP214) functionalized adsorbents. Also, commercial resins investigated in this work have been considered to analyze the comparative efficacy. Table 6.5 presents these findings. Critical insight into these findings is as follows:

a) Among CH-TSC and CH-AZ, the performance of the derivative in terms of adsorption capacity is comparable with respect to glutaraldehyde (175.44, 161.29, and 166.67 mg g^{-1} for CH-AZ, CH-TSC, and glutaraldehyde cross-linked chitosan, respectively). Therefore, the Pd(II) removal of sulfur functionalized adsorbents (CH-TSC and CH-AZ) is similar to that of the nitrogen functionalized adsorbents reported in the literature (glutaraldehyde based resin).

b) With respect to commercial resins investigated in this work and those considered in the literature, the adsorption capacity is excellent (100, 166.67, 185.16 and 172.41 mg g^{-1}) for Amberlyst A21, Amberlite IRA958, Dowex Marathon MSA, and Lewatit TP214 resins, respectively.

c) The desorption characteristics of both CH-AZ and CH-TSC (45.03 and 40.82 %, respectively) are comparable with glutaraldehyde cross-linked chitosan (42.35 %). However, the desorption efficiency is significantly poor in comparison with commercial resins, namely Lewatit TP214, Amberlite IRA958, and Dowex Marathon MSA, whose desorption efficiency values are high and about 66%. Thus, both CH-TSC and CH-AZ can be concluded to be satisfactory but not excellent resins for Pd(II) recovery and reuse from synthetic ELP solutions.

d) The comparison with other literature is not relevant as they have been aqueous media and solutions without any chemistry complexity. However, on good influence is that better adsorption capacity was obtained for CH-TSC and CH-AZ upon comparison with thiourea modified chitosan microspheres (112.4 mg g^{-1}). The desorption data also cannot be compared for these, as the data refers to deploy of expensive eluents.

Table 6.5: Efficacy of Pd(II) adsorption and desorption characteristics of CH-TSC and CH-AZ derivatives with sulfur and nitrogen functionalized adsorbents reported in the literature.

Adsorbent name	Contaminants	Pd(II) concentration (mg L^{-1})	Adsorbent dose (g L^{-1})	pH	Adsorption capacity (mg g^{-1})	Eluent	Desorption (%)	Reference
3-amino-1,2,4 triazole,5-thiol cross-linked chitosan	Pd(II) Na_2EDTA NH_4OH	50-300	1.6	4	175.44	2M HCl	45.03*	Present study
Thiosemicarbazide cross-linked chitosan				2	161.29		40.82*	
Glutaraldehyde cross-linked chitosan		50-500	0.6	8	166.67	0.1M HCl	42.35*	Nagireddi et al. 2017
Lewatit TP214		50-300	2	8	172.41	0.1M HCl	66.95	Nagireddi et al. 2018
Thiourea modified chitosan microspheres	Pd(II) Pt(VI)	400	3.33	2	112.4	0.5M EDTA−0.5M H_2SO_4	98.38	Zhou et al. 2009
Ethylenediamine modified magnetic chitosan nanoparticles		60	0.5	2	138	0.4M H_2SO_4−1.0M Thiourea	90.5	Zhou et al. 2010
Duolite GT-73	Pd(II)	195	500 (0.5g resin/50cm^3Pd(II) ions)	0-7	19.5-35.46	0.5M HCl─0.5M Thiourea	>99.9	Hubicki and Wołowicz 2009
					21.27-31.9			
Lewatit TP-214				0-14	171.9-205.6			
					285.4-306.7			

* All desorption studies were conducted at Pd(II) concentration of 50 mg L^{-1}.

6.5 Surface characterization of raw and Pd(II) loaded resins

6.5.1 FTIR analysis

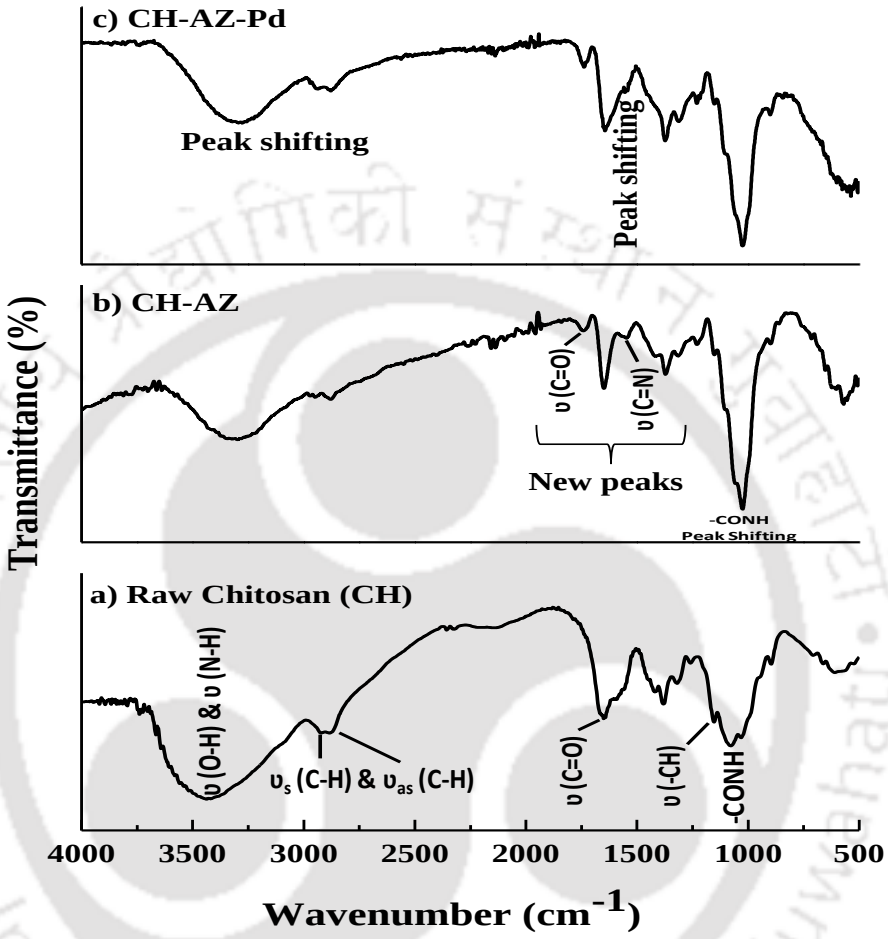

Fig. 6.7: FTIR spectra of (a) Raw chitosan, (b) CH−AZ, and (c) Pd(II) loaded CH−AZ derivative.

Figs. 6.7 a, 6b, and 6c depict the FTIR spectra of raw chitosan, CH-AZ, and Pd adsorbed CH−AZ derivatives, respectively. The existence of peaks corresponding to various functional groups indicates significant interactions of Pd with the derivative. The peaks at 3436 cm^{-1} in the raw chitosan sample (Fig. 6.7a) indicate stretching vibrations of –OH and $–NH_2$ groups and overlapping of intermolecular hydrogen bonds with one another. Further, a secondary amine group is being confirmed with the existence of one amine spike around this peak.

Peaks at 1654 cm^{-1}, 1154 cm^{-1}, and 1078 cm^{-1} indicate stretching vibration of amide I, −CH vibration, and –CONH groups, respectively. The FTIR spectra of CH−AZ sample (Fig. 6.7b) affirm the appearance of new peaks at 1744 and 1553 cm^{-1}. These are attributed to stretching vibrations of C=O and C=N groups, respectively(Lambert et al. 1976, Silverstein et al. 1991) and thereby confirm cross-linking of 3-Amino-1,2,4 triazole,5-thiol onto the chitosan structure. Peak shifting apparent in the wavenumber range of 3436 to 3293 cm^{-1} affirm interaction of Pd species with primary amine groups of the CH−AZ structure (Fig. 6.7c).

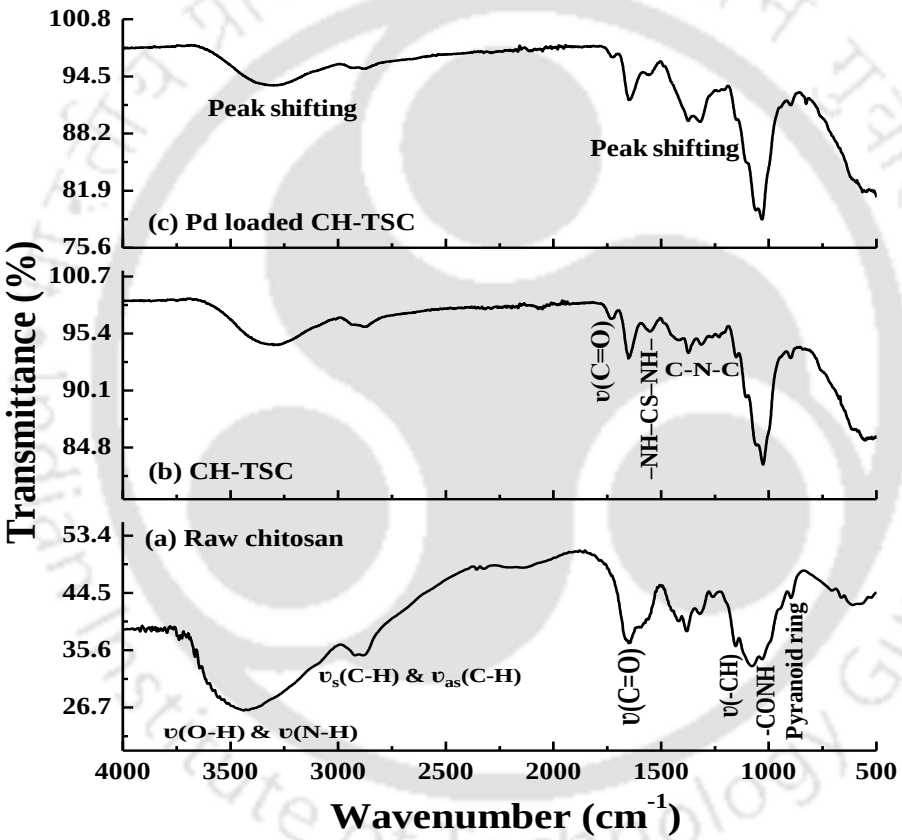

Fig. 6.8: FTIR spectra of (a) Raw chitosan, (b) CH−TSC, and (c) Pd(II) loaded CH−TSC derivative.

Figs. 6.8 a, b, and c illustrate the FTIR spectra of raw chitosan, CH-TSC, and Pd adsorbed CH−TSC derivatives, respectively. Compared with raw chitosan (Fig. 6.8a), the FTIR of CH-TSC can be analyzed to possess a new band at 1550 cm^{-1}. This is attributed to the –NH–CS–NH– group (Zhong et al. 2010)and thereby infers that the CH-TSC had been successfully

obtained through cross-linking of TSC with chitosan (Fig. 6.8b). The Peak shift visible in the wavenumber range of 3436 to 3293 $cm^{-1}$for Pd loaded CH-TSC (Fig. 6.8c) confirms the interaction of Pd species with primary amine groups of the CH−TSC structure.

6.5.2 Surface area analysis

The BET surface area of pure chitosan, CH-TSC, and CH−AZ samples have been determined to be 8.212, 15.89, and 17.16 m^2 g^{-1}. Compared to the chitosan BET surface area, these variations in values indicate that chitosan derivatives have a better surface area due to structural modification of the chitosan.

6.5.3 Thermogravimetric analysis

The thermo-gravimetric analysis plots for chitosan and CH−AZ have been illustrated in Figs. 6.9a and 6.9b, respectively. For chitosan, weight loss occurred in two stages. However, for the CH−AZ, weight loss occurred in three different stages. For both chitosan and CH-AZ, the first stage weight loss is due to the removal of physically adsorbed and fractional hydrogen-bonded water. This corresponds to 14.01% for raw chitosan at 194 °C and 7.59% for CH−AZ at 168 °C. The second stage is likely to occur due to the decomposition of the resins and would involve dehydration of saccharide rings, depolymerization, and decomposition of acetylated and deacetylated resins. The mass loss % for chitosan in the second stage is 55.25% at 750 °C. The corresponding value for CH−AZ is 41.94% at 352 °C. The third and final stage of mass loss for CH−AZ case refers to the contributions from the destruction of pyranose rings with ring-opening reactions and charring of chitosan at a higher temperature. A corresponding mass loss for the CH−AZ derivative during the stage is 19.11% at 750 °C. A comparative analysis of both TGA plots of chitosan and CH−AZ confirms marginally higher thermal stability than that of the raw material. These results and trends are in good agreement

with those presented in the literature (Elwakeel et al. 2016). Similar patterns were obtained for CH-TSC derivative case.

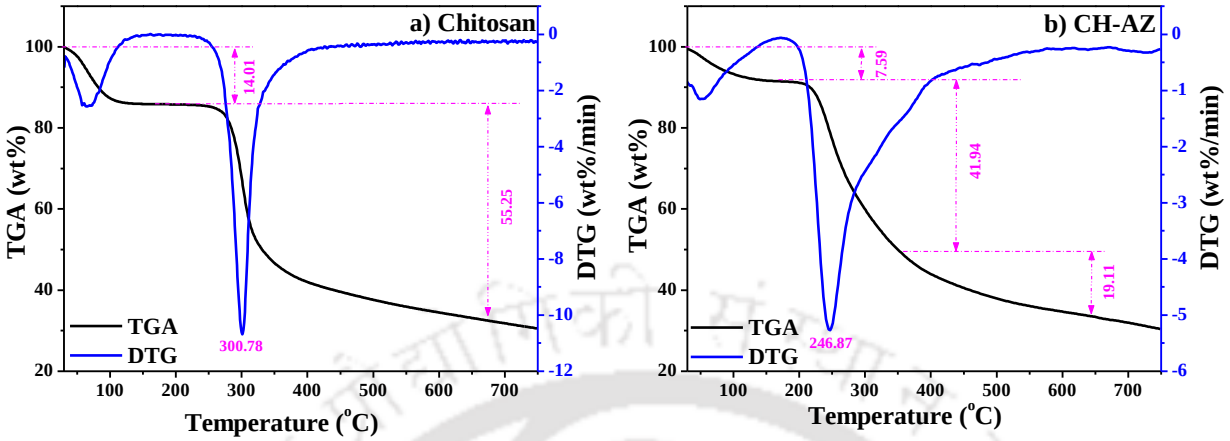

Fig. 6.9: TGA plot of (a) raw chitosan and (b) CH−AZ.

6.5.4 Crystallinity analysis

The X-ray diffraction pattern of raw chitosan, CH−AZ, and Pd loaded CH−AZ has been depicted in Figs. 6.10a−6.10c. The XRD spectra of chitosan are in agreement with the available literature and depict broad and sharp peaks at 9.18 and 19.85° to affirm high crystallinity (Kanai et al. 2008, Ramesh et al. 2008, Zhou et al. 2009). This is due to the formation of strong inter and intra-molecular hydrogen bonds with abundant hydroxyl and amino groups (Zhou et al. 2009). In addition, the regularity in the structure of chitosan also contributes to its higher degree of crystallinity. Fig. 6.10b depicts the XRD spectra of CH−AZ derivative and indicates a lower degree of crystallinity and a greater degree of amorphous nature due to the modification with 3-Amino-1,2,4-triazole-5-thiol. However, the same resin after Pd sorption exhibited crystallinity, as is evident in Fig. 6.10c.

Similar patterns were obtained for CH-TSC derivative case as shown in Fig. 6.11. For the case of Pd-loaded CH-TSC, the material showed higher amorphous nature because of complex form Pd availability on CH-TSC surface (Fig. 6.11c)

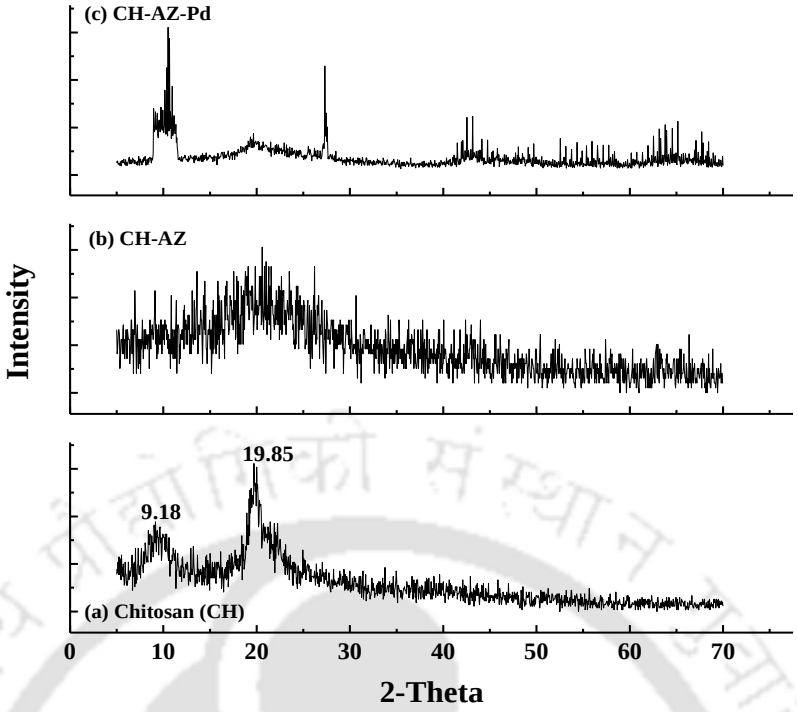

Fig. 6.10: XRD spectra of (a) Raw chitosan, (b) CH−AZ, and (c) Pd(II) loaded CH−AZ derivative.

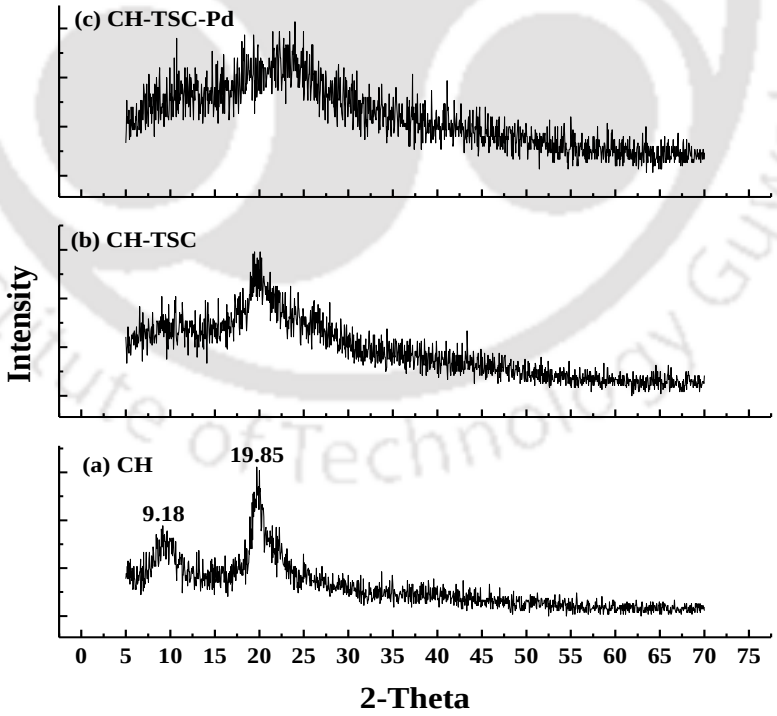

Fig. 6.11: XRD spectra of (a) Raw chitosan, (b) CH−TSC, and (c) Pd(II) loaded CH−TSC derivative.

6.5.5 FESEM and EDX analysis

Figs. 6.12a−6.12d depicts FESEM and EDX spectra of fresh CH−AZ, CH-TSC, and Pd loaded CH−AZ, CH-TSC samples. For the CH−AZ sample, the EDX spectra (Fig. 6.12a) indicates the existence of S (0.6%) due to cross-linking of 3-Amino-1,2,4 triazole,5-thiol with chitosan and S (2.3%) for CH-TSC sample (Fig. 6.12c). The Constitution of other elements in the CH−AZ refers to C (58.5%), O (34.4%), Cl (2.3%), and N (4.2%). On the other hand, CH-TSC consists of other elements as C (55.0%), O (35.2%), Cl (0.4%), and N (7.1%). The Pd loaded CH−AZ, and CH-TSC samples confirmed the existence of a significant amount of Pd (3.7 and 2.9%) on the CH-AZ and CH-TSC surfaces, respectively (Figs. 6.12b and 6.12d).

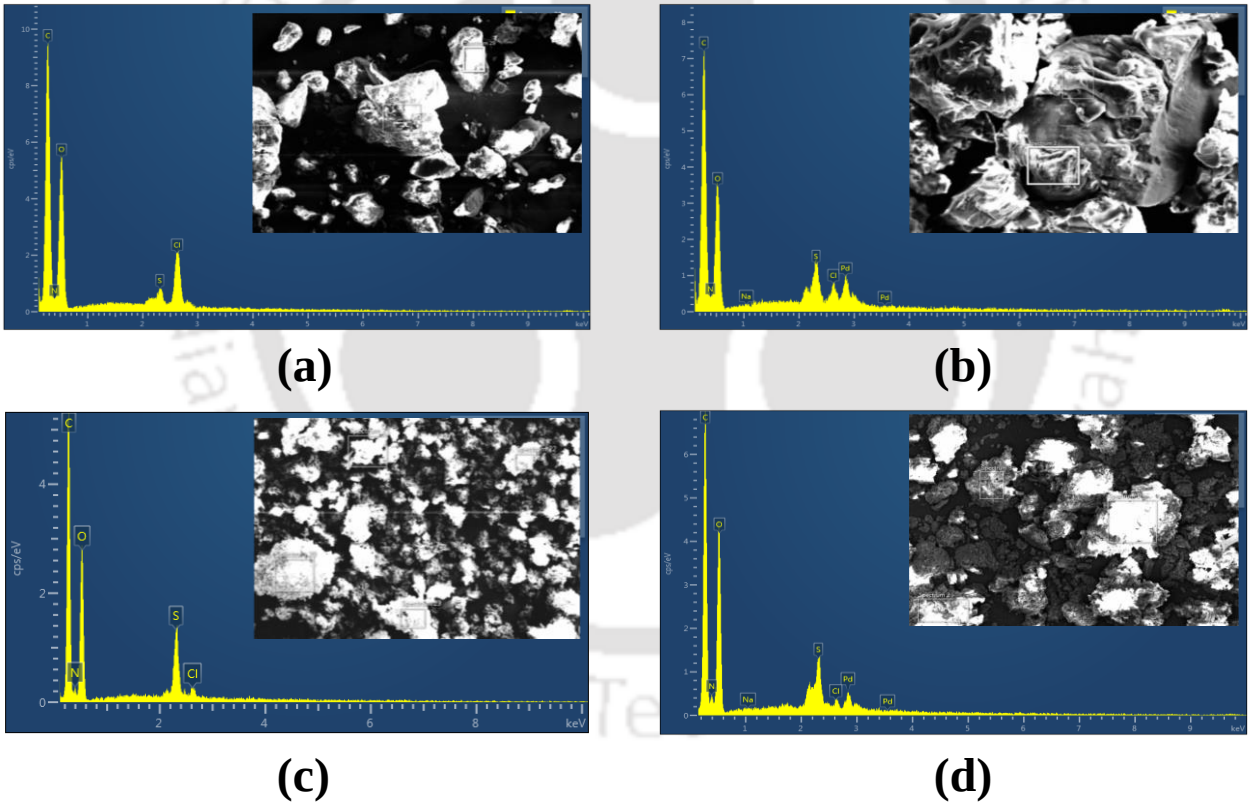

Fig. 6.12: FESEM and Energy dispersive X-Ray spectra of (a) CH-AZ, (b) Pd(II) loaded CH-AZ, (c) CH-TSC, and (d) Pd(II) loaded CH-TSC derivatives.

6.6 Efficacy of alternate resins based on Pd(II) adsorption and desorption characteristics and cost indices

Table 6.6 presents the comparative assessment of adsorption capacity and desorption % for all investigated adsorbents (commercial resins, chitosan derivatives, and chitosan) for both synthetic ELP and aqueous solutions. It can be observed that a marginal reduction in adsorption capacity is apparent for all resins for the synthetic ELP solution case in comparison with the aqueous solution case. This is due to the presence of additives such as Na_2EDTA and NH_4OH in ELP solutions. From the perspective of desorption %, it can be observed that a significant reduction in desorption % is relevant for commercial resins and chitosan derivatives that exhibit higher desorption efficiencies of 55–59% and a marginal variation is apparent for the other chitosan derivatives. The significant reduction in desorption efficiency of the commercial resins and CH-ME resin is probably due to the existence of other impurities on the adsorbent surface in terms of additives in the synthetic ELP solutions that may strongly deter desorption using inexpensive eluents. However, for lower desorption efficiency values, the variations are not significant due to the minor contribution of additives as impurities influencing the surface related interactions during adsorption. In summary, it can be opined that significant variation in the adsorption and desorption characteristics does not exist for the chosen resins in terms of additives playing an influential role in detrimenting desired effect of higher Pd(II) recovery and reuse. Therefore, it is recommended that the prepared resins and chosen commercial resins are efficient to serve for the commercial needs associated to Pd(II) removal, recovery, and reuse from synthetic ELP solutions. The findings are to be further supplemented with retail and conceptual cost analysis and relevant indices.

Table 6.6: Summary of Pd(II) adsorption and desorption characteristics of alternate resins considered in this work and reported in the literature.

Adsorbent	Functional groups	pH	Adsorbent doasage ($g\ L^{-1}$)	Contact time (min)	Adsorption capacity for ELP solutions ($mg\ g^{-1}$)	Adsorption capacity for aqueous solutions ($mg\ g^{-1}$)	Desorption eluent	Desorption for ELP solutions (%)	Desorption for aqueous solutions (%)
Raw chitosan	Nitrogen	6	1.6	540	24.56	-	2M NaOH	6.31	
Amberlyst A21	Nitrogen	2	1.6	840	24.62	29.62	0.1M NaOH	59.66	48.05
Amberlite IRA958	Nitrogen	4	1.6	720	26.55	29.93	2M KOH	66.80	51.45
Dowex Marathon MSA	Nitrogen	4	1.4	780	31.56	35.66	2M KOH	68.08	57.02
Melamine cross-linked chitosan derivative (CH-ME)	Nitrogen	2	1.6	840	22.22	27.73	2M H_2SO_4	59.82	53.03
Triethylenetetramine cross-linked chitosan derivative (CH-TETA)	Nitrogen	2	1	300	40.76	45.54	2M HCl	39.68	38.72
Thiosemicarbazide cross-linked chitosan derivative (CH-TSC)	Sulfur and Nitrogen	2	1.6	720	30.27	30.31	2M HCl	40.82	39.39
3-amino-1,2,4-triazole-5-thiol cross-linked chitosan derivative (CH-AZ)	Sulfur and Nitrogen	4	1.6	120	30.96	30.88	2M HCl	45.03	46.38
Glutaraldehyde cross-linked chitosan derivative (Nagireddi *et al*., 2018)	Nitrogen	8	0.6	300	166.67	-	0.1M HCl	66.95	-
Lewatit TP214 (Nagireddi *et al*., 2017)	Sulfur and Nitrogen	8	2	300	172.41	-	0.1M NaOH	42.35	-
Raw chitosan (Sharififard *et al*., 2013)	Nitrogen	2	10	300					

Table 6.7: Performance and cost indices of alternate resins investigated in the thesis.

S. No	Adsorbent Name	Adsorption capacity (mg g^{-1})	Desorption efficiency (%)	Adsorbent cost ($ g^{-1})	Adsorption based index		Desorption based index	
					Performance	Cost	Performance	Cost
1	Raw chitosan	24.44	6.31	0.977	0.782	0.748	0.043	0.041
2	Amberlyst A21	20.74	59.66	0.102	0.788	7.240	0.333	6.112
3	Amberlite IRA958	29.49	66.80	0.229	0.826	3.364	0.540	2.200
4	Dowex Marathon MSA	31.44	68.08	0.418	0.880	2.248	0.560	1.430
5	CH-ME	22.64	59.82	2.029	0.815	0.333	0.380	0.156
6	CH-TETA	43.53	39.68	2.027	0.819	0.604	0.309	0.228
7	CH-TSC	30.43	40.82	2.058	0.974	0.442	0.623	0.113
8	CH-AZ	30.96	45.03	2.873	0.991	0.322	0.335	0.109

Table 6.7 summarizes the performance and cost indices of alternate resins investigated in the thesis. The provided data is interesting from the perspective of performance and cost indices, which is very much missing in the available literature. The table provides several useful insights. Firstly, the adsorption based performance index of alternative materials is similar (0.782-0.991) with a maximum value obtained for CH-AZ derivative. However, the corresponding cost index affirms poor cost index for CH-AZ (0.322), CH-ME (0.333), and marginally better values for CH-TETA (0.604); but excellent values for Amberlyst A21 (7.240) followed by Amberlite IRA 958 (3.364) and Dowex Marathon MSA (2.248). The corresponding cost index for Chitosan is marginally promising (0.748). Secondly, from the desorption perspective, best performance index value was confirmed for CH-TSC derivative (0.623), Dowex Marathon MSA commercial resin (0.560), Amberlite IRA 958 (0.540) and CH-ME derivative (0.380). Corresponding value for Chitosan is very low (0.043). However, the corresponding cost index is highest for Amberlyst A21 (6.112), followed by Amberlite IRA 958 (2.200) and Dowex Marathon MSA (1.430). Chitosan derivatives referred to poor values of desorption based cost index (0.228 for CH-TETA, 0.156 for CH-ME, 0.113 for CH-TSC, and 0.109 for CH-AZ). This is due to the high cost of chitosan (0.977 $ g^{-1}), which enormously contributed to its derivative cost. Thus, among all resins, commercial resin

Amberlyst A21 followed by Amberlite IRA 958 performed best in terms of all indices including cost indices for the removal and recovery of Pd(II) from synthetic ELP solutions.

6.7 Summary

The carried out experimental investigations provided several useful insights. Firstly, for synthetic ELP solutions, CH-AZ and CH-TSC provided Pd(II) removal characteristics but satisfactory and average Pd(II) recovery and reuse characteristics. The optimality of Pd(II) batch adsorption parameters refers to pH 2, 1.6 g L^{-1} adsorbent dosage, and 720 min contact time for CH-TSC and pH 4, 1.6 g L^{-1} adsorbent dosage and 120 min contact time for CH-AZ derivative. Corresponding adsorption characteristics are 30.43−143.17 mg g^{-1} adsorption capacity and 97.38−76.35 % removal for CH-TSC and 30.96−156.72 mg g^{-1} adsorption capacity and 99.08−83.58 % removal for CH-AZ in the Pd(II) solution concentration range of 50−300 mg L^{-1}. The most useful insight of the work is with respect to the limited desorption of sulfur and nitrogen functionalized chitosan derivatives with respect to nitrogen functionalized chitosan derivatives. This not reported in the literature for synthetic ELP solutions. Therefore, it is highly relevant to target research on stoichiometric and synthesis variations to enhance the Pd(II) desorption characteristics with synthetic ELP solutions. Also, for both derivatives, model fitness studies indicated best fitness of Freundlich isotherm and pseudo-second-order kinetic. Speciation analysis confirmed the role of $PdEDTA^{-2}$ species to functionally adsorb Pd(II) with amine and sulfur groups of the CH-TSC and CH−AZ derivatives. With moderate Pd(II) desorption characteristics and excellent Pd sorption characteristics, CH-TSC and CH−AZ derivatives can be concluded to be a comparable resin with available commercial resins such as Lewatit TP214 for Pd(II) recovery and reuse.

Chapter 7:

Conclusions and Future Work

Conclusions and Future Work

This chapter summarizes important conclusions, possible directions, and scope for future work.

7.1 Conclusions

Based on experimental and modeling studies associated to removal, recovery, and reuse of Pd(II) from synthetic ELP solutions, various conclusions deduced for commercial resins, and chitosan derivatives are presented in the following sub-sections for the set objectives.

7.1.1 Speciation analysis in ELP solutions

- In the entire range of pH investigated in this work (1 – 10) and for synthetic ELP solutions, Pd(II) can exist as $PdEDTA^{2-}$, $PdCl_4^{2-}$, $PdCl_3^-$, $PdCl_2$ (aq), $PdCl^+$, $Pd(NH_3)_4^{2+}$ and $Pd(NH_3)_3^{2+}$.
- For synthetic ELP solutions, in the lower pH range (1-6) and basic pH range (7-10), Pd(II) mostly exists as $PdEDTA^{2-}$ and $Pd(NH_3)_4^{2+}$, respectively.

7.1.2 Performance characteristics of raw chitosan

- For raw chitosan, the optimal adsorption parameters are initial solution pH of6, Cl^- concentration of 33 mg L^{-1}, adsorbent dose of 1.6 g L^{-1}, and contact time of 540 min.
- For an initial Pd(II) concentration range of 50−300 mg L^{-1}, the raw chitosan provided Langmuir adsorption capacity (90.91 mg g^{-1}), which is marginally higher than that reported in the literature for raw chitosan (62.5 mg g^{-1}) (Sharififard, Ashtiani et al. 2013).

- For raw chitosan, for an initial concentration range of 50−300 mg L^{-1}, the adsorption characteristics have been evaluated as 24.44−74.69 mg g^{-1} adsorption capacity and 78.21−39.83 removal %.
- Pd(II) adsorption studies for raw chitosan indicated the fitness of Langmuir equilibrium isotherm and pseudo-second-order kinetic models. Further, Pd(II) adsorption with this adsorbent has been evaluated to be exothermic and spontaneous in nature.
- The desorption efficiency from Pd loaded chitosan has been evaluated as 6.31 % (eluent: 2N NaOH), which is very less compared with other literature values.

7.1.3 Pd(II) adsorption and desorption characteristics of commercial resins

- The optimal adsorption parameters were evaluated as initial solution pH of 2, 4, and 4; an adsorbent dose of 1.6, 1.6, and 1.4 g L^{-1} and contact time of 840, 720, and 780 min for Amberlyst A21, Amberlite IRA958 and Dowex Marathon MSA resins, respectively.
- The adsorption capacities for the reins were obtained as20.74−73.81, 29.49−122.85, and 31.44−138.19 mg g^{-1} for Amberlyst A21, Amberlite IRA958, and Dowex Marathon MSA resins, respectively at an initial Pd(II) concentration range of 50−300mg L^{-1}. Corresponding % removal were 78.78−44.30, 82.57−57.33, and 88.02−64.49, respectively.
- Among equilibrium models, best fitness models correspond to Freundlich isotherm for Dowex MSA and Amberlite IRA 958 and Langmuir isotherm for Amberlyst A21. For all resins, Pd(II) adsorption kinetic were represented by the pseudo-second-order model. For all resins, exothermic and spontaneous Pd(II) adsorption occurred.

- The best desorption efficiencies were obtained as 59.66 (0.1M NaOH), 66.80 (2M KOH), and 68.08 % (2M KOH) for Amberlyst A21, Amberlite IRA958 and Dowex Marathon MSA resins, respectively.

7.1.4 Pd(II) adsorption and desorption characteristics of nitrogen functionalized chitosan based derivatives

- The optimal adsorption parameters obtained were to be pH of 2, adsorbent dose of 1.6 and 1 g L^{-1} and, contact time of 840 and 300 min for CH-ME and CH-TETA derivatives, respectively.
- For a variation in Pd(II) solution concentration of 50−300 mg L^{-1}, the metal uptakes varied as 22.64−85.58 and 43.53−117.08 mg g^{-1} for CH-ME and CH-TETA derivatives, respectively. Corresponding metal removal % were 81.50−51.35 and 87.05−39.03, respectively.
- Freundlich and Langmuir equilibrium isotherms have been evaluated to be the best fit models for CH-ME and CH-TETA derivatives, respectively. The pseudo-second-order kinetic model has been evaluated to be the best fit model for both the derivatives. Thermodynamic evaluations indicated that the Pd(II) adsorption is spontaneous and exothermic nature for both resins.
- The best desorption efficiencies were obtained as 59.82 (2M H_2SO_4) and 39.68 % (2M HCl) for CH-ME and CH-TETA derivatives, respectively.

7.1.5 Pd(II) adsorption and desorption characteristics of nitrogen and sulfur functionalized chitosan based derivatives

The optimal adsorption parameters refer to be pH of 2 and 4, adsorbent dose of 1.6 g L^{-1}, contact time of 720, and 120 min for CH-TSC and CH-AZ derivatives, respectively.

- For synthetic ELP solutions, for a variation in Pd(II) solution concentration from 50−300 mg L^{-1}, the noble metal uptake varied from 30.43−143.17 and 30.96−156.72 mg g^{-1} for CH-TSC and CH-AZ derivatives, respectively. Corresponding metal removal % varied from 97.33−76.35 and 99.08−83.58 %.
- From modelling perspective, both derivatives followed Freundlich equilibrium isotherm and pseudo-second-order kinetic models. Thermodynamic evaluations indicated that the Pd(II) adsorption is spontaneous and exothermic nature for both resins.
- The maximum desorption efficiencies were obtained as 40.82 and 45.03 % with 2M HCl eluent for CH-TSC and CH-AZ derivatives, respectively.

The best results obtained in this work along with the data available in few most competent literature, the following can be outlined as the most promising conclusions of the Ph.D. thesis:

a) All chitosan derivatives and commercial resins provided promising Pd(II) adsorption capacities from synthetic ELP solutions.

b) Compared to aqueous solutions data in the literature, among all resins, Dowex Marathon MSA resin and CH-AZ derivative exhibited best adsorption capacities of 185.16 and 175.44 mg g^{-1}, respectively.

c) Among all resins, Dowex Marathon MSA and Amberlite IRA958 exhibited best desorption efficiencies of 68.08 and 66.80 % (2M KOH eluent), respectively.

d) CH-AZ derivative exhibited the highest adsorption capacity (175.44 mg g^{-1}) but not desorption efficiency (45.03 %).

e) Nitrogen functionalized chitosan derivative CH-ME performed better than sulfur functionalized chitosan derivative CH-AZ in terms of desorption efficiency. Other derivatives, namely CH-TSC and CH-TETA performance is satisfactory but not excellence.

f) Literature findings affirm the average adsorption capacity of chitosan in comparison with chitosan derivatives and commercial resins.

g) Compared to nitrogen functionalized resins such as CH-ME and Amberlyst A21, Amberlite and Dowex, the literature reported findings as well affirm satisfactory but not excellent desorption efficacy of nitrogen and sulfur functionalized resins (Lewatit TP214).

h) Overall, among all considered resins, commercial resin Dowex Marathon MSA performed the best followed with derivative CH-AZ in terms of Pd(II) removal, recovery, and reuse.

FTIR, BET, FESEM, EDXA, TGA analyses have been conducted for alternate commercial, and chitosan functionalized resins for which Pd(II) adsorption and desorption characteristics have also been obtained. Deeper insight into the obtained data and trends indicates the following inferences with respect to the synergy or irrelevance of the results obtained from such characterization studies with respect to obtained trends for Pd(II) adsorption and desorption characteristics:

- ✓ The data from BET surface area analysis is not highly synergistic with the Pd(II) adsorption and desorption characteristics. This is due to the fact that chemical and functional group interactions have a stronger role to influence and enhance the measured Pd(II) adsorption and desorption characteristics.
- ✓ The mechanistic understanding with respect to Pd(II) adsorption process is indicative of the said mechanisms by following a pseudo-second-order model, which is in good agreement with the FTIR analysis for all resins and raw chitosan. However, the analysis does not account upon the trends obtained for the desorption characteristics. Hence, further research is required to this extent.
- ✓ EDX analysis affirmed the existence of Pd and nitrogen on the adsorbent surface after adsorption and after functional modification, respectively. Such analysis is useful to correlate towards the observed enhancement of Pd(II) adsorption of functionalized chitosan with respect to the raw chitosan.
- ✓ FESEM analysis enabled morphological analysis, which is insignificant to elaborate upon trends obtained from Pd(II) adsorption and desorption studies for both commercial, and chitosan functionalized resins.
- ✓ The crystallinity of the resins has been indicated by the XRD analysis. Based on the observed trends, chitosan crystallinity decreased after modification with suitable functional groups. Also, the adsorbent surface became amorphous after treatment with EDTA complex of the Pd prevalent in the synthetic ELP solutions.
- ✓ TGA analysis indicated the thermal stability of the adsorbents even at higher temperatures (up to 300 °C) and hence the efficacy of the resins to function with respect to Pd(II) adsorption and desorption at a lower temperature (≤60 °C).

- ✓ Regeneration studies affirmed that Dowex Marathon MSA resin facilitates grater desorption efficiency (93.99%) in comparison with CH-ME derivative (78.47%) after three cycles of desorption without any intermittent adsorption. Reusability studies confirm that a significant reduction in adsorption efficiency of about 30% for both resins. Therefore, it is apparent that strong chemical interaction between functional sites and adsorbate molecules occurred that restricted desorption of Pd(II) from the surface of the adsorbent.

In summary, Pd(II) adsorption and desorption characteristics cannot be fully understood from surface characterization analyses. These analyses at the maximum, provide a qualitative understanding of the associated resin chemistry information. Adsorbent reusability is very much dependent on its desorption characteristics, which are always influenced by the complex chemistry of the eluents and associated functional interactions. Therefore, the cyclic performance of the commercial resins and associated functional group interactions need to be considered in the near future based on finer FTIR analysis before and after adsorption/desorption of every cycle to correlate with the trends indicated by the cyclic Pd(II) adsorption/desorption studies. Such studies would be useful to provide useful insights into the complex chemistry of eluents and resin reusability.

Also, among tested adsorbents, commercial resins provided reasonable adsorption efficiencies and better desorption efficiencies in comparison with the synthesized chitosan derivatives. Overall, all adsorbents provided better Pd(II) adsorption efficiencies, and reasonable desorption efficiencies in comparison with the literature reported data that involved either aqueous solutions or complex eluents or both. Since Pd(II) adsorption is stronger, a significant portion of the Pd(II) exists on the adsorbent even after consistent desorption. Such stable adsorbent can have utility as

a catalyst for Suzuki cross-coupling reactions, degradation of organic compounds, hydro-dehalogenation, and dehydro-dearomatization process.

7.2 Future work

The following areas of work have been identified to consider in the near future to consolidating future challenging and exciting research in the vast field of noble metal recovery and reusing from complex waste solutions:

- Synthetic ELP solutions with variations in stabilizer (Na_2EDTA) type and concentrations and solution pH (NH_4OH or NaOH) can be targeted to further delineate upon the effect of these on Pd(II) recovery and reuse characteristics of said resins be targeted.
- Solution with more complex solution chemistry and real wastewater samples are to be targeted for Pd(II) recovery and reuse.
- Variations to reaction stoichiometry and synthesis procedures are to be targeted to enhance desorption efficiency from 40−45% to 65−75% for both nitrogen and, nitrogen and sulfur functionalized resins. Further, the utilization of inexpensive reagents and laboratory extracted chitosan are to be targeted to significantly reduce the cost of chitosan derivatives and foster their cost competitiveness close to that of commercial resin. This will be a very exciting field of research.
- Commercial resins and chitosan modified derivatives with S/N/O and their combination functional groups to be investigated for the recovery and reuse of other noble metals (Pt and Au) and their combinations with Pd from solutions with complex and chelating chemistry associated to other metals and additives.

- Investigations towards adsorption and desorption cycles and resin efficacy based on best performance in the content of repetitive usage.
- Reaction kinetics, desorption, and engineering studies associated to catalytic properties of Pd/Pt loaded chitosan derivatives in various reactions such as Suzuki cross-coupling reaction, degradation of organic compounds, hydro-dehalogenation and dehydro-dearomatization process.
- Column studies to optimize the performance of chitosan derivatives and commercial resins for continuous adsorption and desorption of Pd(II) from synthetic ELP solutions
- Development of super-efficient chelating resins with enhanced noble metal desorption characteristics based on chelation and functional group chemistry.
- Detailed cost analysis for all resins reported till date for their cost efficacy towards noble metal recovery from spent and waste adsorbate systems with variant solution chemistry complexity.
- Research commercialization and technology transfer of most cost competitive adsorbents for noble metal recovery and reuse from real waste streams and adsorbate systems.

References

References

Aharoni, C. and M. Ungarish (1977). "Kinetics of activated chemisorption. Part 2—Theoretical models." Journal of the Chemical Society **73**: 456-464.

Ahmad, M., S. Ahmed, B. L. Swami and S. Ikram (2015). "Preparation and characterization of antibacterial thiosemicarbazide chitosan as efficient Cu(II) adsorbent." Carbohydrate Polymers**132**: 164-172.

Arrascue, M. L., H. M. Garcia, O. Horna and E. Guibal (2003). "Gold sorption on chitosan derivatives." Hydrometallurgy**71**: 191–200.

Atia, A. A., A. M. Donia and A. M. Yousif (2005). "Comparative Study of the Recovery of Silver(I) from Aqueous Solutions with Different Chelating Resins Derived from Glycidyl Methacrylate." Journal of Applied Polymer Science**97**(806-812): 806.

Awual, M. R. and M. M. Hasan (2015). "Fine-tuning mesoporous adsorbent for simultaneous ultra-trace palladium(II) detection, separation and recovery." Journal of Industrial and Engineering Chemistry**21**: 507–515.

Awual, M. R., M. A. Khaleque, Y. Ratna and H. Znad (2015). "Simultaneous ultra-trace palladium(II) detection and recovery from wastewater using new class meso-adsorbent." Journal of Industrial and Engineering Chemistry**21**: 405–413.

Awual, M. R., M. M. Hasan and H. Znad (2015). "Organic–inorganic based nano-conjugate adsorbent for selective palladium(II) detection, separation and recovery." Chemical Engineering Journal**259**: 611–619.

Awual, M. R., M. M. Hasan, M. Naushad, H. Shiwaku and T. Yaita (2015). "Preparation of new class composite adsorbent for enhanced palladium(II) detection and recovery." Sensors and Actuators B**209**: 790–797.

Awual, M. R., T. Yaita, S. A.El-Safty, H. Shiwaku, Y. Okamoto and S. Suzuki (2013). "Investigation of palladium(II)detection and recovery using ligand modified conjugate adsorbent." Chemical Engineering Journal**222**: 172–179.

Azarova, Y. A., A. V. Pestov, A. Y. Ustinov and S. Y. Bratskaya (2015). "Application of chitosan and its N-heterocyclic derivatives for preconcentration of noble metal ions and their determination using atomic absorption spectrometry." Carbohydrate Polymers**134**: 680-686.

Baba, Y., T. Oshima and S. Kanemaru (2011). "A Quantitative Consideration for Template Effect of Palladium(II) Using N-[Pyridylmethyl] Chitosan." Solvent Extraction and Ion Exchange**29**(3): 509-517

Baba, Y., Y. Aoya, K. Ohe, S. Nakamura and T. Ohshima (2005). "Adsorption removal of copper(II) on N-Methylene phosphonic chitosan derivative." Journal of Chemical Engineering of Japan**38**(11): 887-893.

Barakat, M. A., M. H. H. Mahmoud and Y. S. Mahrous (2006). "Recovery and separation of palladium from spent catalyst." Applied Catalysis A: General**301**: 182–186.

Belver, C., M. J. Lopez-Munoz, J. M. Coronado and J. Soria (2003). "Palladium enhanced resistance to deactivation of titanium dioxide during the photocatalytic oxidation of toluene vapors." Appl. Catal., B**46**: 497–509.

Bernardis, F. L., R. A. Grant and D. C. Sherrington (2005). "A review of methods of separation of the platinum-group metals through their chloro-complexes." Reactive & Functional Polymers**65**: 205–217.

Bilba, D., D. Bejan and L. Tofan (1998). "Chelating Sorbents in Inorganic Chemical Analysis." Croatica Chemica Acta**71**(1): 155-178.

Birinci, E., M. Gülfen and A. O. Aydın (2009). "Separation and recovery of palladium(II) from base metal ions by melamine–formaldehyde–thiourea (MFT) chelating resin." Hydrometallurgy**95**: 15–21.

Boucher, L. J. and J. J. Katz (1967). "The Infared Spectra of Metalloporphyrins (4000-160 cm^{-1})." J. Am. Chem. Soc. **89**(6): 1340-1345.

Bratskaya, S. Y., A. Y. Ustinov, Y. A. Azarova and A. V. Pestov (2011). "Thiocarbamoyl chitosan: Synthesis, characterization and sorption of Au(III), Pt(IV), and Pd(II)." Carbohydrate Polymers**85**(4): 854-861.

Bratskaya, S., Y. Privar, A. Ustinov, Y. Azarova and A. Pestov (2016). "Recovery of Au(III), Pt(IV), and Pd(II) Using Pyridylethyl-Containing Polymers: Chitosan Derivatives vs Synthetic Polymers." Industrial & Engineering Chemistry Research**55**: 10377−10385.

Butewicz, A., K. C. Gavilan, A. V. Pestov, Y. Yatluk, A. W. Trochimczuk and E. Guibal (2009). "Palladium and Platinum Sorption on a Thiocarbamoyl-Derivative of Chitosan." Journal of Applied Polymer Science**116**: 3318–3330.

Camel, V. (2003). "Solid phase extraction of trace elements." Spectrochimica Acta Part B**58**: 1177–1233.

Chassary, P., T. Vincent, J. S. Marcano, L. E. Macaskie and E. Guibal (2005). "Palladium and platinum recovery from bicomponent mixtures using chitosan derivatives." Hydrometallurgy**76**: 131–147.

Colombo, C. (2007). "Complexation of platinum, palladium and rhodium with inorganic ligands in the environment." Geochemistry: Exploration, Environment, Analysis**8**: 1-11.

Dean, J. A. (1999). Lange's Handbook of Chemistry. New York, McGRAW-HILL, INC.

Ding, S., X. Zhang, X. Feng, Y. Wang, S. Ma, Q. Peng and W. Zhang (2006). "Synthesis of *N,N'*-diallyl dibenzo 18-crown-6 crown ether crosslinked chitosan and their adsorption properties for metal ions." Reactive & Functional Polymers**66**: 357–363.

Donia, A. M., A. A. Atia and K. Z. Elwakeel (2005). "Gold(III) recovery using synthetic chelating resins with amine, thio and amine/mercaptan functionalities." Separation and Purification Technology**42**: 111–116.

El-Safty, S. A., M. A. Shenashen, M. Ismael, M. Khairy and M. R. Awual (2013). "Mesoporous aluminosilica sensors for the visual removal and detection of Pd(II) and Cu(II) ions." Microporous and Mesoporous Materials**166**: 195–205.

Elwakeel, K. Z., S. El-Kousy, H. G. El-Shorbagy and M. A. A. El-Ghaffar (2016). "Comparison between the removal of Reactive Black 5 from aqueous solutions by 3-amino-1,2,4 triazole,5-thiol and melamine grafted chitosan prepared through four different routes." Journal of Environmental Chemical Engineering**4**(1): 733-745.

Freundlich, H. M. F. (1906). "Over the adsorption in solution." The Journal of Physical Chemistry **57**: 385-470.

Fujiwara, K., A. Ramesh, T. Maki, H. Hasegawa and K. Ueda (2007). "Adsorption of platinum (IV), palladium (II) and gold (III) from aqueous solutions onto L-lysine modified crosslinked chitosan resin." Journal of Hazardous Materials**146**: 39–50.

Ge, H., H. Chen and S. Huang (2012). "Microwave preparation and properties of O-crosslinked maleic acyl chitosan " Journal of Applied Polymer Science**125**(4): 2716-2723.

Goldberg, S. (2005). Equations and Models Describing Adsorption Processes in Soils. Soil Science Society of America, 677 S. Segoe Road, Madison, WI 53711, USA.

Guadalupe, R., H. E. Reynel-Avila, A. Bonilla-Petriciolet, I. Cano-Rodríguez, C. Velasco-Santos and A. L. Martínez-Hernández. (2008). Recycling poultry feathers for Pb removal from

wastewater: kinetic and equilibrium studies. World Academy Of Science, Engineering And Technology.

Guibal, E. (2004). "Interactions of metal ions with chitosan-based sorbents: a review." Separation and Purification Technology**38**: 43–74.

Guibal, E., M. Ruiz, T. Vincent, A. Sastre and R. Navarro-Mendoza (2001). "Platinum and palladium sorption on chitosan derivatives." Separation Science and Technology**36**(5&6): 1017–1040.

Guibal, E., N. V. O. Sweeney, M. C. Zikan, T. Vincent and J. M. Tobin (2001). "Competitive sorption of platinum and palladium on chitosan derivatives." International Journal of Biological Macromolecules**28**: 401-408.

Guibal, E., N. V. O. Sweeney, T. Vincent and J. M. Tobin (2002). "Sulfur derivatives of chitosan for palladium sorption." Reactive & Functional Polymers **50**: 149–163.

Ho, Y. S. and G. McKay (1999). "Pseudo-second order model for sorption processes." Process Biochemistry**34**: 451-465.

Hubicki, Z. and A. Wołowicz (2009). "A comparative study of chelating and cationic ion exchange resins for the removal of palladium(II) complexes from acidic chloride media." Journal of Hazardous Materials**164**: 1414–1419.

Hubicki, Z. and A. Wołowicz (2009). "Adsorption of palladium(II) from chloride solutions on Amberlyst A 29 and Amberlyst A 21 resins." Hydrometallurgy**96**: 159–165.

Hubicki, Z., M. Leszczyńska, B. Łodyga and A. Łodyga (2007). "Recovery of palladium(II) from chloride and chloride–nitrate solutions using ion-exchange resins with S-donor atoms." Desalination**207**(1-3): 80-86.

Jana, N. R., Z. L. Wang and T. Pal (2000). "Redox Catalytic Properties of Palladium Nanoparticles: Surfactant and Electron Donor-Acceptor Effects." Langmuir**16**: 2457-2463.

Jermakowicz-Bartkowiak, D., B. N. Kolarz and A. Serwin (2005). "Sorption of precious metals from acid solutions by functionalised vinylbenzyl chloride–acrylonitryle–divinylbenzene copolymers bearing amino and guanidine ligands." Reactive & Functional Polymers**65**: 135–142.

Kanai, Y., T. Oshima and Y. Baba (2008). "Synthesis of Highly Porous Chitosan Microspheres Anchored with 1,2-Ethylenedisulfide Moiety for the Recovery of Precious Metal Ions." Industrial & Engineering Chemistry Research**47**: 3114-3120.

Kato, T., S. Igarashi, O. Ohno, S. Saito and R. Ando (2016). "Homogeneous Liquid-Liquid Extraction (HoLLE) of Palladium in Real Plating Wastewater for Recovery." Journal of Environmental Protection**7**: 277-286.

Khunathai, K., K. Inoue, K. Ohto, H. Kawakita, M. Kurata, K. Atsumi, H. Fukuda and S. Alam (2013). "Adsorptive Recovery of Palladium(II) and Platinum(IV) on the Chemically Modified-Microalgal Residue." Solvent Extraction and Ion Exchange**31**(3): 320-334.

Kim, K. M., J. H. Son, S. K. Kim, C. L. Weller and M. A. Hanna (2006). "Properties of Chitosan Films as a Function of pH and Solvent Type." Journal of Food Science**71**(3): 119-124.

Kim, S., M.-H. Song, W. Wei and Y.-S. Yun (2015). "Selective biosorption behavior of Escherichia coli biomass toward Pd(II) in Pt(IV)–Pd(II)binary solution." Journal of Hazardous Materials**283**: 657–662.

Labosova, L., M. Stofkova and J. Kracunovska (2006). "The study of possibilities of selective recovery of palladium (ii) from chlorides solutions by ion exchange resin Lewatit TP-214." Acta Metallurgica Slovaca**12**: 235-241.

Lambert, B., H. F. Shurvell, L. Verbit, R. G. Cooks and G. H. Stout (1976). Organic Structural Analysis. New York Macmillan Publishing Co., Inc.

Langmuir, I. (1918). "The adsorption gases on plane surface of glass, mica and platinum." Journal of the American Chemical Society**40**(9): 1361-1403.

Li, M., Z. Zhang, R. Li, J. J. Wang and A. Ali (2016). "Removal of Pb(II) and Cd(II) ions from aqueous solution by thiosemicarbazide modified chitosan." International Journal of Biological Macromolecules**86**: 876-884.

Liao, B., W.-y. Sun, N. Guo, S.-l. Ding and S.-j. Su (2016). "Equilibriums and kinetics studies for adsorption of Ni(II) ion on chitosan and its triethylenetetramine derivative." Colloids and Surfaces A: Physicochemical and Engineering Aspects**501**: 32-41.

Lin, S., W. Wei, X. Wu, T. Zhou, J. Mao and Y.-S. Yun (2015). "Selective recovery of Pd(II) from extremely acidic solution using ion-imprinted chitosan fiber: Adsorption performance and mechanisms." Journal of Hazardous Materials**299**: 10–17.

Liu, Y. (2009). "Is the Free Energy Change of Adsorption Correctly Calculated?" Journal of Chemical & Engineering Data**54**(7): 1981–1985.

Lu, Y., L. Xu, Y. Li, H. Yang, Z. Liu, L. Jiang and A. Zhang (2018). "Highly selective adsorption for palladium removal by impregnation preparation of a macroporous N-based functional composite." Solvent Extraction and Ion Exchange**36**(1): 1-16.

Middlesworth, J. M. V. and S. A. Wood (1999). "The stability of palladium(II) hydroxide and hydroxy–chloride complexes: An experimental solubility study at 25–85°C and 1 bar." Geochimica et Cosmochimica Acta**63**(11/12): 1751–1765.

Mohan, S. and J. Karthikeyan (1997). "Removal of lignin and tannin color from aqueous solution by adsorption on to activated carbon solution by adsorption on to activated charcoal." Environmental Pollution**97**: 183-187.

Monier, M., D. A. Abdel-Latif and Y. G. A. El-Reash (2016). "Ion-imprinted modified chitosan resin for selective removal of Pd(II) ions." Journal of Colloid and Interface Science**469**: 344–354.

Morcali, M. H. and B. Zeytuncu (2015). "Investigation of adsorption parameters for platinum and palladium onto a modified polyacrylonitrile-based sorbent." International Journal of Mineral Processing**137**: 52–58.

Nachtigall, D., S. Artelt and G. Wunsch (1997). "Speciation of platinum–chloro complexes and their hydrolysis products by ion chromatography Determination of platinum oxidation states." Journal of Chromatography A**775**: 197–210.

Nagireddi, S., A. K. Golder and R. Uppaluri (2018). "Role of protonation and functional groups in Pd(II) recovery and reuse characteristics of commercial anion exchange resin-synthetic electroless plating solution systems." Journal of Water Process Engineering**22**: 227-238.

Nagireddi, S., V. Katiyar and R. Uppaluri (2017). "Pd(II) adsorption characteristics of glutaraldehyde cross-linked chitosan copolymer resin." International Journal of Biological Macromolecules**94**(Part A): 72-84.

Nska, D. K., J. Ryczkowski and Z. Hubicki (2008). "FT-IR/PAS studies of chelates adsorp-tion on anion exchangers." The European Physical Journal Special Topics**154**: 339–343.

Nski, G. W., S. Pasieczna-Patkowska and Z. Hubicki (2008). "Mechanism of sorptionsulphoderivative organic chelating agents on strong base anion exchanger Amberlite IRA-402 by FT-IR/PAS and DRS methods." The European Physical Journal Special Topics **154**: 377–380

Rajesh, Y. (2015). Adsorption Characteristics of Activated Carbon Adsorbents for the Recovery of Pd (II) from Synthetic Electroless Plating Solutions. PhD, Indian Institute of Technology Guwahati.

Ramesh, A., H. Hasegawa, W. Sugimoto, T. Maki and K. Ueda (2008). "Adsorption of gold(III), platinum(IV) and palladium(II) onto glycine modified crosslinked chitosan resin." Bioresource Technology**99**: 3801–3809.

Ruiz, M., A. M. Sastre and E. Guibal (2000). "Palladium sorption on glutaraldehyde-crosslinked chitosan." Reactive & Functional Polymers**45**: 155–173.

Saita, K., S. Nagaoka, T. Shirosaki, M. Horikawa, S. Matsuda and H. Ihara (2012). "Preparation and characterization of dispersible chitosan particles with borate crosslinking and their antimicrobial and antifungal activity." Carbohydrate Research**349**: 52-58.

Sharififard, H., F. Z. Ashtiani and M. Soleimani (2013). "Adsorption of palladium and platinum from aqueous solutions by chitosan and activated carbon coated with chitosan." Asia-Pacific Journal of Chemical Engineering**8**(3): 384-395.

Silverstein, R. L., G. C. Baddler and T. C. Morrill (1991). Spectrometric Identification of Organic Compounds, John Wiley & Sons Ink

Socrates, G. (2001). Infrared and Raman Characteristic Group Frequencies: Tables andCharts. Chichester, New York, John Wiley & Sons Ltd.

Tripathi, S., G. K. Mehrotra and P. K. Dutta (2009). "Physicochemical and bioactivity of cross-linked chitosan-PVA film for food packaging applications." International Journal of Biological Macromolecules**45**(4): 372-376.

Wołowicz, A. and Z. Hubicki (2012). "The use of the chelating resin of a new generation Lewatit MonoPlus TP-220 with the bis-picolylamine functional groups in the removal of selected metal ions from acidic solutions." Chemical Engineering Journal**197**: 493–508.

Wołowicz, A. and Z. Hubicki (2014). "Adsorption characteristics of noble metals on the strongly basic anion exchanger Purolite A-400TL." Journal of Material Science**49**: 6191–6202.

Z.Elwakeel, K., S. El-Kousy, H. G. El-Shorbagy and M. A. A. El-Ghaffar (2016). "Comparison between the removal of Reactive Black 5 from aqueous solutions by 3-amino-1,2,4 triazole,5-thiol and melamine grafted chitosan prepared through four different routes." Journal of Environmental Chemical Engineering**4**(1): 733-745.

Zakaria, Z., Z. Izzah, M. Jawaid and A. Hassan (2012). "Effect of degree of deacetylation of chitosan on thermal stability and compatibility of chitosan polyamide blend." BioResources**7**: 5568-5580.

Zhong, Z., Z. Zhong, R. Xing, P. Li and G. Mo (2010). "The preparation and antioxidant activity of 2-[phenylhydrazine (or hydrazine)-thiosemicarbazone]-chitosan." International Journal of Biological Macromolecules**47**: 93-97.

Zhou, L., J. Liu and Z. Liu (2009). "Adsorption of platinum(IV) and palladium(II) from aqueous solution by thiourea-modified chitosan microspheres." Journal of Hazardous Materials**172**: 439–446.

Zhou, L., J. Xu, X. Liang and Z. Liu (2010). "Adsorption of platinum(IV) and palladium(II) from aqueous solution by magnetic cross-linking chitosan nanoparticles modified with ethylenediamine." Journal of Hazardous Materials**182**(1–3): 518–524.

Publications

List of Publications

Published articles in international refereed journals

[1] **S Nagireddi**, AK Golder, R Uppaluri. Investigation on Pd (II) removal and recovery characteristics of chitosan from electroless plating solutions. Journal of Water Process Engineering 2017; 19: 8-17.

[2] **S Nagireddi**, AK Golder, R Uppaluri. Role of protonation and functional groups in Pd(II) recovery and reuse characteristics of commercial anion exchange resin-synthetic electroless plating solution systems. Journal of Water Process Engineering 2018; 22: 227- 238.

[3] **S Nagireddi**, AK Golder, R Uppaluri. Role of EDTA on the Pd(II) adsorption characteristics of chitosan cross-linked 3-amino-1,2,4-triazole-5-thiol derivative from synthetic electroless plating solutions. International Journal of Biological Macromolecules 2019; 127:320-329.

[4] **S Nagireddi**, AK Golder, R Uppaluri. Combinatorial Optimality of functional groups, process parameters and Pd(II) adsorption-desorption characteristics for commercial anion exchange resins-synthetic electroless plating systems. Environmental Science and Pollution Research 2019; 1-13.

Communicated/Under preparation

[1] **S Nagireddi**, AK Golder, R Uppaluri. Challenges and opportunities for the development of low cost Pd(II) adsorptive chelating resin: A review. (To be submitted)

[2] **S Nagireddi**, AK Golder, R Uppaluri. Efficacy of triethylenetetraamine cross-linked chitosan derivative towards Pd(II) removal and recovery synthetic electroless plating solutions. (To be submitted)

[3] **S Nagireddi**, AK Golder, R Uppaluri. Optimality of sulfur and nitrogen functionalized derivative for recovery and reuse of Pd(II) from synthetic electroless plating solutions. (To be submitted)

[4] **S Nagireddi**, AK Golder, R Uppaluri. Role of EDTA and NH4OH on the Pd(II) adsorption characteristics of chitosan cross-linked melamine derivative from synthetic electroless plating solutions. (To be submitted)

Conference Presentations (National and International)

[1] **S Nagireddi**, AK Golder, R Uppaluri. International Conference on Challenges in Environmental Science & Engineering (CESE-2018), 04-08 November, 2018, Bangkok, Thailand.

[2] **S Nagireddi**, AK Golder, R Uppaluri. Indo-Japan Bilateral Symposium on Future Perspective of Bioresource Utilization in North-Eastern Region (IJBS 17), 01-04 February, 2018, IIT Guwahati, India.

[3] **S Nagireddi**, V Katiyar, R Uppaluri. Indo-Japan Bilateral Symposium on Future Perspective of Bioresource Utilization in North-Eastern Region (IJBS 17), 01-04 February, 2018, IIT Guwahati, India

Appendix

Appendix A: Calibration Curve for The Determination of Pd(II) Solution Concentration

Atomic absorption spectrophotometer (AAS) (Make: M/S Varian BV, Model: Spectra AA 220FS) operated in flame mode at a wavelength of 244.8 nm was used to determine the absorbance of Pd(II) adsorbate samples before and after adsorption. A calibration curve has been prepared to serve as a supplementary database to determine the concentrations of the fresh and spent adsorbate solutions. Using solution concentrations reported in Table 2.2, 3-15 ppm Pd(II) solutions have been prepared using dilution approaches of stock solutions. Thereafter, for all standard samples, AAS was used to measure the absorbance. Based on the measured absorbances for various Pd(II) solution concentrations of synthetic ELP solutions, Figure A1 illustrates the relevant calibration curve. As shown, the mean absorbance of the samples varied linearly with Pd(II) concentrations.

A calibration curve is required to determine the Pd(II) solution concentration from measured adsorbate absorbance value. Since it would be possible to obtain different calibration curves for synthetic Pd(II) ELP solutions have been prepared.

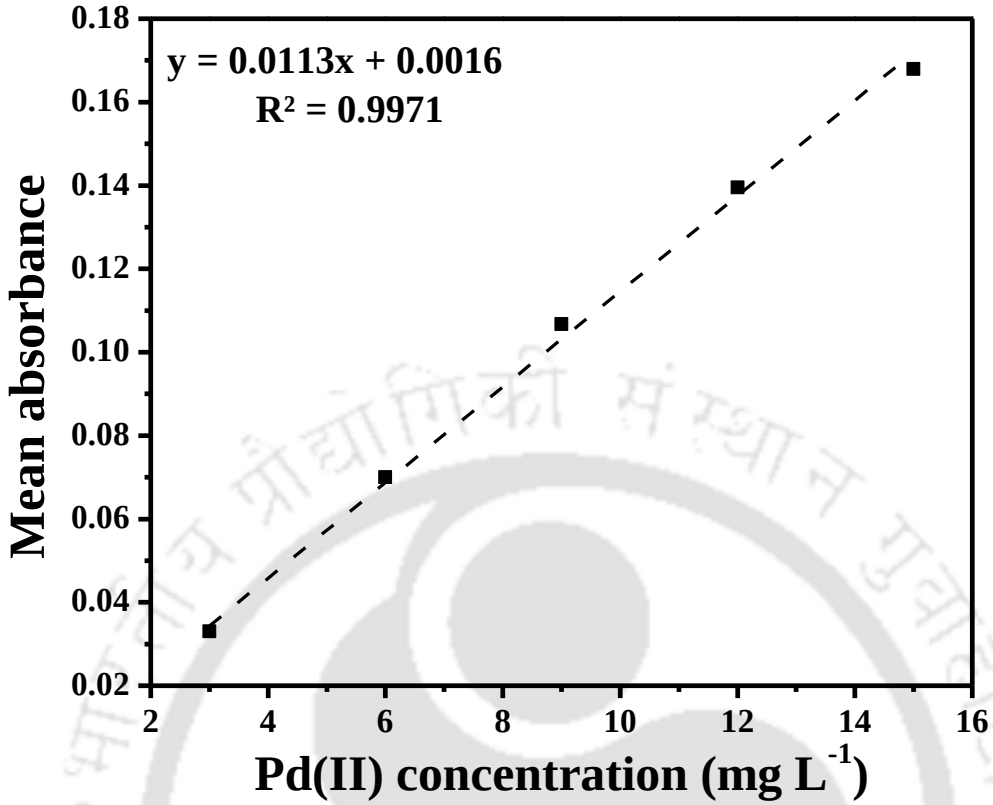

Fig. A1: Calibration curve for the determination of Pd(II) in synthetic electroless plating solutions.

Appendix B: Batch Adsorption Sample Calculations

The following steps summarize the evaluation of Pd (II) adsorption characteristics of raw chitosan:

a) Adsorption parameters: Adsorbent Dosage: 1.6 g L^{-1} (80 mg); Volume of Pd(II) solution: 50ml; Contact Time: 540 min; Initial Concentration: 50 mgL^{-1}.

b) Final equilibrium Pd(II) solution concentration (C_{eq}): From AAS and calibration curve, C_{eq} = 10.895mgL^{-1}.

c) Using eq. (**2.1**), % Adsorption $= \frac{(50-10.895)}{50} \times 100 = 78.21\%$

d) Using eq. (**2.2**), Metal Uptake= $\frac{(50-10.895)}{80} \times 50 = 24.44\,mg/g$

e) Langmuir isotherm Parameters:

The determination of Langmuir isotherm parameters requires adsorption equilibrium data. Using the data, for the plot of $\frac{C_{eq}}{Q_{eq}}$ vs C_{eq}, the slope, intercept and regression coefficient (R^2)have been obtained as0.011, 0.330 and 0.999, respectively.

Using slope, q_{max} (monolayer capacity) = $\frac{1}{\text{slope}}$ = 90.91mg g^{-1}.

Using intercept and q_{max}, b = $\frac{1}{(q_{max} \times \text{intercept})}$ = 0.0333.

f) Freundlich isotherm parameters:

For a plot drawn between $\log C_{eq}$ and $\log q_{eq}$, the slope, intercept and regression coefficient have been obtained as 0.399, 1.006 and 0.966, respectively.

Using slope, $n = \frac{1}{m} = 2.506$.

Using intercept, $K_f = 10^{1.006} = 10.136$

g) Psuedo-second order model parameters

For a plot drawn between tvs $\frac{t}{q_t}$, the slope, intercept and regression coefficient have been obtained as, 0.039, 0.802 and 0.997, respectively.

Using slope, $Q_e = \frac{1}{0.039} = 25.64 \text{ mg g}^{-1}$

Using intercept, $k_2 = \frac{1}{(Q_e^2 \times \text{intercept})} = 0.0019$.

h) Thermodynamic model parameters:

For a plot drawn between $\frac{1}{T}$ and $\ln K_c$, the slope, intercept and regression coefficient have been obtained as 1878, -4.738 and 0.974.

Using slope and intercept, the thermodynamic parameters can be evaluated as

$\Delta H^o = -(\text{slope} \times R) = -15.614 \text{ kJ mol}^{-1}$

$\Delta S^o = (\text{intercept} \times R) = -39.392 \text{J K}^{-1}\text{mol}^{-1}$

$\Delta G^o = \Delta H^o - T\Delta S^o = -3.875 \text{ kJ mol}^{-1}$

Appendix C: Batch Desorption Sample Calculations

The following steps summarize the evaluation of Pd (II) desorption characteristics of raw chitosan:

a) Adsorption parameters: Adsorbent Dosage: 1.6 g L^{-1} (80 mg); Volume of Pd(II) solution: 50mL; Contact Time: 540 min; Initial Concentration: 50 mg L^{-1}.

Final Pd(II) solution concentration (C_f) = 16.247 mg L^{-1}

Concentration of Pd(II) on adsorbent (A) = $C_i - C_f$ = 33.753 mg L^{-1}

b) Desorption parameters: Adsorbent Dosage: 1.6 g L^{-1} (80 mg); Volume of eluent: 50ml; Contact Time: 540 min.

$$B = \frac{V_{sol} \times A}{W_{adsorbent}} = \frac{50 \times 33.753}{80} = 21.10$$

$$\text{Desorption, \%} = \frac{(C \times V_{eluent})}{(B \times W_{adsorbent})} \times 100 = \frac{(2.131 \times 50)}{(21.10 \times 80)} \times 100 = 6.31\%$$

Appendix D: Sample Calculations to Evaluate Performance and Cost Index of Chitosan Derivatives

The following sections summarize sample calculations associated to the determination of performance and cost index for epoxy chitosan and 3-amino-1,2,4-triazole-5-thiol cross-linked chitosan derivative (CH-AZ).

A. Preparation of epoxy chitosan

Experimental conditions and chemicals utilized	**Retail cost**	**Estimated cost of various entities in the synthesis**
Raw chitosan = 5 g	Chitosan (250 g) = Rs. 17014.50	Chitosan (5 g) = Rs. 340.29
2% acetic acid = 250 mL	Acetic acid (500 mL) = Rs. 420	2% acetic acid (5 mL) = Rs. 4.2
0.1M NaOH = 1 L	NaOH (500 g) = Rs. 360	0.1M NaOH (1 L) = Rs. 2.88
Dimethylformamide = 50 mL	Dimethylformamide (1 L) = Rs. 5613.56	Dimethylformamide (50 mL) = Rs. 280.68
Epichlorohydrin = 25 mL	Epichlorohydrin (500 mL) = Rs. 1603.60	Epichlorohydrin (25 mL) = Rs. 80.18
Ethanol = 200 mL	Ethanol (500 mL) = Rs. 101.48	Ethanol (200 mL) = Rs. 40.59
Temperature = 80 °C	Electricity (1 KWH) = Rs. 5	Electricity ((24 h) = Rs. 240
Time = 24 h		
Total cost = Cost of chitosan + 2% acetic acid + 0.1M NaOH + Dimethylformamide + Epichlorohydrin + Ethanol + Electricity		
Total cost for 6 g of epoxy chitosan = Rs. 988.82		

B. Preparation of CH-AZ

Experimental conditions and chemicals utilized	**Retail cost**	**Estimated cost of various entities in the synthesis**
3-amino-1,2,4-triazole-5-thiol = 3 g Epoxy chitosan = 6 g Methanol = 100 mL Acetone = 100 mL Temperature = 100 °C Time = 12 h	3-amino-1,2,4-triazole-5-thiol (10 g) = Rs. 1533.30 Methanol (1 L) = Rs. 1390 Acetone (1 L) = Rs. 2550	3-amino-1,2,4-triazole-5-thiol (3 g) = Rs. 459.99 Epoxy chitosan (6 g) = Rs. 988.82 Methanol (100 mL) = Rs. 139 Acetone (100 mL) = Rs. 255 Electricity (12 h) = Rs. 120

Total cost = Cost of 3-amino-1,2,4-triazole-5-thiol + Epoxy chitosan + Methanol + acetone + electricity.

Total cost for 10 g of CH-AZ = Rs. 1962.81

Miscellaneous operating cost = 2% of total cost = Rs. 39.26

Therefore, **Grand total** = Cost of CH-AZ + Miscellaneous operating cost = Rs. 2002.06

Cost of 1 kg CH-AZ = Rs. 200206.62 = $ 2866.36

C. Performance index

Pd(II) concentration = 50 mg L^{-1}

Volume of Pd(II) solution = 50 mL

Amount of Pd present in the 50 mL of solution = 2.5 mg

Amount of adsorbent used = 80 mg

Amount of Pd adsorbed for 1 g of adsorbent = 30.96 mg g^{-1}

Amount of Pd adsorbed in mg = $30.96\times80\times10^{-3}$ = 2.4768 mg

$$\text{Performanceindex} = \frac{\text{Amount of Pd adsorbed in mg}}{\text{Amount of Pd present in the 50 mL of solution}} = 0.9907$$

D. Cost index

$$\text{Costindex} = \frac{\text{Amount of Pd adsorbed in mg} \times \text{Pd cost for 1 g}}{\text{Amount of adsorbent used} \times \text{cost of adsorbent}} = 0.3219$$

Appendix E: Images of Laboratory Research

Raw adsorbents **Pd loaded adsorbents**

Chitosan

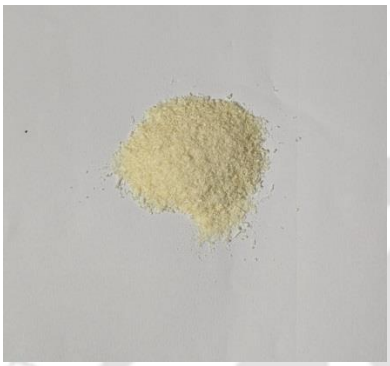


Amberlyst A21


Amberlite IRA958

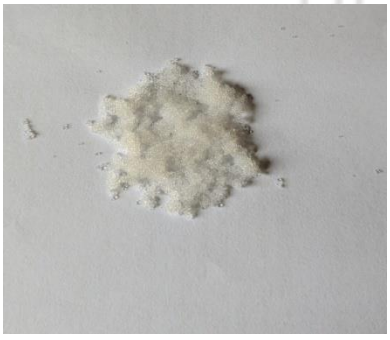


Dowex Marathon MSA

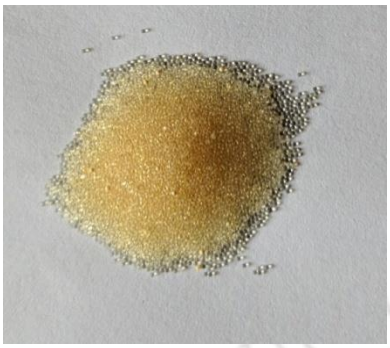

CH-ME

CH-TETA

CH-TSC

CH-AZ

Appendix F: Regenerative and Reusable Efficacy of Most Competent Adsorbents

The following section summarizes Regenerative and reusable efficacy of most competent adsorbents, namely CH-ME and Dowex marathon MSA resins.

The regenerative and reusable efficacy of most competent adsorbents that exhibited best Pd(II) desorption characteristics has been additionally targeted. These resins are Dowex Marathon MSA (commercial resin) and chitosan cross-linked melamine (CH-ME) (synthesized resin). The regenerative and reusability characteristics of these resins have been presented in Table F1. These studies have been carried out in three cycles and without involving Pd(II) adsorption in the intermediate cycles. As shown, for Dowex Marathon MSA resin, the desorption efficiency enhanced from 69.31 to 93.99% in three consecutive cycles. Corresponding desorption efficiency values were comparatively lower (58.79 to 78.47%) for the chitosan functionalized CH-ME resin. The reusability capacity of the resins also indicated such variations, thereby confirming that reusability reduced the adsorption capacities significantly.

Table F1: Recycling and reusability efficacies of Dowex Marathon MSA and CH-ME adsorbents.

Adsorbent name	Pd(II) concentration (mg L^{-1})	Removal (%)	Adsorption capacity (mg g^{-1})	Cycle	Desorption efficiency[1] (%)	Reusability capacity[2] (mg g^{-1})	Reusability Efficiency[3] (%)
Dowex Marathon MSA	50	82.68	29.53	1	69.31	18.68	52.31
				2	88.90		
				3	93.99		
CH-ME		78.94	24.67	1	58.79	14.25	45.61
				2	75.88		
				3	78.47		

[1] $Desorption\ efficiency, (\%) = \frac{C_i - (C_i - C_{f,absorbed})}{C_i} \times 100$

[2] $Reusability\ capacity, (mg\ g^{-1}) = \frac{(C_i - C_{f,absorbed})}{W} \times V$

[3] $Reusability\ efficiency, (\%) = \frac{(C_i - C_{f,absorbed})}{C_i} \times 100$

Appendix G: Statistical Analysis (ANOVA analysis) of CH-ME and Dowex Marathon MSA Resins

The following section summarizes statistical analysis (ANOVA analysis) of CH-ME and Dowex marathon MSA resins.

Table G (1-4) and G (5-6) summarize Pd(II) adsorptive removal efficiency data obtained after conducting one-way statistical (Analysis of variance or ANOVA) analysis of CH-ME and Dowex marathon MSA, respectively. For each resin, three trails have been considered for variations in four alternate adsorption process parameters namely pH, dosage, time and concentration. For all cases, high F-values have been obtained and thereby infer upon significancy of the Pd(II) batch adsorption characteristics. For CH-ME, highest F-value was obtained for initial Pd(II) solution concentration followed by time, adsorbent dosage and pH. Hence, it is apparent that among all four adsorption process parameters, concentration has the highest influence and pH has the lowest influence upon the removal efficiency of Pd(II) from synthetic ELP solutions using CH-ME resin. The trends are opposing for the case of Dowex Marathon MSA commercial resin where the pH has maximum influence and concentration has lowest influence on the Pd(II) removal efficiency from synthetic ELP solutions. For all cases, a lower p-value has been obtained (< 0.0001), which again affirms upon the significancy of the experiments. In summary, the ANOVA analysis affirm confidence with respect to the Pd(II) adsorption characteristics of the said resins using synthetic ELP solutions.

Table G1: Statistical analysis data of CH-ME derivative resin for pH influence on Pd(II) removal efficiency.

pH	Trail 1	Trail 2	Trail 3	Mean	Standard Deviation	SE of Mean	F-Value	P-Value
0.5	55.62	56.66	56.14	56.14	0.52	0.30		
1	59.96	60.82	60.39	60.39	0.43	0.25		
2	72.40	73.11	72.76	72.76	0.35	0.20		
4	63.64	64.53	64.09	64.09	0.44	0.26	659.03	$2.22E^{-16}$
6	61.49	60.86	61.17	61.17	0.32	0.18		
8	57.76	57.02	57.39	57.39	0.37	0.21		
10	56.38	56.90	56.64	56.64	0.26	0.15		

Table G2: Statistical analysis data of CH-ME derivative resin for dosage influence on Pd(II) removal efficiency.

Dose (mg)	Trail 1	Trail 2	Trail 3	Mean	Standard Deviation	SE of Mean	F-Value	p-Value
10	56.82	56.04	56.43	56.43	0.39	0.22		
20	58.56	57.62	58.09	58.09	0.47	0.27		
30	63.20	64.00	63.60	63.60	0.40	0.23		
40	67.44	66.80	67.12	67.12	0.32	0.18		
50	72.93	71.78	72.36	72.36	0.57	0.33		
60	74.96	74.02	74.49	74.49	0.47	0.27	1411.91	<0.0001
70	76.64	76.00	76.32	76.32	0.32	0.18		
80	77.99	77.75	77.87	77.87	0.12	0.07		
90	79.19	78.39	78.79	78.79	0.40	0.23		
100	79.16	78.55	78.86	78.86	0.31	0.18		

Table G3: Statistical analysis data of CH-ME derivative resin for contact time influence on Pd(II) removal efficiency.

Time (min)	Trail 1	Trail 2	Trail 3	Mean	Standard Deviation	SE of Mean	F-Value	p-Value
5	42.82	41.78	42.30	42.30	0.52	0.30	3505.13	<0.0001
15	46.00	45.26	45.63	45.63	0.37	0.21		
30	47.44	46.33	46.89	46.89	0.56	0.32		
60	49.29	48.35	48.82	48.82	0.47	0.27		
240	61.97	61.93	61.96	61.96	0.03	0.02		
420	66.41	67.83	67.12	67.12	0.71	0.41		
600	72.38	73.26	72.82	72.82	0.44	0.26		
780	78.34	79.28	78.81	78.81	0.47	0.27		
960	80.39	79.70	80.04	80.04	0.35	0.20		
1080	80.60	80.10	80.35	80.35	0.25	0.14		

Table G4: Statistical analysis data of CH-ME derivative resin for initial Pd(II) solution concentration influence on Pd(II) removal efficiency.

Concentration (mg L^{-1})	Trail 1	Trail 2	Trail 3	Mean	Standard Deviation	SE of Mean	F-Value	p-Value
50	82.02	80.98	81.50	81.50	0.52	0.30	3769.04	$6.15E^{-13}$
100	69.98	70.86	70.42	70.42	0.44	0.25		
200	53.50	54.33	53.92	53.92	0.41	0.24		
300	51.24	51.46	51.35	51.35	0.11	0.06		

Table G5: Statistical analysis data of Dowex Marathon MSA resin for pH influence on Pd(II) removal efficiency.

pH	Trail 1	Trail 2	Trail 3	Mean	Standard Deviation	SE of Mean	F-Value	p-Value
2	60.04	60.29	60.17	60.17	0.13	0.07		
4	86.50	86.65	86.57	86.57	0.08	0.05		
6	77.43	77.82	77.63	77.63	0.19	0.11	1933.06	$2.15E^{-14}$
8	69.77	70.33	70.05	70.05	0.28	0.16		
10	68.46	70.04	69.25	69.25	0.79	0.46		

Table G6: Statistical analysis data of Dowex Marathon MSA resin for dosage influence on Pd(II) removal efficiency.

Dose (mg)	Trail 1	Trail 2	Trail 3	Mean	Standard Deviation	SE of Mean	F-Value	p-Value
10	66.76	65.20	65.98	65.98	0.78	0.45		
20	79.76	80.76	80.26	80.26	0.50	0.29		
30	85.80	86.57	86.18	86.18	0.39	0.22		
40	88.52	89.13	88.82	88.82	0.31	0.18		
50	90.99	91.59	91.29	91.29	0.30	0.17	1429.29	<0.0001
60	91.80	92.36	92.08	92.08	0.28	0.16		
70	92.00	92.58	92.29	92.29	0.29	0.17		
80	92.38	92.93	92.65	92.65	0.28	0.16		
90	92.62	93.18	92.90	92.90	0.28	0.16		
100	92.86	93.29	93.07	93.07	0.21	0.12		

Table G7: Statistical analysis data of Dowex Marathon MSA resin for contact time influence on Pd(II) removal efficiency.

Time (min)	Trail 1	Trail 2	Trail 3	Mean	Standard Deviation	SE of Mean	F-Value	p-Value
5	57.60	62.40	60.00	60.00	2.40	1.39	95.99	$1.79E^{-14}$
15	67.16	69.06	68.11	68.11	0.95	0.55		
30	79.36	80.71	80.03	80.03	0.67	0.39		
60	79.78	82.29	81.03	81.03	1.25	0.72		
240	81.72	86.12	83.92	83.92	2.20	1.27		
420	83.76	87.11	85.44	85.44	1.68	0.97		
600	85.76	90.17	87.96	87.96	2.21	1.27		
780	86.54	90.42	88.48	88.48	1.94	1.12		
960	87.18	90.40	88.79	88.79	1.61	0.93		
1080	87.40	90.52	88.96	88.96	1.56	0.90		

Table G8: Statistical analysis data of Dowex Marathon MSA resin for initial Pd(II) solution concentration influence on Pd(II) removal efficiency.

Concentration ($mg\ L^{-1}$)	Trail 1	Trail 2	Trail 3	Mean	Standard Deviation	SE of Mean	F-Value	p-Value
50	84.26	91.77	88.02	88.02	3.75	2.16	41.26	$3.26E^{-05}$
100	72.65	78.76	75.70	75.70	3.05	1.76		
200	66.06	70.82	68.44	68.44	2.38	1.37		
300	63.05	65.93	64.49	64.49	1.44	0.83		